universität wien

MASTERARBEIT / MASTER'S THESIS

Titel der Masterarbeit / Title of the Master's Thesis

„Interaction of EGFR and MET in acquired EGFR inhibitor resistance“

verfasst von / submitted by

Taraneh Beikbaghban

angestrebter akademischer Grad / in partial fulfilment of the requirements for the degree of

Master of Science (MSc)

Wien, 2019 / Vienna 2019

Studienkennzahl lt. Studienblatt / degree programme code as it appears on the student record sheet:	A 066 877
Studienrichtung lt. Studienblatt / degree programme as it appears on the student record sheet:	Masterstudium Genetik und Entwicklungsbiologie
Betreut von / Supervisor:	Univ.-Prof. Dr. Mag. Walter Berger

Abstract:

Non-small cell lung cancer (NSCLC) accounts for ~85% of all lung cancers. EGFR mutations in this tumor are common causes for aggressiveness and thus represent a valuable therapeutic target. However, after initial therapy response, resistance develops by various mechanisms including overexpression of other RTKs like Met or acquisition of secondary mutations, e.g. T790M. In this study, we analyzed resistance mechanisms using the human EGFR-driven NSCLC cell line HCC827.

First, resistant sublines against the EGFR inhibitors erlotinib (HCC827/Erlo) and gefitinib (HCC827/Gefi) were generated. Array Comparative Genomic Hybridization (aCGH) and Fluorescence in situ hybridization (FISH) analyses revealed high-level amplification of the EGFR gene locus in the parental cell line, which was reduced but still present in the resistant sublines. Reduction of the EGFR amplicon was accompanied by gain of the MET gene amplification, which interestingly had a different pattern in the two EGFR inhibitor-resistant models.

Met upregulation resulted in EGFR inhibitor resistance in the HCC827/Erlo and HCC827/Gefi sublines. Upon Met inhibition by crizotinib, HCC827/Erlo and HCC827/Gefi were re-sensitized towards EGFR inhibitor treatment.

Next, the selection was expanded by additional inhibition of Met. For both the HCC827/Erlo and HCC827/Gefi cell lines two additional sublines were generated: one receiving only crizotinib (HCC827/ErloCrizo, HCC827/GefiCrizo) and one with continuous application of the initial EGFR inhibitor and crizotinib (HCC827/Erlo+Crizo, HCC827/Gefi+Crizo). In the sublines selected only with crizotinib, indirect aCGH revealed loss of MET but no change or even gain of EGFR gene copies.

Concomitant selection with both RTK inhibitors resulted in a pronounced loss of both amplicons. In these sublines, combination experiments with crizotinib and EGFR inhibitors showed no re-sensitizing effect towards EGFR inhibitors. Interestingly, in the Erlo+Crizo model, a new high-level amplification on chromosome 17q12 was observed, containing the gene locus for SOCS7, a gene involved in JAK/STAT and MET signaling. Besides that, ErbB family members, AXL and FGFR1 were significantly upregulated in EGFR/MET inhibitor resistant subline. Summarizing, in the double-selected cell models neither MET amplification/overexpression nor the T790M mutation is responsible for EGFR TKI resistance.

Zusammenfassung:

Non Small Cell Lung Cancer (NSCLC) macht ~ 85% aller Lungenkrebs. EGFR-Mutationen in diesem Tumor sind häufige Ursachen für Aggressivität und stellen somit ein wertvolles therapeutisches Ziel dar. Nach anfänglicher Therapieantwort entwickelt sich die Resistenz jedoch durch verschiedene Mechanismen einschließlich der Überexpression anderer RTKs wie Met oder dem Erwerb von sekundären Mutationen, zum Beispiel T790M. In dieser Studie analysierten wir Resistenzmechanismen mithilfe der humanen EGFR-gesteuerten NSCLC-Zelllinie HCC827.

Zunächst wurden resistente Sublinien gegen die EGFR-Inhibitoren erlotinib (HCC827/Erlo) und Gefitinib (HCC827/Gefi) generiert. Vergleichende genomische Array-Hybridisierungs- (aCGH) und Fluoreszenz-in-situ-Hybridisierungs (FISH) Analysen zeigten eine hohe Amplifikation des EGFR-Genlocus in der parentalen Zelllinie, die reduziert war, aber immer noch in den resistenten Sublinien vorhanden war. Die Reduktion des EGFR-Amplikons wurde von einem Gewinn der MET-Genamplifikation begleitet, die interessanterweise ein anderes Muster in den zwei EGFR-Inhibitor-resistenten Modellenaufwies. Die Met-Hochregulation führte zu einer EGFR-Inhibitor-Resistenz in den HCC827/Erlo und HCC827/Gefi Sublinien. Nach der Met-Hemmung durch Crizotinib wurden HCC827/Erlo und HCC827/Gefi erneut gegenüber einer EGFR-Inhibitor-Behandlung sensibilisiert. Als nächstes wurde die Selektion durch zusätzliche Hemmung von Met erweitert. Für die HCC827/Erlo und HCC827/Gefi Zelllinien wurden zwei zusätzliche Sublinen erzeugt: eine, die nur Crizotinib (HCC827/ErloCrizo, HCC827/GefiCrizo) und eine mit kontinuierlicher Anwendung des ersten EGFR-Inhibitors und Crizotinib (HCC827/Erlo+Crizo, HCC827/Gef+Crizo). In den nur mit Crizotinib ausgewählten Sublinen zeigte indirektes aCGH den Verlust von MET, aber keine Änderung oder sogar Zunahme von EGFR-Genkopien.

Die gleichzeitige Selektion mit beiden RTK-Inhibitoren führte zu einem ausgeprägten Verlust beider Amplikons. In diesen Sublinen zeigten Kombinationsexperimente mit Crizotinib und EGFR-Inhibitoren keine re-sensibilisierende Wirkung gegenüber EGFR-Inhibitoren. Interessanterweise wurde im Erlo+Crizo-Modell eine neue hochgradige Amplifikation auf Chromosom 17q12 beobachtet, die den Genlocus für SOCS7, ein Gen, das an der JAK/STAT und Met-Signalisierung beteiligt ist, enthält. Darüber hinaus wurden die Mitglieder der ErbB-Familie, AXL und FGFR1, in der EGFR/MET Inhibitor-resistenten Subline signifikant hochreguliert. Zusammenfassend ist in den doppelt selektierten Zellmodellen weder die MET-Amplifikation/-

Überexpression noch die T790M-Mutation für die EGFR-TKI-Resistenz verantwortlich.

Acknowledgment:

Herewith I would like to thank all people, that this study was not possible without their help.

First, I am deeply grateful to Prof. Dr. Mag. Walter Berger, who trusted me and accepted me in his group. It is being an honor for me to perform my master thesis in your lab and under your supervision. I am grateful for the pleasant cooperative atmosphere in the lab.

Special thanks to Dr. Christine Pirker, for all help and support. She opened the door of arrays to me and led me to the right scientific way with her expertise and patience. You taught me so many things and helped me a lot by correcting my master thesis. Many thanks go to Dr. Kushtrim Kryeziu who taught me a lot and helped me during my thesis. I would like to acknowledge, our cooperating Partner at AIT, Assoc. Prof. Oliver Langer for financing my master thesis.

I am thankful to my father and brother for motivating me through my path during the last years. Finally, a very special word of thank goes to my husband and love of my life, Abouzar, who has tried his bests to support me during my study.

Table of Contents:

1 Introduction

1.1 Lung Cancer:

Lung cancer is the first cause of cancer-related death in both women and men worldwide [1]. Upon their microscopic appearance, lung cancers are categorized into two following categories [2-4]:

- Small cell lung cancer (SCLC)
- Non-small cell lung cancer (NSCLC)

SCLC (also known as oat cell cancer) includes 15-20% of all cases and is the most aggressive lung cancer. NSCLC accounts for more than 80-85% of the cases, and thus, it is the most common type of lung cancer [5]. There are three types of NSCLC (see Figure 1) [6]:

- Adenocarcinoma
- Squamous cell carcinoma
- Large cell carcinoma

Most adenocarcinomas arise in the outer or peripheral area of the lungs. They can also spread to the lymph nodes and beyond, leading to metastasis [7]. It has already been shown that long term tobacco smoking increases lung cancer incidence. Several countries perform screening for lung cancer. For instance, Canadian arm forces perform low-dose computed tomography (CT) for smokers with at least 30 pack-year smoking history and who smoke or quit smoking less than 15 years ago, and in Japan, lung cancer screening by chest radiography from age 40 onward is suggested [8].

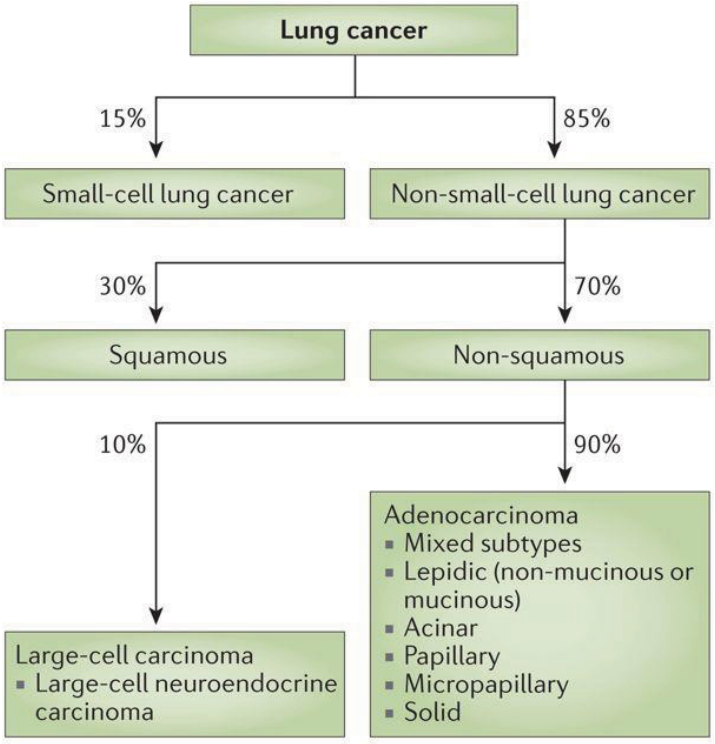

Figure 1: lung cancer classification. Copyright © 2015 Springer Nature, reprinted, with permission, from Springer Nature [6].

Positron emission tomography (PET) and CT are two methods widely used for diagnosis. Medical imaging systems, tumor biopsy and physiological analysis, which are widely used to assess the degree of malignancy, determine the treatment regimen used. However, the value of biopsy for diagnosis has limitations regarding the accessibility of the tumor site as well as intra-tumoral heterogeneity [9, 10].

1.2 Lung Cancer Therapy:

First stages of NSCLC often show no respiratory symptoms and thus escape early detection. Many patients are only diagnosed at stage III or IV with poor prognosis and low progression-free survival rate [11, 12]. Despite large therapy achievements during the last decade, advanced-stage lung cancer represents a fatal and incurable disease [13]. In late-stage patients, most commonly diagnosed with advanced NSCLC upon rapid disease progression, surgery is not appropriate anymore [14-16].

1.2.1 Surgery

In early stages of NSCLC, provided that the tumor has not spread to other parts, surgery is used to remove the cancerous lobe of the lung (lobectomy) and to further determine the stage of the adenocarcinoma.

1.2.2 Chemotherapy

In the most general term, cancer chemotherapy might be defined as cancer therapy using drugs that induce cancer cell death (cytotoxic) and/or inhibit cancer cell proliferation (cytostatic). Various chemotherapeutic agents are applied depending on cancer type and stage. Depending on their biological characteristics and mode of actions, chemotherapies are classified differently [17, 18]. However, they all have a common goal, that is, to prevent cancer cells from dividing and growing. This can be achieved, for example, by intercalating into the DNA or crosslinking DNA strands, causing abnormal base pairing and DNA breakage.

Nevertheless, chemotherapeutic agents not only affect fast-growing cancerous cells but also highly proliferating healthy cells like white blood cells, intestinal cells in the gut, and hair follicle cells in the skin. This leads to well-known side effects such as increased risk for infection, intestinal problems, fatigue, hair loss, etc. that can severely impact patient's quality of life. In some cases, chemotherapy might be combined with other therapies, like radiotherapy or targeted approaches, and most recently, also with immunotherapy [19].

1.2.3 Radiotherapy:

Radiotherapy is another type of cancer treatment that uses high doses of radiation to kill cancer cells or to reduce their size. There are two types of radiation therapy:

- External beam radiation therapy (EBRT). Here, patients are exposed to high doses of ionizing radiation. This is even stronger than X-ray radiation and aims to kill cancer cells. However, it also kills healthy cells that are near the tumor cells.
- Internal beam radiation therapy (IBRT), also known as brachytherapy or seed implantation. In this treatment, radioactive materials (also known as seeds) are implanted at the tumor site in the patient's body [9].

Radiotherapy is used as monotherapy or in combination with surgery and chemotherapy.

1.2.4 Immunotherapy:

Malignant cells are capable to stimulate immunosuppressive mechanisms, which promote proliferation and survival of cancerous cells [20-22]. Programmed cell death (PD-1) receptor is a cell surface receptor mainly expressed on T lymphocytes following an activating immune response, thus preventing the onset of autoimmune reactions. PD-1 receptor inhibits T cell activation and immune response through interaction with its ligands (PD-L1 and PD-L2). This is one of the so-called immune checkpoints abused by cancer cells to shut off an antitumor immune response and escape immunosurveillance [23, 24]. PD-1/PD-L1 has been found upregulated in different cancer types including NSCLC. Several antibodies targeting PD-1 or PD-L1, developed to (re-)activate the anticancer immune response, have already been approved for treatment of lung cancer (reviewed in [25] and [26]). It has already been shown that activation of oncogenic pathways, such as the EGFR pathway, can modify the tumor microenvironment via PD-1/PD-L1 upregulation as immunosuppressive molecules and that oncogenic pathway inhibition may increase the antitumor immunity [27]. Thus, targeting oncogenic pathways together with immunotherapy as combinational therapy could improve treatment outcome. Such, combination of the EGFR inhibitor gefitinib with a PD-L1 nanobody was effective to overcome EGFR T790M-associated resistance in NSCLC patients [28]. However, it should be mentioned here, that treatment response to checkpoint inhibitor therapy in lung cancer often only weakly correlates with expression levels of PD-1/PD-L1, and a reliable biomarker characterizing those patient subgroups that might profit most is still missing [27, 29].

1.2.5 Targeted Therapy:

In the past decades, different agents have been developed to block one or more pathways involved in tumor formation, growth, metastasis, and angiogenesis. Prominent among these new generation agents are small molecule tyrosine kinase inhibitors (TKIs) [30]. Specific inhibitors targeting epidermal growth factor receptor (EGFR) mutations, anaplastic lymphoma receptor tyrosine kinase/ROS proto-oncogene 1 (ALK/ROS1) fusions, or B-Raf proto-oncogene, serine/threonine Kinase (BRAF) mutations are prominent examples for several US food and drug administration (FDA)-approved drugs. Besides that, KRAS mutations, erbB2 receptor tyrosine-protein kinase (ERBB2) mutations, and hepatocyte growth factor receptor (HGFR or MET, see below chapter 1.4.3) alterations [31], are also susceptible targets in NSCLC therapies

[13]. Patients are treated with chemotherapy or receive tyrosine kinase inhibitors (TKIs) according to the molecular profile and disease state of each patient ("personalized therapy") [32]. For example, patients harboring a tumor with ALK rearrangements or an EGFR mutation are treated with ALK or EGFR TKIs, respectively [33]. EGFR TKI targeted therapy improved the progression-free survival (PFS) and overall survival rate (OS) and also increased the quality of life of the patients. The first and second generations of EGFR TKIs have shown promising effects in EGFR mutated NSCLC especially exon 19 deletions or an exon 21 L858R mutation (see below chapter1.4.2).

1.3 Therapy Resistance:

Despite frequently observed successful initial therapy response, resistance inevitably develops and stays the main problem in cancer therapy [13, 15, 34, 35].

1.3.1 Multi-Drug Resistance and ATP Binding Cassette (ABC) Transporters:

ABC transporters are transmembrane proteins that play an important role in the transportation of different molecules across intra- and extracellular membranes [36]. In fact, hydrolysis of two ATP molecules is required to transfer every molecule through the membrane [37]. The ABC transporter superfamily includes several different subfamilies. Under physiological circumstances, ABC transporters are important for secretion and absorption and also for protection from toxins, e.g. in the blood-brain barrier (B.B.B.), where high levels of ABCB1 are expressed. Overexpression of several ABC transporters leads to multi-drug resistance in cancer cells including NSCLC. It has been shown that overexpression of ABCB1, as well as ABCG2, are responsible for acquired multi-drug resistance in NSCLC cells treated with targeted therapy [38].

ABC transporters consist of ATP-binding and transmembrane domains (TMDs). In most of the cases, they contain two TMDs and two ATP binding domains (e.g. ABCB1). These four domains, working together as one polypeptide chain, are called full transporter [39]. However, several ABC transporters contain only one transmembrane and one ATP binding domain (e.g. ABCG2) and are called half transporters (see Figure 2) [37]. These half transporters form either homo- or heterodimers for generation of a functional transporter.

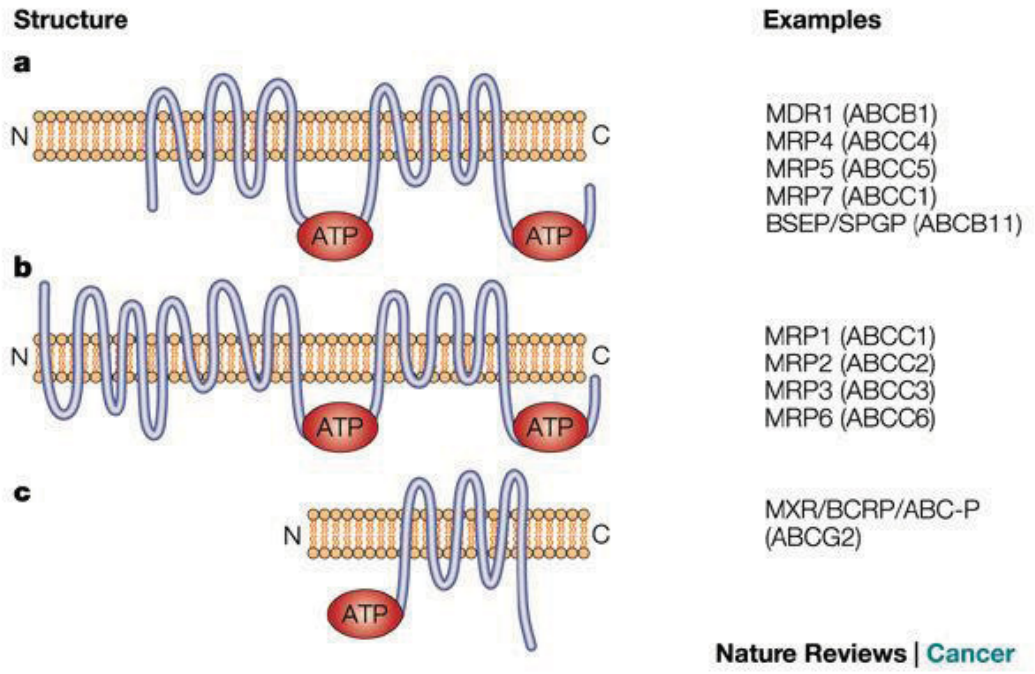

Figure 2: structure of the ABC transporters. Copyright © 2002 Springer Nature, reprinted with permission from Springer Nature [37].

ABC proteins utilize the energy derived from ATP hydrolysis to perform a directed transmembrane movement of their substrates (primary active transporters), open or close a specific membrane channel (e.g. ion-channels) or regulate the permeability of multi-protein channel complexes (receptors). In the ABC proteins which act as primary active transporters, the transport function depends on the hydrolysis of ATP within the nucleotide binding domains (NBDs) [36].

1.3.2 Targeted Therapy Resistance:

Despite the first successful response to targeted therapy, most tumors become resistant after 9 to 12 months [13]. Resistance to targeted therapy in NSCLC can be divided into “on target” and “off-target” resistance [13]. “On target” resistance refers to resistance due to (new) alterations in the targeted oncogene, whereas “off-target” resistance is caused by alteration/activation of other pathways or downstream molecules than the original target.

Drug-induced alterations in oncogenic kinases such as EGFR, ROS1, and ALK are common resistance mechanism against targeted therapeutics in various NSCLC subtypes [40]. Among them, the T790M mutation in the tyrosine kinase domain of the EGFR has the highest incidence and leads to acquired resistance to first-generation EGFR TKIs. Thus, a combination of various targeted therapeutic agents not only increases the treatment outcome but can also more efficiently prevent/overcome the development of acquired resistance [32, 41]. This is the

main topic of the *in vitro* investigations of this study and will be discussed in detail in the discussion part.

1.4 Receptor Tyrosine Kinases (RTKs):

RTKs are a class of growth factor receptor which have tyrosine kinase activity [42]. Well-known examples comprise the EGFR, platelet-derived growth factor receptors (PDGFRs), fibroblast growth factor receptors (FGFRs), vascular endothelial growth factor receptor (VEGFR), hepatocyte growth factor receptor, also called scatter factor receptor or mesenchymal-epithelial transition factor (HGFR, SFR, MET), ephrin receptors (EPH receptors), and the insulin receptor (INSR). RTKs are essential components of cellular signaling pathways.

1.4.1 EGFR and Downstream Cascade:

EGFR is one of the Erythroblastosis Oncogene B (ErbB)/HER family members. The human ErbB family includes 4 members (ErbB1 to 4). EGFR, also known as ErbB1 or HER1, is one of the RTKs often highly upregulated in different cancer types including lung cancer [43]. It contains three major domains: an extracellular domain, a transmembrane domain, and a cytoplasmic domain. There are different growth factors that are capable to act as ligands for EGFR such as epidermal growth factor (EGF) and transforming growth factor alpha (TGFα). Binding of the ligand to the extracellular domain leads to a conformational change of the cytoplasmic domain, resulting in receptor dimerization and autophosphorylation. EGFR can form homo and/or heterodimers with other members of the ErbB-family [44]. This further induces the phosphorylation of several proteins and downstream signaling pathways. There are various phosphorylation sites on the receptor kinase domain which activate different downstream proteins.

Figure 3 shows downstream signaling pathways which can be activated by EGFR.

Activation of EGFR can lead to activation of signal transducer and activator of transcription 1 (STAT1), STAT3 and STAT5. Activated STAT1 translocate to the nucleus and regulates different genes responsible for cell survival, proliferation and oncogenesis [45].

Activated EGFR can increase cell survival not only by activating the JAK-STAT pathway but also by activating the PI3K-AKT downstream cascade. This is explained further in 1.4.4 (Phosphatidylinositol 3-kinase (PI3K) Pathway).

As Figure 3 shows, also the RAS-MAPK pathway can be upregulated by activation of EGFR. This can lead to cell cycle progression (as explained in chapter1.4.5 (Mitogen-Activated Kinase (MAPK) Pathway).
EGFR activation can also result in phospholipase c- γ (PLCγ) activation, which induces hydrolyzation of phosphatidylinositol 4,5-bisphosphate (PIP2) into to diacylglycerol (DAG) and inositol triphosphate (IP3). This leads to the activation of PKC, which results in cell cycle progression, transformation, and apoptosis.

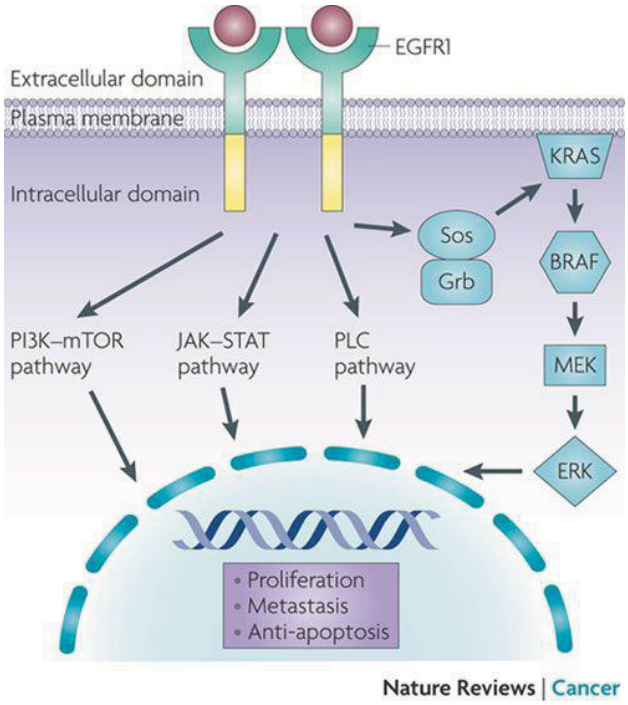

Figure 3: The main downstream signaling pathways regulated by EGFR. Copyright © 2011 Springer Nature, reprinted with permission from Springer Nature [46].

1.4.2 EGFR Tyrosine Kinase Inhibitors (EGFR TKIs):

EGFR TKIs are one of the most successful molecular targeted therapy agents which are used to treat NSCLC. There are 3 generations of FDA-approved EGFR TKIs, which are used as first-line treatment in EGFR-mutated NSCLC patients [47].
The first generation of EGFR TKIs binds to the ATP binding pocket of the EGFR tyrosine kinase domain, where they compete with ATP for binding. Both erlotinib and gefitinib are reversible ATP mimetic quinazoline derivatives that are classified as the first generation of EGFR TKIs [48]. It is proven that first generation EGFR TKIs increase the progression-free survival in comparison to standard chemotherapy in large phase III trials [49]. NSCLC cells harboring EGFR sensitizing mutations show high sensitivity towards erlotinib. However, also

10% of NSCLC with wild type (wt) EGFR respond to EGFR-TKIs due to unknown molecular mechanisms [50].

The second generation of EGFR TKIs binds covalently to the EGFR ATP binding site and thus leads to irreversible inhibition of the tyrosine kinase domain. Afatinib binds to the C797 amino-acid residue of EGFR [51][49]. Erlotinib, gefitinib, and afatinib are used worldwide as the first line treatment for lung adenocarcinomas harboring EGFR-exon 19 deletions or EGFR-L858R mutations.

The third generation of inhibitors binds irreversibly to the EGFR tyrosine kinase domain and is designed to overcome secondary resistance mutations. This generation of TKIs is capable to inhibit EGFR with the activating mutations as well as EGFR harboring the T790M resistance mutation. However, they have only limited efficacy against wild-type EGFR. Osimertinib, an FDA approved third-generation EGFR-TKI, inhibits metastatic, EGFR T790M mutation-positive NSCLC. It is a mutant-selective EGFR-TKI and has a different structure from other first and second-generation inhibitors. Unfortunately, the promising results achieved by therapy with this selective EGFR TKI are limited by the development of tertiary resistance mutations. Such, it has already been shown that a cysteine-797 to serine-790 (C797S) mutation causes acquired resistance towards osimertinib [52].

As shown in Figure 4, two types of EGFR mutations can be distinguished: sensitizing (primary) and secondary (therapy-induced) mutations. The former can be targeted by the first generation of inhibitors, however, application of these inhibitors causes the development of secondary resistance mutations [53].

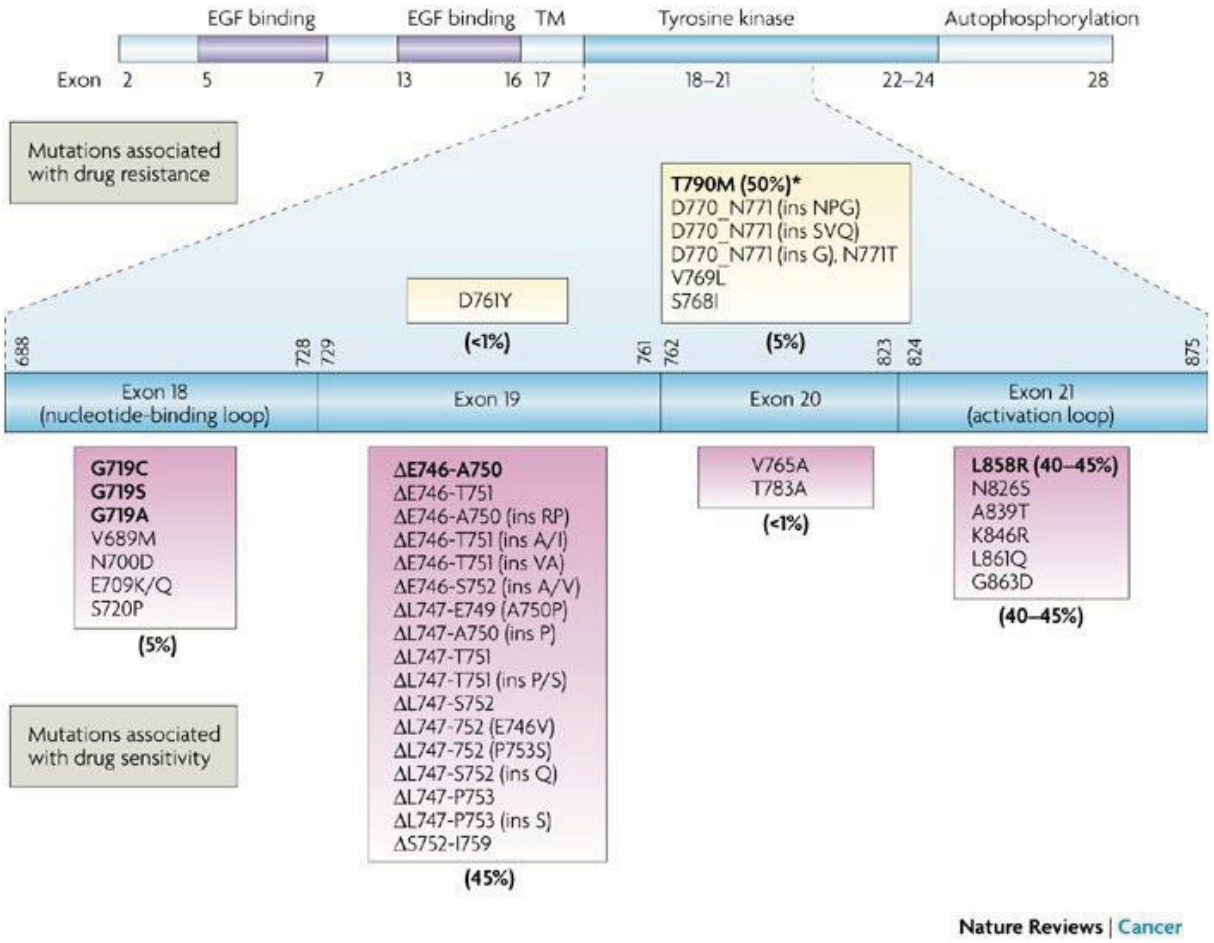

Figure 4: EGFR mutations in NSCLC. Copyright © 2007 Springer Nature, reprinted with permission from Springer Nature [53].

1.4.3 Mesenchymal-Epithelial Transition Factor (MET) Pathway

It has been shown that the MET pathway contributes to many physiological mechanisms during embryogenesis as well as during the development of muscle and nervous system. It has an important role in epithelial to mesenchymal transition (EMT). The Met pathway is also involved in wound healing, and MET expression is found on endothelial cells, neurons, hepatocytes, hematopoietic cells and neonatal cardiomyocytes [54-56]. In cancer, MET pathway dysregulation leads to proliferation, invasion, migration, and metastasis. It is also implicated in many malignancies including NSCLC [54]. MET pathway regulates many cellular responses including cell survival and proliferation, angiogenesis, and cell motility. Deregulation of these functions is relevant to tumorigenesis, invasion, and metastasis (Figure 5). As the MET pathway is frequently upregulated in cancer, it represents an important target for targeted cancer therapy [57]. Upregulation of MET signaling can be due to gene amplification or overexpression the receptor [58]. MET mutations are observed in different solid tumors such as lung, gastric, colorectal, pancreas,

breast, hepatic, head and neck, and brain cancer [45, 59, 60]. MET activation plays a dual role not only as a primary oncogenic driver of NSCLC but also as an important mechanism of acquired resistance against EGFR TKIs [31, 54, 55, 61, 62]. TKIs targeting MET, such as crizotinib, are used to overcome acquired resistance due to EGFR TKI treatment [63, 64].

After activation of the receptor by binding to its high-affinity ligand HGF, autophosphorylation occurs and leads to recruitment of proteins belonging to the downstream cascade. These include growth factor receptor-bound protein 2 (GRB2) and GRB2-associated binding protein 1 (GAB1). This can then activate various downstream signaling pathways [57], e.g. the Ras-Raf-MEK cascade or the phosphatidylinositol 3 kinase pathway (compare 1.4.4 and 1.4.5), leading to enhanced cell proliferation and motility as well as cell survival and apoptosis resistance.

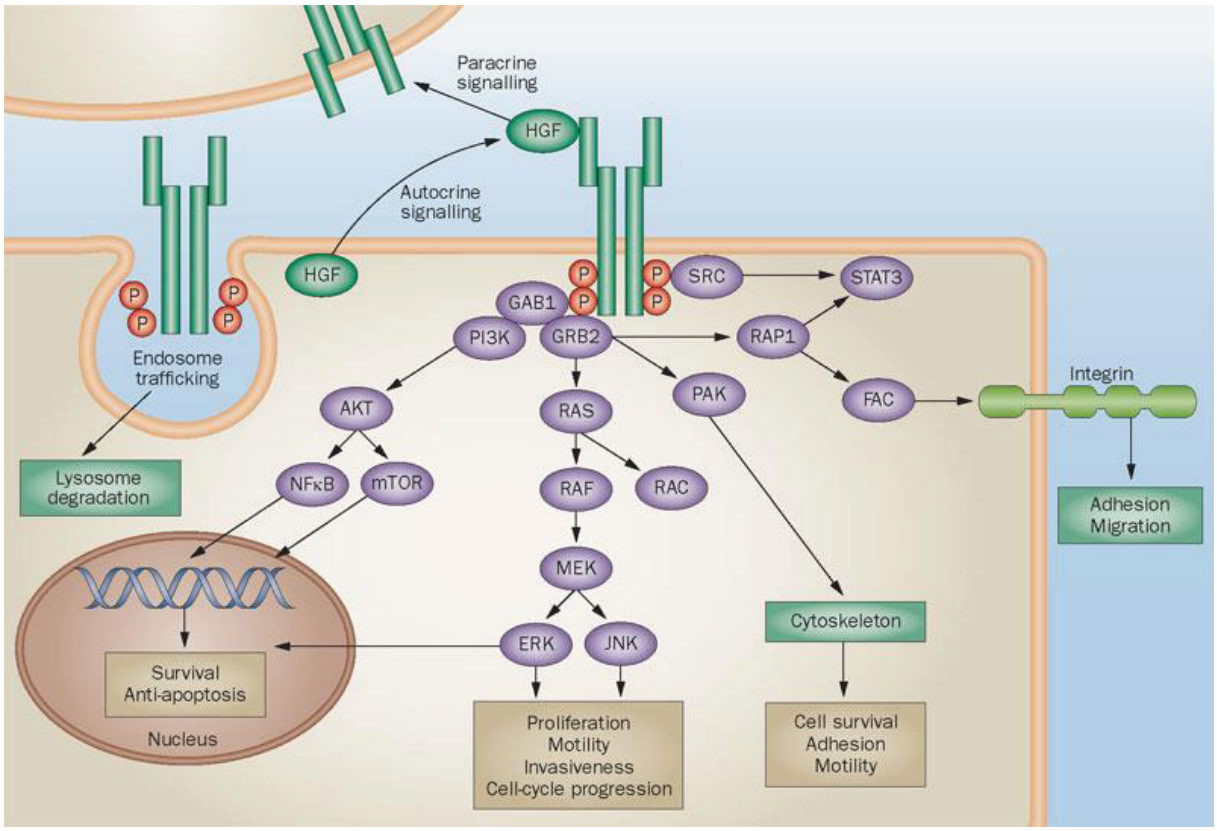

Figure 5: c-MET signaling pathway and different hallmarks of cancer regulated due to c-MET pathway upregulation. Copyright © 2012 Springer Nature, reprinted with permission from Springer Nature [57].

1.4.4 Phosphatidylinositol 3-kinase (PI3K) Pathway

PI3K activation triggers a downstream cascade which leads to cancer cell growth and cell cycle, cell survival, and also angiogenesis [65, 66].

PI3Ks could be activated by RTKs or G-protein-coupled receptors (GPCRs). Upon activation by e.g. growth factor binding, PI3K generates phospholipids that act as second messengers activating AKT (a serine-threonine kinase named after its homologous protein in the retrovirus AKT8, also called protein kinase B or PKB) and multiple downstream targets [65, 67]. The active PI3K migrates to the inner side of the cell membrane and binds to phosphatidylinositol-3, 4-diphosphate (PIP2), which is a regular component of the membrane and is anchored by its two fatty acids in the lipid layer of the membrane. PI3K phosphorylates PIP2 to phosphatidylinositol-3, 4, 5-triphosphate (PIP3). PIP3 can then recruit the kinase AKT to the cell membrane where it gets activated. AKT serine-threonine kinase is a proto-oncogene with many substrates and downstream effects [68]. The tumor suppressor phosphatase and tensin homolog (PTEN) dephosphorylates PIP3 to PIP2, thus inhibiting activation of AKT.

One well-described effect in cancer biology is the inhibition of apoptosis. AKT binds to Bax and prevents it from translocating from the cytosol to the mitochondrial membrane. In the absence of AKT, Bax induces mitochondrial membrane permeabilization, release of cytochrome c and proapoptotic factors, and finally caspase activation and apoptosis

AKT also activates protein synthesis (translation), by a multi-step protein cascade. It begins with the activation of the protein Rheb by AKT. Then, Rheb activates another protein called mammalian target of rapamycin (mTOR). mTOR itself interacts with and activates the translation factor S6 kinase (S6K) by binding to the large subunit of ribosomes. S6K, together with several other proteins, is necessary for initiation of translation [68].

In addition, AKT may lower the concentration of the tumor suppressor protein FOXO1, a transcription factor, by phosphorylating FOXO1. Phosphorylated FOXO1 is a substrate of the enzyme ubiquitin ligase which transfers ubiquitin peptides onto the proteins. Subsequently, ubiquitinated FOXO1 is destroyed by a complex of proteases in the proteasome. Thus, AKT prevents FOXO1-induced transcription of genes that can inhibit proliferation and induce apoptosis (Figure 6).

The PI3K/AKT pathway is aberrantly regulated in many cancers, and increased activity of this pathway is often involved in resistance to cancer therapies. Upregulation of PI3K signaling pathway can be a result of different mechanisms such as mutations, amplification of tyrosine kinase or of PI3K itself.

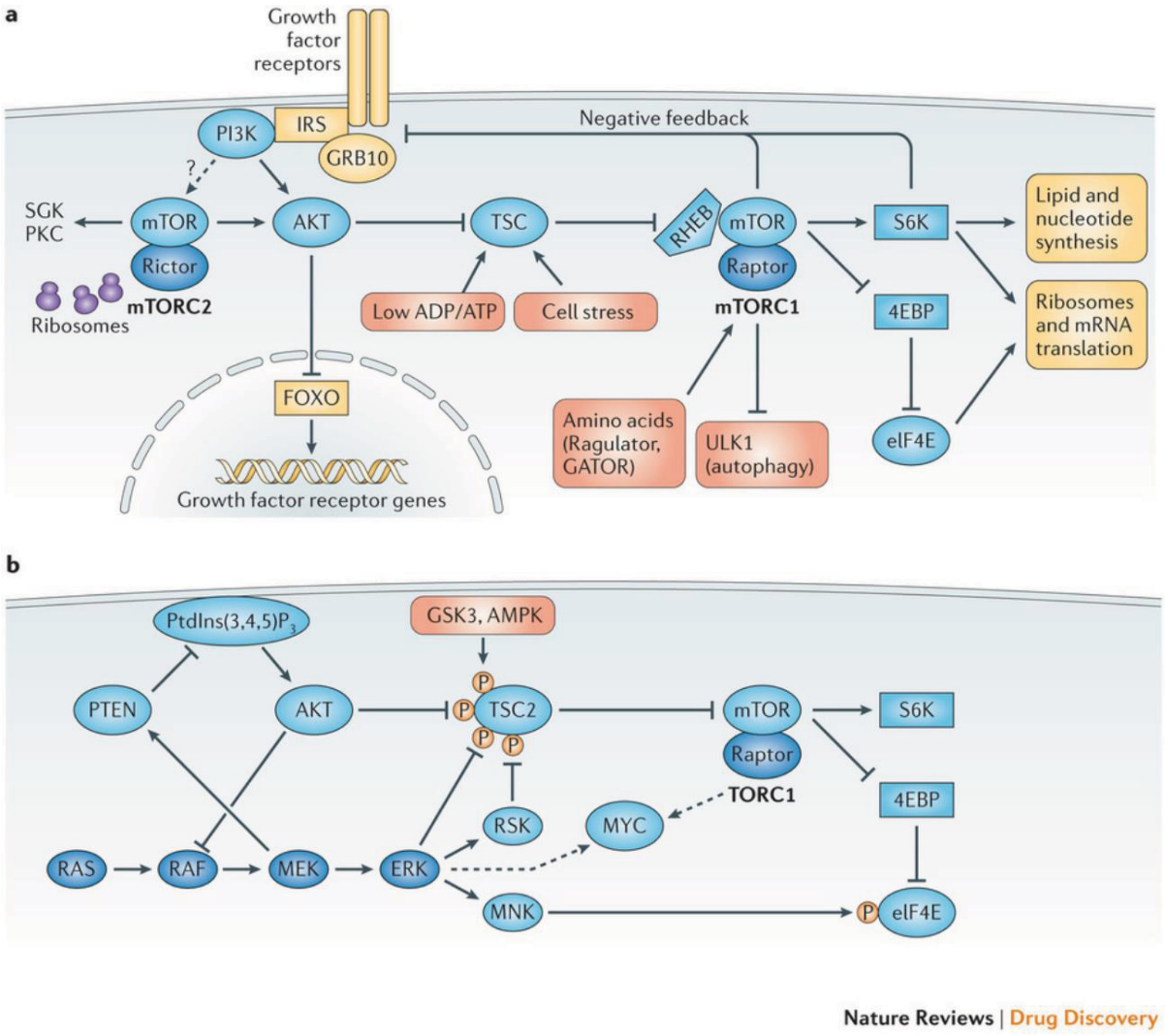

Figure 6: Signaling through the phosphatidylinositol-3-kinase (PI3K)/AKT pathway. Copyright © 2014 Springer Nature, reprinted with permission from Springer Nature [65].

1.4.5 Mitogen-Activated Kinase (MAPK) Pathway

MAPK signaling has an important role in cell cycle progression, development, and differentiation. The MAPK pathway can be activated by various mechanisms including G protein-coupled receptors (GPCR), RTKs, inflammatory cytokines, and environmental stresses. Aberrant MAPK signaling is a key feature of several tumor types and is caused by various mechanisms like e.g. activation of receptor via upregulation of ligands or KRAS and BRAF activating mutations. Upregulated MAPK pathway leads to uncontrolled cell proliferation, resistance to apoptosis, and is involved in resistance development against different therapies [65].

MAPK signaling pathway is activated through binding of a ligand (e.g. EGF) to the extracellular domain of an RTK (e.g. EGFR). This leads to conformation changes of the receptor molecule and receptor dimerization. Next, GRB2 and

son of sevenless (SOS) signaling molecules are activated and bind to the phosphorylated internal domain of the receptors. This results in the activation of RAS on the inner membrane and subsequent phosphorylation of RAF (Figure 7). RAS triggers a phosphorylation cascade including RAF, MEK, and ERK proteins, leading to ERK activation. ERK then translocate to the nucleus where it activates several transcription factors and regulates transcription of many genes that can contribute to cell proliferation and survival.

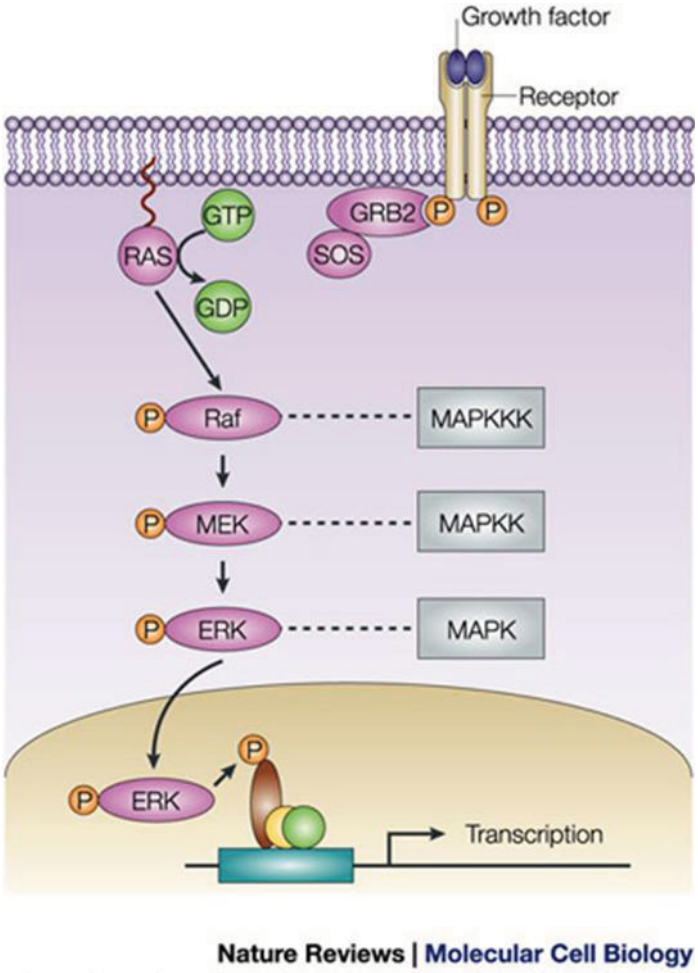

Figure 7: MAPK and its downstream signaling cascade. Copyright © 2004 Springer Nature, reprinted with permission from Springer Nature [69].

2 The aim of the study:

The aim of this study was to investigate different resistance mechanisms towards EGFR-TKIs with a special focus on erlotinib. Various mechanisms for acquired EGFR TKI resistance are already known. Among them, we focused on the following topics

- EGFR resistance mutations (T790M), activation of alternative pathways (overexpression of MET), and upregulation of ABC transporters (ABCB1 and ABCG2) were investigated. To accomplish this, characterization of HCC827 cells as well as sublines with acquired EGFR-TKI resistance, established at the Institute of Cancer Research, Vienna, were investigated. Next, genome-wide changes in gene dose alterations (gains, losses, amplifications, and deletions), as well as gene expressions levels of the EGFR-TKI sensitive parental and resistant sublines were analyzed.
- Analysis of genomic and gene expression data by bioinformatics and systems biology approaches in comparison with international studies on EGFR-TKI resistance.
- Confirmation of prominent cellular response mechanisms and signaling pathways alterations in EGFR-TKI-sensitive versus -resistant cells were investigated at the protein level, and further dissected by using pharmacological or genetic inhibitors as appropriate.
- Investigation of the role of MET receptor overexpression and MET gene amplification on EGFR-TKI resistance.
- Investigation of the role of MDR mechanisms by
    - Analyzing EGFR-TKI responsiveness of cells that overexpress ABC transporters and interactions of EGFR-TKIs with the activity of ABC transporter substrate drugs, and,
    - Analyzing expression and functional activity of ABC transporter in EGFR-TKI-sensitive as compared to resistant cell models.
- Investigation of the impact of EGFR-TKI resistance on tumor growth, in vivo erlotinib accumulation (in vivo imaging) and treatment response.

3 Materials and Methods:

3.1 Drugs:

The following table represents all compounds used in this study.

Table 1: Compounds used in this study.

Drugs	Targets	Used as	FDA approval for Tumor Type	Source
Afatinib (Geotrif)	EGFR	EGFR TKI	NSCLC EGFR exon 19 deletions or exon21 (L858R)	Institute of Cancer Research (ICR)
GW120918 (Elacridar)	ABCB1, ABCBG2	ABCB1 inhibitor		Austrian Institute of Technology (AIT)
Erlotinib (Tarceva)	EGFR	EGFR TKI	NSCLC as monotherapy after failure of at least one prior chemotherapy (2004) Advanced pancreatic cancer in combination with gemcitabine for patients who have not received previous chemotherapy (2005)	LC laboratories
Crizotinib (Xalkori)	ALK inhibitor	c-MET TKI	ALK positive NSCLC (2012)	LC labratories
Doxorubicin (Adriamycin)	Topoisomerase II	ABCB1 substrate		Ebewe pharma
Gefitinib (Iressa)	EGFR		Locally advanced	LC laboratories

			metastatic NSCLC cancer after failure of both platinum-based and docetaxel chemotherapies (2003	
Methotrexate (amethopterin)	Dihydrofolate reductase inhibitor			Fluka
Mitoxantrone	Topoisomerase II	ABCG2 substrate		Ebewe pharma
Osimertinib (AZD9291)	EGFR & HER2	EGFR exon 20 T790M	EGFR T790M mutation-positive NSCLC	ICR
PHA-665752	c-MET			ICR
Tariquidar (XR9576)	ABCB1 inhibitor	ABCB1 modulator		AIT
Verapamil (Isoptin)	calcium ion influx inhibitor (calcium ion antagonist)	Cytotoxic agent		ICR
Vincristine sulfate	Tubulin, Is also a substrate of P-gp	Cytotoxic agent	adult patients with Philadelphia chromosome-negative (Ph-) acute lymphoblastic leukemia (ALL) in second or greater relapse or whose disease has progressed following two or more anti-leukemia	ICR

			therapies.	
Geneticin	aminoglycoside antibiotic blocks polypeptide synthesis by inhibiting the elongation step	Selection antibiotic		
Hygromycin	aminoglycoside antibiotic inhibits protein synthesis	Selection antibiotic		Stem cell technologies

3.2 Cell culture

3.2.1 Cancer cell models:

Cell models investigated in this study are shown in the following table.

Table 2: cancer cell lines investigated in this study.

Cell line	Histology	Specification	Growth medium	Source
HCC827	NSCLC Adenocarcinoma	EGFR mutated (delE746-A750)	RPMI-1640	American type culture collection (ATCC)
HCC827/Dox	derived from HCC827	resistant to doxorubicin	RPMI-1640	Selected in the frame of this study
HCC827/ABCB1	NSCLC Adenocarcinoma	ABCB1 transfected, overexpressing ABCB1	RPMI-1640	Selected in frame of this study
HCC827/Erlo	derived from HCC827	resistant to erlotinib	RPMI-1640	Institute of Cancer Research (ICR) (selected by

				Kushtrim Kryeziu)
HCC827/ErloDox	derived from HCC827/Erlo	resistant to doxorubicin	RPMI-1640	Selected in the frame of this study
HCC827/ErloMX	derived from HCC827/Erlo	resistant to MX	RPMI-1640	Selected in the frame of this study
HCC827/ErloCrizo	derived from HCC827/Erlo	resistant to crizotinib	RPMI-1640	Selected in the frame of this study
HCC827/Erlo+Crizo	derived from HCC827/Erlo	resistant to erlotinib and crizotinib	RPMI-1640	Selected in the frame of this study
HCC827/Gefi	derived from HCC827	resistant to gefitinib	RPMI-1640	ICR (selected by Kushtrim Kryeziu)
HCC827/GefiMX	derived from HCC827/Erlo	resistant to MX	RPMI-1640	Selected in the frame of this study
HCC827/GefiCrizo	derived from HCC827/Gefi	resistant to crizotinib	RPMI-1640	Selected in the frame of this study
HCC827/Gefi+Crizo	derived from HCC827/Gefi	resistant to gefitinib and crizotinib	RPMI-1640	Selected in the frame of this study
HCC827/EPR	NSCLC Adenocarcinoma	resistant to erlotinib and PHA 6657-52	RPMI-1640	Dr. Kenichi Suda Kinki University, Japan
HCC827/eGFP	NSCLC	GFP	RPMI-	ICR

	Adenocarcinoma	transfected, resistant against geneticin	1640	
PC9	NSCLC Adenocarcinoma		RPMI-1640	ATCC
DMS114	Small cell lung carcinoma (SCLC)	overexpression of FGFR1	RPMI-1640	ATCC
DMS114/NIN	derived from DMS114	overexpression of ABCB1, resistant to nintedanib	RPMI-1640	ICR (selected by Bernhard Englinger)
A431	Human squamous carcinoma		RPMI-1640	ATCC

3.2.2 EGFR TKI selection:

HCC827 cells were selected with two different EGFR TKI inhibitors, erlotinib, and gefitinib.

The selection was performed as below:

1. **Erlotinib Selection:** The parental cells received 20 µM erlotinib once a month.
2. **Gefitinib selection:** the parental cells received 20 µM gefitinib once a month.

3.2.3 Crizotinib selection:

The HCC827/Erlo and HCC827/Gefi cell lines were both further selected with crizotinib. This second selection was performed in two different ways (Table 3).

1. The parental cells received only crizotinib (HCC827/ErloCrizo & HCC827/GefiCrizo).
2. The parental cells were selected with crizotinib as well as primary selection drug (HCC827/Erlo+Crizo & HCC827/Gefi+Crizo).

Table 3: Crizotinib Selection

Cell line	1µM Erlotinib	1µM Crizotinib	1µM Gefitinib
HCC827/ErloCrizo	-	+	-
HCC827/Erlo+Crizo	+	+	-
HCC827/GefiCrizo	-	+	-
HCC827/Gefi+Crizo	-	+	+

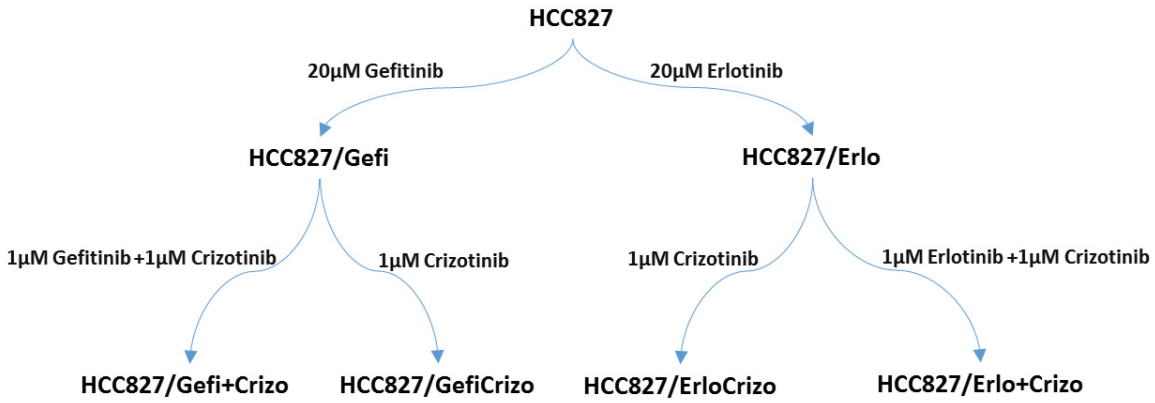

Figure 8: crizotinib selection of the EGFR-TKI selected sublines HC827/Erlo and HCC827/Gefi. HCC827/Erlo and HCC827/Gefi were provided by Kushtrim Kryeziu.

3.2.4 Doxorubicin selection:

The HCC827 and HCC827/Erlo cells were further selected by adding different doxorubicin concentrations (50, 100, 200 nM). As doxorubicin is a substrate for ABCB1 this should lead to ABCB1 overexpression.

3.2.5 Mitoxantrone selection:

HCC827/Erlo and HCC827/Gefi resistant sublines were selected with 1 µM Mitoxantrone as an ABCG2 substrate in order to induce overexpression of ABCG2 (HCC827/Gefi MX and HCC827/ErloMX). The cells received drug regularly after each feeding. They incubated with treatment 3 to 5 day at 37°C.
An overview of all selections including sensitive parental cell model as well as resistant sublines.

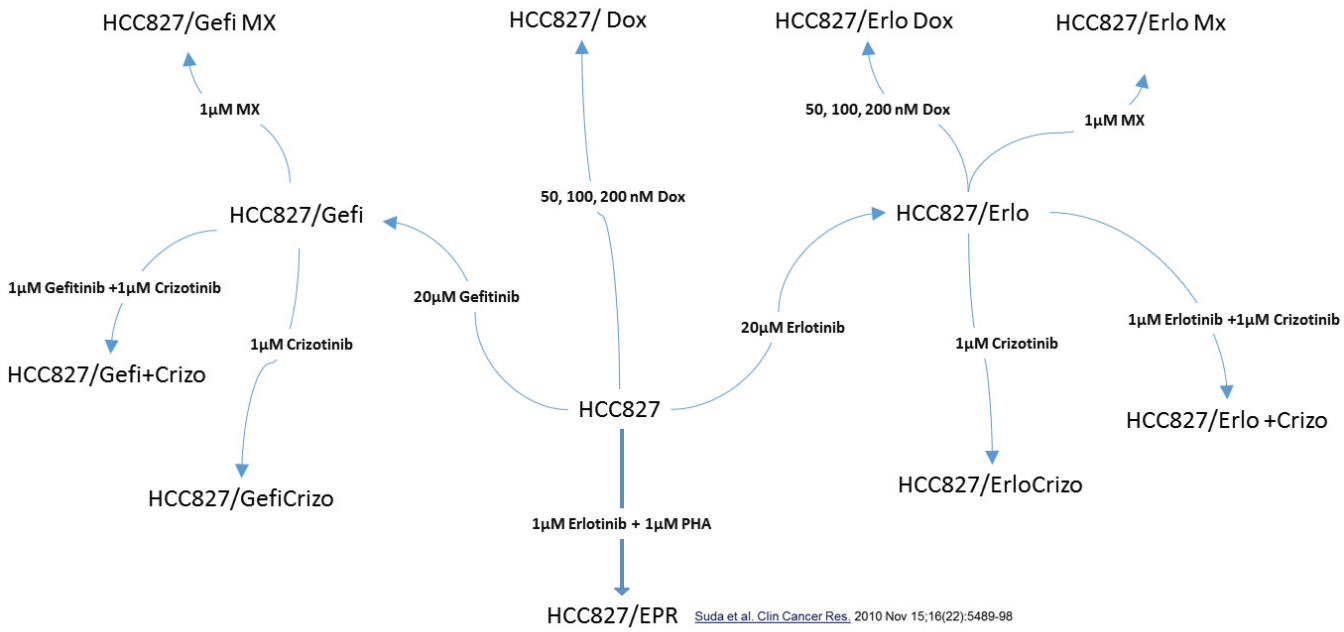

Figure 9: Scheme of HCC827-derived sublines with acquired TKI resistance.

3.3 Viability assay

3.3.1 Theoretical background:

Metabolically active cells are capable to reduce the water-soluble 3-(4, 5-dimethyl thiazolyl-2)-2,5-diphenyltetrazolium bromide (MTT) to formazan by the enzyme mitochondrial reductase. Formazan is not water soluble and shows an orange staining indicating mitochondrial activity of viable cells (Figure 10). The optical density is then measured by colorimeter at 450 nm.

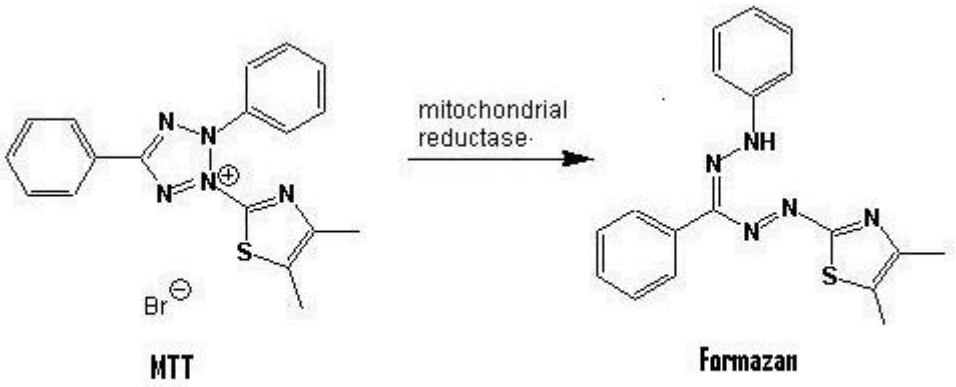

Figure 10: MTT is reduced to formazan by mitochondrial reductase enzyme.

3.3.2 Procedure:

2-4×10^3 cells/well were seeded into 96-well microtiter plates (100µL per well). The plates were incubated for 24 hours and then treated further with

increasing concentrations of the respective drugs. Control wells contained only media without the drug. Drugs were diluted in 100µl/well with the respective culture media. In single drug MTT experiments, 2x final drug concentrations were added to the wells, whereas in combination treatment 4x final drug concentrations were used to reach the final volume of 200 µL per well. The treated cells were further incubated for 72 hours. After removal of drug-containing media, MTT developing solution was added and cells were incubated again for 1-5 hours. Formazan absorbance was detected at 450nm. Data were normalized to values of the first 3 wells containing only medium and no cells and analyzed further by GraphPad Prism 5 software.

3.4 Protein analysis

3.4.1 Protein Isolation:

Cells were seeded into 6-well plates ($3.5x10^5$ cells/well in 1ml culture medium for HCC827 as well as HCC827/Erlo cells and $4.5x\ 10^5$ cells/well for all other resistant sublines). After 24 hours of incubation at 37°C, cells were treated by adding 1ml drug (2x final concentration) and incubated further for 24 hours at 37°C. Cells were scratched into media, collected in falcon tubes and centrifuged at 240xg for 5min, then re-suspended again in 1ml cold 1xPBS and centrifuged again. After removal of PBS, cells were lysed in 30-50µl lysis buffers for 30min on ice. To disrupt the cell membrane, samples were treated 3-5min with ultrasound sonicator. Finally, they were centrifuged for 15min at 18.200xg at 4°C. Supernatants containing protein lysates were collected and stored at -80°C.

Receipts:
500 µl lysis buffer: 50mM Tris
300 mM NaCl
0.5% Triton X-100
5µl phenylmethanesulfonylfluoride (PMSF) - serine protease inhibitor, (Roche)
12.5 µl complete protease inhibitor tablets, (Roche)
25µl Phospho-STOP Phosphatase inhibitor tablets, (Roche)

3.4.2 Western Blotting:

3.4.2.1 Theoretical background:

Western blotting is an immunochemical method. It enables us to separate proteins according to their molecular weight. First, proteins isolated from cell

culture or tissues are separated on a gel. Next, they are transferred to a membrane where they can be detected by using specific antibodies.

3.4.2.2 Sodium Dodecyl Sulfate Polyacrylamide Gel Electrophoresis (SDS-PAGE):

SDS-PAGE is a method commonly used to separate the proteins. Two acrylamide gels (with different acrylamide concentrations) are prepared. SDS is a detergent which destructs disulfide bonds and tertiary structures of proteins, thus making them linear. It also coats proteins uniformly with negative charges, enabling protein separation by electrophoresis according to molecular weight independent of charge. SDS was also added to other buffers used for preparing the gel. Percentage of acrylamide can vary according to target protein size. A high percentage provides small pores of the gel suitable for detection of smaller proteins. A low percentage of acrylamide was used for separation and detection of larger proteins.

For electrophoresis, two gels were used together, stacking and separating gel. The stacking gel was layered on the top of the separating gel. It contained less acrylamide and lower pH than the separating gel. During electrophoresis, it brought proteins rapidly to the same level and prepared them for proper separation by the separating gel.

Cell lysates were diluted in lysis buffer to equal concentrations. Loading buffer containing ß-mercaptoethanol was added to the samples for the more efficient unfolding of the proteins. Next, samples were loaded on the gel and electrophoresis ran at 90 Volt for 2.5 hours.

3.4.2.3 Semi-dry blotting:

The separated proteins were transferred on a membrane by performing semidry blotting. Six filter sheets, as well as one polyvinylidene fluoride (PVDF) membrane, were cut at the same size as the gel. Three blotting sheets were soaked with methanol blotting buffer and other three sheets with SDS blotting buffer. Figure 11 shows how a blotting sandwich was made by putting the gel and membrane together, between blotting paper sheets. The membrane was activated by adding 96% methanol to it. Next, it was washed with Methanol blotting buffer. It was put on the top of 3 blotting sheets soaked with methanol buffer The SDS phage gel and 3 blotting sheets soaked with SDS buffer were added to them respectively (From down to up). The proteins were transferred by an electric current from the gel to the membrane, where they were immobilized.

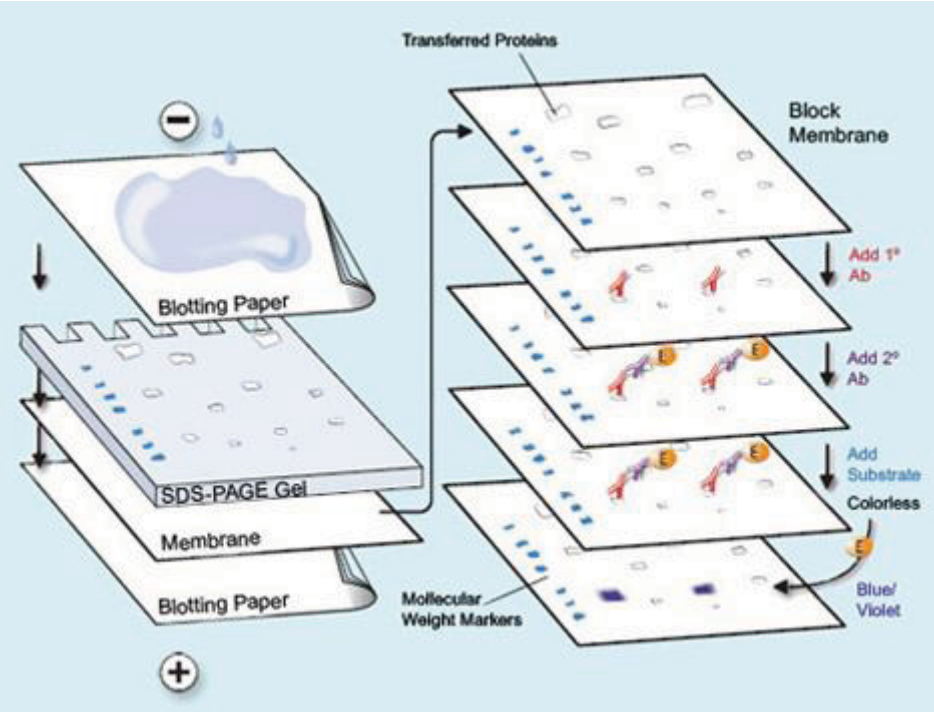

Figure 11: semidry blotting. Of the proteins which have been already separated by SDS Phage Electrophoresis.

Next, the blotting was investigated by incubating the blotted membrane was with Ponceau. The proteins were dyed in red after
The membrane was then washed with TBST 2 times for 5 minutes.
The membrane was blocked by adding the blocking solution for 1 hr. This prevents antibodies from unspecific binding to the membrane.

3.4.2.4 Protein detection:

The blocked membrane was incubated with primary antibody and incubated overnight at 4 °C. Table 4 depicts all primary antibodies used in this study. Next, the membrane was washed with TBST in order to remove all unbound primary antibodies. After all washing steps, the secondary antibody was added to the membrane and incubated 1 hour at room temperature (Table 5).
It was washed 3 times with TBST, before adding a chemiluminescent agent.
The result was visualized in the darkroom by adding a film on the membrane. The film became dark where the proteins were blotted on the membrane.

Table 4 Primary antibodies used for western blotting.

Primary Antibody	specification	Dilution	Company
AXL	monoclonal rabbit	1:1000	Cell signaling
α tubulin	monoclonal		Sigma-Aldrich

	mouse		
ß-actin	monoclonal mouse	1:5000	Sigma
AKT	polyclonal rabbit	1:1000	Cell signaling
pAKT ser 473	polyclonal rabbit	1:1000	Cell signaling
BCRP	monoclonal mouse	1:500	Chemicon
EGFR	polyclonal rabbit	1:1000	Cell signaling
pEGFR Y1068	polyclonal rabbit	1:1000	Cell signaling
MET	monoclonal mouse	1:1000	Cell signaling
pMET Y1234/35	monoclonal rabbit	1:1000	Cell signaling
PARP	polyclonal rabbit	1:1000	Cell signaling
Cleaved PARP	polyclonal rabbit	1:1000	Cell signaling
P-gp (C-219)	polyclonal rabbit		Calbiochem
S6	polyclonal mouse	1:1000	Cell signaling
pS6	polyclonal rabbit	1:1000	Cell signaling

Table 5 Secondary antibodies used for western blotting.

Secondary antibody	Specification	Dilution	Company
Goat anti-mouse	IgG conjugated to Horseradish peroxidase (HRP)	1:10000	Santa Cruz
Goat anti-rabbit	IgG conjugated to Horseradish peroxidase (HRP)	1:10000	Santa Cruz

Table 6

Separating gel		
	10% Acrylamide	7.5% Acrylamide
Contents		
H_2O	3.65 ml	4.1 ml
Acrylamide	1.875 ml	1.4 ml
TrisHCl1.5 M, pH 8.8	1.875 ml	1.875 ml
20% SDS	75 µl	75 µl
10% APS	25 µl	25 µl
TEMED	5 µl	5 µl

Table 7

Stacking Gel	
	4.5 % Acrylamide
Contents	
H_20	1.56 ml
Acrylamide	0.281
Tris-HCL; 0.5M, pH 6.8	0.625 ml
20 % SDS	25 µl
10 % APS	12.5 µl
TEMED	2.5 µl

Receipts:

Tris –HCl 1.5 M, PH=8.8:

18.2 g (150mM) Tris

∑ 100 ml ddH2O, pH=8.8

Tris-HCL 0.5 M, pH=6.8

3 g (25 mM) Tris

∑ 50 mL ddH2O, bring it to pH=6.8

Lysis Buffer:

50 mM Tris-HCL, pH=7.6

300 mM NaCl

0.5% Triton X-100

∑ 500 ml ddH2O

4x Sample loading buffer:

4 ml 10% Glycine

2ml 2-Mercaptoethanol

0.92 g SDS

2.5 ml 1 M Tris-HCl (pH=6.8)

∑ 10 ml ddH2O

Blocking solution:

TBST

+1% powdered milk (fat free)

+0.5 % Bovine Serum Albumine (BSA)

10x TBS:
120g Tris
90g NaCl
∑ 1 L ddH2O & pH =7.6

1x TBST:
100 mM Tris
0.9 M NaCl
1% Tween (polyoxyethylene sorbitan monolaurate, Bio-Rad)

10x Laemmli –Electrophoresis buffer:
30 g (250 mM) Tris
144 g (1.92M) Glycine
10 g (35 mM) SDS
∑ 1 L ddH2O

Bjerrum buffer with Methanol:
5.82 g (48 mM) Tris
2.93 g (39 mM) Glycine
200 ml (12.3 mM) Methanol
∑ 1 L ddH2O

Bjerrumbuffer with SDS:
5.82 g (48 mM) Tris
2.93 g (39 mM) Glycine
0.375 g (1.3 mM) SDS
∑ 1 L ddH2O
Ponceau solution (0.25 mg/ml):
(0.1 % (w/v) Ponceau in 5 %(v/v) acetic acid)
1g Ponceau
50ml acetic acid
∑ 1L ddH2O

3.5 Fluorescence In Situ Hybridization (FISH):

3.5.1 Theoretical background:

FISH is a cytogenetic technique for detection of DNA or RNA sequences. It is based on specific hybridization (self-annealing ability) of 2 DNA or RNA strands. A fluorescently labeled probe is used for detection of the counterpart on the

sample of interest (e.g. chromosomes). FISH can be used for detection of amplifications, translocations, deletions as well as investigating aneuploidy (by adding various centromere probes and counting the distribution of centromeres among the cells fixed on the slide) [70].
In this study, we performed FISH on metaphase chromosome preparations for detection of specific gene amplifications.

3.5.2 Procedure:

3.5.2.1 Metaphase chromosome preparation:

Metaphase chromosomes were prepared according to the following protocol (see below). Cells were seeded into one or two T75 cell culture flasks and incubated until they were 70-80% confluent. Ideally, many mitotic cells were present. Metaphase chromosome preparation protocol was as follows:
100 µl Colchicine (KaryoMAX COLCEMID Solution, Gibco life technologies, Waltham, MA, USA) per 10 ml medium is put onto the cells and incubated for 15 – 60 min at 37 °C.
Hypotonic Solution and Fixation Solution were prepared as below:
Hypotonic Solution: 19 parts 0.075 M KCL (5.6 g / l) + 1 part 0.8% (0.8 g / 100 ml) Na-Citrate. 10 ml per sample, pH 7.4, is prepared at 37°C
Fix. Solution: 3 parts Methanol, 1-part Acetic Acid
35 ml per sample (In fact, 3 x 10 ml plus few additional mls) were prepared and put at -20 °C. Note that they need to be prepared freshly. Slides were put in cold Ethanol abs./HCL (80 ml + 3 ml HCl) overnight.
It is important to mention that slides were put in cold Aqua dest before dropping.
The medium was removed and collected in 50 ml tube. Cells were washed carefully with Trypsin/E (T/E), and this was added to the tube. In addition, T/E was added to the cell layer. It is important to monitor carefully when mitotic cells start to float off and adherent cells start to detach. Then, mitotic and detaching cells were transferred into the tube.
The next step was to centrifuge for 10 min at 200xg. The supernatant was removed (not completely, so that about 0.5-1 ml was left in the tube). The pellet was resuspended using a Pasteur-pipette and transferred into a 10-12ml tube.
Hypo (37 °C) was added dropwise using a Pasteur-pipette, while the tube was shaking constantly with a slow pace at the beginning. The filled tube was incubated for 7 min at 37 °C. Next, it was centrifuged for 10 min at 200xg. The

supernatant (Hypo) was removed (not completely, so that about 0.5-1 ml was left in the tube). The pellet was resuspended using a Pasteur-pipette.

1. Fix. Step: Cold Fix was added dropwise using a Pasteur-pipette, while the tube was shaking constantly with a slow pace at the beginning. The tube was filled up to 10 ml, and incubated at -20 °C for 30 min.

Next, it was centrifuged for 10 min at 200xg. The supernatant (Fix) was removed (not completely, so that about 0.5-1 ml was left in the tube). The pellet was resuspended using a Pasteur-pipette.

2. Fix. Step: Cold Fix was added dropwise using a Pasteur-pipette, while the tube was shaking constantly with a slow pace at the beginning. The tube was filled up to 10 ml and incubated at -20 °C for 1 h. Next, it was centrifuged for 10 min at 200xg. The supernatant (Fix) was removed (not completely, so that about 0.5-1 ml was left in the tube). The pellet was resuspended using a Pasteur-pipette.

3. Fix. Step: Cold Fix was added dropwise using a Pasteur-pipette, while the tube was shaking constantly with a slow pace at the beginning. The tube was filled up to 10 ml and incubated at -20 °C for 1 h. Next, it was centrifuged for 10 min at 200xg. The supernatant (Fix) was removed (not completely, so that about 0.5-1 ml was left in the tube). The pellet was re-suspended by adding a small volume of fix solution using a Pasteur-pipette. Next, it was dropped onto slides. 1-3 drops were added to each cold slide.

It was left to be air dried and monitored by a fluorescent microscope.

Prior to FISH analysis, chromosome preparations were stored at room temperature for at least overnight and additionally put on an 80 °C heating plate for 1 hour ("aging" of the chromosomes to make the DNA strands more accessible for the FISH probes).

FISH for EGFR or MET was performed using either EGFR/CEN-7 FISH Probe Mix together with the cytology FISH Accessory Kit (DAKO Glostrup Denmark) or the MET Spectrum Red FISH Probe Kit together with a CEP 7 Spectrum Green Probe (Abbott Molecular Inc. Des Plaines IL USA). The protocols for both procedures were provided by the respective companies (see below). The EGFR and MET genes are both located on chromosome 7, EGFR on 7p11.2 and MET on 7q31.2.

3.5.2.2 EGFR/CEN7 FISH:

Protocol:

Principle steps	working steps	temperature	time	Comment
fixation of	3.7%	R.T.	2´	

nuclei and chromosomes on the slide	Formaldehyde			
	Wash buffer Nr1	R.T.	5´	1:20 diluted
	1x PBS	R.T.	5´	
dehydration of slides	ethanol 70%	R.T.	2´	
	ethanol 85%	R.T.	2´	
	ethanol 96%	R.T.	2´	
	air dry	R.T.	10´	
application of the probes onto the metaphase preparations	apply 3.0µl probe mix*	R.T.		
	put on coverslip (12 mm Ø)	R.T.		without bubbles
	close with Fixogum	R.T.		
co-denaturation of probes and chromosomes	put slides on a hot heating block	82°C	5´	specific for probe and company!!!
hybridization	put slides in a dark, humid chamber	45°C	overnight	
	remove Fixogum	R.T.		
washing steps (avoid light)	2x SSC/0.1% NP-40	R.T.	5´	to lose the coverslip
		73^{o}	2´	stringent wash
	2x SSC/0.1% NP-40	R.T.	1´	
	air dry	R.T.	10´	
	DAPI pipetting (8µl)	R.T.		
	put on coverslip	R.T.		without bubbles
	look under microscope			

3.5.2.3 MET/CEN7 FISH:

Protocol:

Principle **steps**	**working steps**	**temperature**	**time**	**pH**	**Comment**
pretreatment of slides	2xSSC	73°	2´		
	protease(pepsin)-solution	37°	4´	2.0	Optional
	1x PBS	room temperature (R.T.)	2x5´		
fixation of nuclei and chromosomes on the slide	1x PBS/50mM $MgCl_2$	R.T.	5´		
	3.7% Formaldehyde	R.T.	10´		
	1x PBS	R.T.	5´		
dehydration of slides	ethanol 70%	R.T.	2´		
	ethanol 85%	R.T.	2´		
	ethanol 100%	R.T.	2´		
	air dry	R.T.	10´		
application of the probes onto the metaphase preparations	apply 3.0µl probe mix*	R.T.			
	put on coverslip (12 mm Ø) to put on	R.T.			without bubbles
	close with Fixogum	R.T.			
co-denaturation of probes and chromosomes	put slides on the hot heating block	75°C	5´		specific for probe and company!!!
hybridization	put slides in a dark, humid chamber	37°C	overnight		
	remove Fixogum	R.T.			

washing steps (avoid light)	2x SSC/0.1% NP-40	R.T.	5´		to lose the coverslip
	0.4x SSC/0.3% NP-40	73°	2´		stringent wash
	2x SSC/0.1% NP-40	R.T.	1´		
	air dry	R.T.	10´		
	DAPI pipetting (8µl)	R.T.			
	put on coverslip	R.T.			without bubbles
	look under microscope				

*1 µl MET Spectrum Red, 1µl CEP 7 Spectrum Green, 7µl hybridization buffer, 1µl H_2O.
Pictures were captured on a Leica DMRXA microscope using the Visy View software.

3.6 (Array) Comparative Genomic Hybridization (aCGH)

3.6.1 Theoretical background

CGH is a cytogenetic FISH technique which enables analysis of changes in gene copy number (gains and losses) across the whole genome [70].
It is based on hybridization of the differentially labeled test (tumor) and reference DNA (normal genomic DNA) on either normal human chromosomes (conventional CGH) or oligonucleotides spotted on a glass slide (microarray) (Figure 12). Tumor DNA and normal reference DNA are labeled with red and green, respectively (or vice versa). Equal amounts of both labeled DNA samples are then mixed together and hybridized to normal chromosomes or oligonucleotides. The slides are examined under a microscope or by a laser scanner, and the color intensity of the two dyes is compared (the red to the green ratio or vice versa) (Figure 13). If a chromosomal/gene region is gained/amplified the red to green ratio is >1. In case of loss/deletion, the ratio is <1. In case of no alteration intensity of the red and green color is identical corresponding to a ratio of 1.
While the resolution of conventional CGH is limited to the level of light microscopy and thus only allows detection of gains/losses of certain chromosomal regions. Array CGH can give direct information about the gene dose alterations at a certain locus.

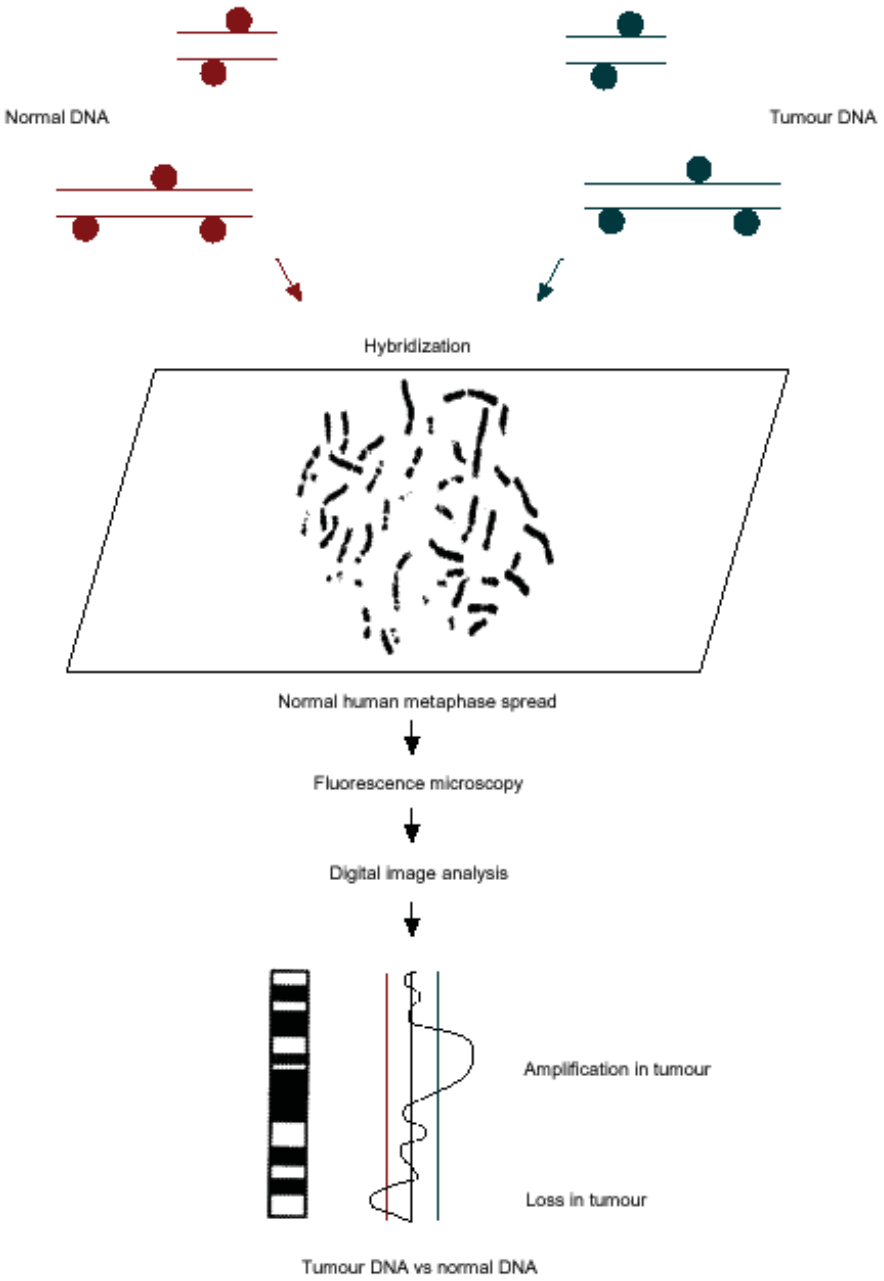

Figure 12: Principle of comparative genomic hybridization

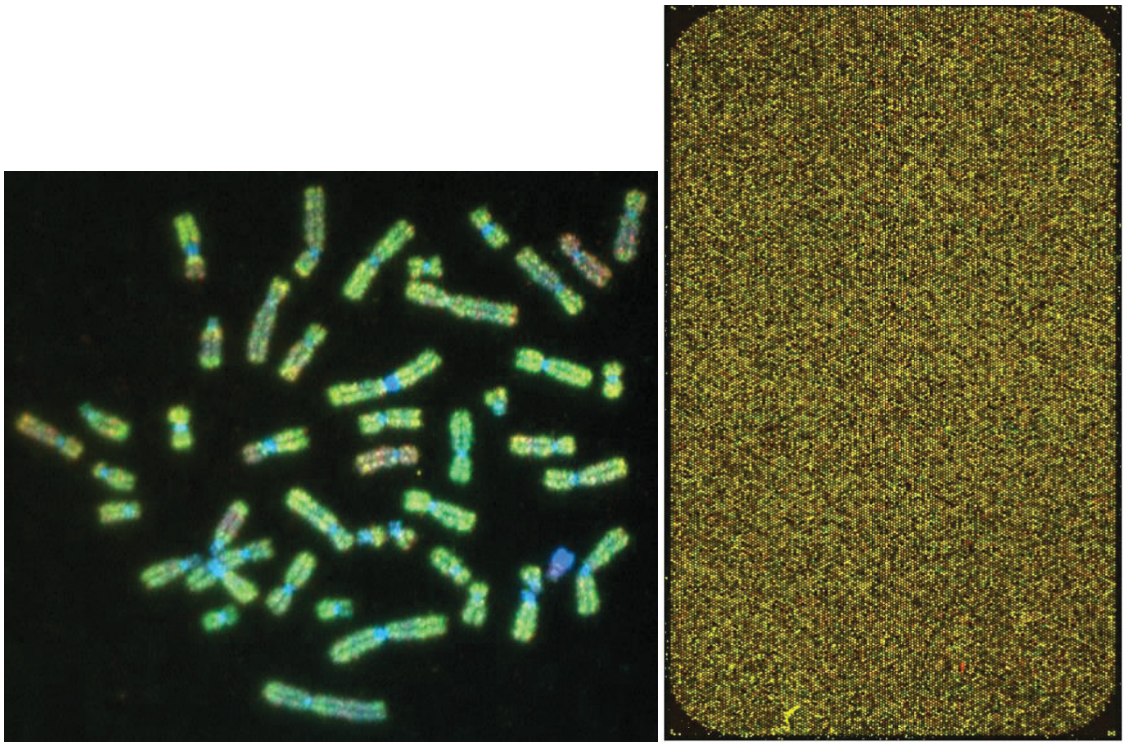

Figure 13: CGH on chromosomes (left) or on a microarray (right). Each dot on the microarray corresponds to one specific oligonucleotide sequence (gene sequence) spotted on the slide.

3.6.2 Procedure:

3.6.2.1 Isolation of genomic DNA:

DNA was isolated using the QIAamp DNA Blood Mini Kit (Qiagen) following the manufacturer's instructions.

3.6.2.2 Array CGH (aCGH):

aCGH was performed using 2x400K whole genome oligonucleotide-based arrays (Agilent Cancer Research Array + SNP, # G5956A). Labeling and hybridization procedures were performed according to the instructions provided by Agilent using the Sure-Tag DNA Labelling Kit and the "Agilent Oligonucleotide Array-Based CGH for Genomic DNA Analysis" protocol. Shortly**,** 500 ng of tumor DNA and reference DNA (human male genomic DNA, Promega) were digested with AluI and RsaI, then differentially labeled by random priming with Cyanine 5- and Cyanine 3-dUTP, respectively. After purification, the two labeled samples were mixed together with Blocking Agents, Hybridization Buffer (Oligo aCGH/Chip-on-Chip Hybridization Kit, Agilent) and cot-DNA (Roche) and hybridized onto 4x44K oligonucleotide arrays. In case of indirect aCGH, the respective parental cell line was used as a reference DNA. Hybridization was carried out for 48 h at 67°C in a hybridization oven (Agilent). Afterwards, slides were washed according to the protocol and scanned with a G2600D Microarray Scanner (Agilent). Feature extraction and

data analysis were carried out using the Feature Extraction (version 10.7.3.1) and Agilent Genomic Workbench software (version 7), respectively.
In case of HCC827, HCC827/Erlo, HCC827/Gefi and HCC827/EPR cells direct aCGH was performed using human male genomic DNA as a reference. In case of HCC827/ErloCrizo and HCC827/Erlo+Crizo cells, indirect aCGH was performed using HCC827/Erlo as a reference.

3.7 Expression array

3.7.1 Theoretical background:

Whole genome gene expression array is performed for determining genome-wide mRNA expression patterns as well as characterizing gene expression alterations between e.g. drug-resistant cancer cell lines in comparison to sensitive cells.

3.7.2 Procedure:

The cells were seeded in 6 well plates at a comparable density. After 48-hour incubation at 37 °C, RNA isolation was performed using the RNeasy Mini Kit (Qiagen). From each sample, at least two or three biological replicates were isolated for microarray analysis.

3.7.3 RNA Isolation

Cells were put on ice. The medium was removed, and cells were washed with 4ml cold PBS and lysed using 300µl Buffer RLT per well. Cells were scratched, and lysates collected in 1.5 ml tubes. Next, cells were homogenized 5x by a needle and syringe. Afterwards, 1 volume of 70% ethanol was added, the lysate was mixed by pipetting, and everything was transformed into a spin column. Washing and RNA elution steps were performed according to the protocol provided by Qiagen. The quantity of RNAs was measured on a Nanodrop. Samples were stored at -80°C.

3.7.4 Determination of RNA quality:

The quality of RNA samples was determined on an Agilent 2100 Bioanalyzer with the Agilent RNA 6000 Nano Kit (both from Agilent). Only samples with an RNA integrity number (RIN) between 9 and 10 were used for further microarray analysis.

3.7.5 Labeling and hybridization procedure:

Gene expression arrays were performed using 4x44K (v2) whole genome oligonucleotide-based gene expression arrays (Agilent, # G4845A). Labeling and hybridization procedures were exactly performed according to the instructions provided by Agilent (Two-Color Microarray-Based Gene Expression Analysis Protocol) using the Quick Amp Labeling Kit and the. Shortly, in a first step

250ng (for two-color experiments) of total RNA were converted into cDNA using a T7 promoter primer. In a second labeling and amplification step, cDNA was converted into cRNA. After purification of labeled cRNA with the RNeasy Mini Kit (Qiagen), 825ng Cy5- and 825ng Cy3-labeled cRNA were incubated for 30 minutes at 60 °C (heat fragmentation). Hybridization was carried out for 17 h at 65 °C in a hybridization oven (Agilent). Afterwards, slides were washed according to the protocol and scanned with a G2505B MicroArray Scanner (Agilent).

Feature extraction and data analysis were carried out using the Feature Extraction and Gene Spring software, respectively.

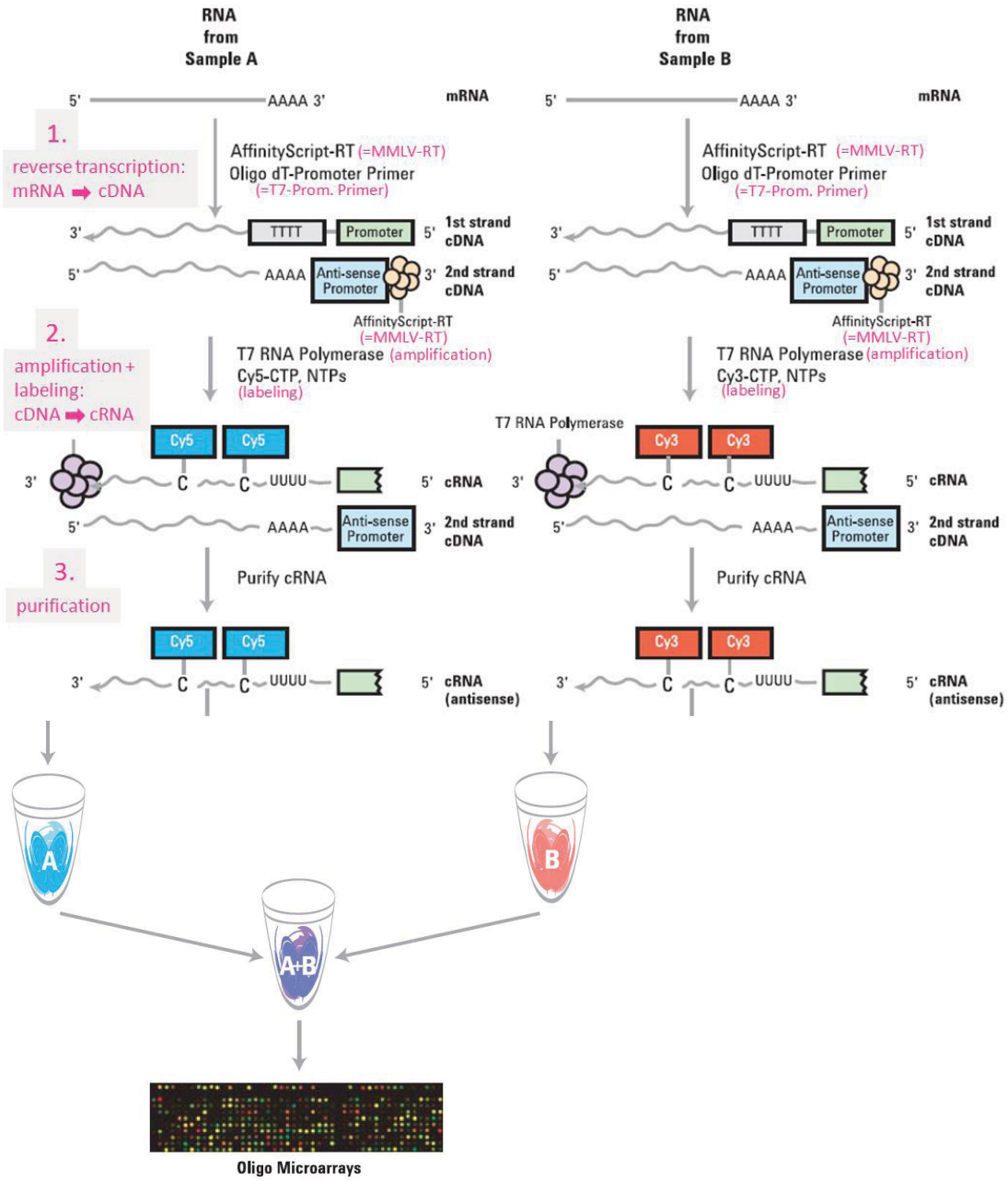

Figure 14: The schematic procedure of the Agilent two-color protocol

3.8 Gene transfer Via Lipofectamine:

3.8.1 Theoretical background:

Lipofectamine is used as a transfection reagent to increase the efficiency of RNA (mRNA or siRNA) or DNA plasmid transfection. It is a cationic-based reagent.

Positively charged nitrogen atoms play a key role in this context. In fact, they allow interactions between the transfection reagent and the negatively charged sugar-phosphate backbone of nucleic acid molecules. Considering that positively charged head group can contain one or more positively charged nitrogen atoms, enables transfection with higher efficiency.

The positive charge on the surface of the liposome generates an electrostatic interaction with nucleic acids and facilitates contact with the negatively charged cell membrane. The neutral co-lipid mediates fusion of the liposome with the cell membrane affecting the entry of the nucleic acid. To achieve expression of the transgene, DNA must reach the nucleus of the cell and become accessible to the transcriptional machinery. In actively dividing cells, transfected DNA may simply become trapped in the nucleus following the reassembly of the nuclear envelope at the end of mitosis

3.8.2 Procedure:

To establish an ABCB1 overexpressing cell model, HCC827 cells were transfected with a YFP-ABCB1 overexpressing (Figure 15) and eGFP plasmid separately. Lipofectamine R 2000 (Thermo Fischer) was used to transfer the related gene of interest (ABCB1& eGFP as control). $5x10^5$ HCC827, as well as PC9 cells, were seeded into 6 well plates (1ml per well). After 24 hours incubation at 37°C, the media was removed, and 1.5 ml fresh media was added to each well. 10 µl lipofectamine 2000 mixed with 240 µl RPMI (without serum) was incubated for 20 minutes on ice.2µg/500µl Plasmid DNA was added to lipofectamine and the whole mixture was added to each well. After 24 hours incubation at 37°C, media was refreshed.

YFP-ABCB1 and eGFP transfected cells were selected by treating with 100 µg/ml hygromycin and geneticin respectively as

ABCB1 overexpressing plasmid the hygromycin resistance gene, transfected cells were afterwards selected by treatment with 100 µg/ml hygromycin.

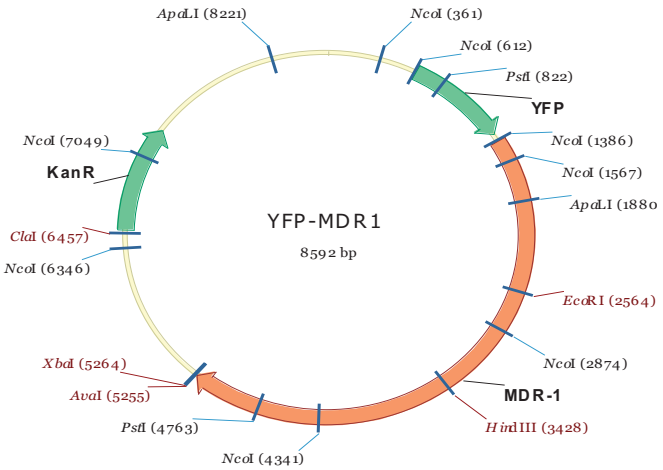

Figure 15: YFP-ABCB1 Vector scheme including single-cutting sites (in brown) and other restriction enzyme sites (in black).

3.9 In vivo xenograft mouse model:

To create the tumor xenograft mouse models, *BALB/c Nude Mice* (5-6 weeks old) from *Charles River Laboratories International, Inc. were* used.

3.9.1 Procedure:

3.9.1.1 Inoculation:

To create the tumor xenograft mouse models 1-5x10^6 cells (depending on the cell line) were re-suspended in medium/PBS and inoculated in 100 µL medium/PBS/Matrigel. The inoculation was done subcutaneously into the left shoulder of the mouse. 10 mice were inoculated with one cell line to account for not growing tumors. Body weight (scale) and tumor volume (caliper rule) were checked biweekly. For calculating the tumor volume, the following equation was used:

$$Tumor\ Volume = \frac{Length \times Width^2}{2}$$

3.9.1.2 PET/MR measurements:

PET measurements were performed after the tumor reached a volume of ~250 mm³. As radiotracers ^{11}C-erlotinib and ^{18}F-Fluorodeoxyglucose (^{18}F-FDG) were used, each animal was undergone three, and in certain cases four, PET/MR measurements in total, where the first two PET measurements were on the same day. The third and fourth PET measurement was performed on the following day, to allow the animals to recover from anesthesia. ^{18}F-FDG and MR measurements were performed to localize the tumor and visualize possible metastases that might be already present.

Mice were anesthetized with isoflurane and laid on the pre-warmed MR torpedo. Body temperature and breathing rate were monitored continuously.

Mice tail veins were catheterized. T_1-weighted MR scan was performed for 15 minutes. Attenuation scan was performed further for 10 minutes using a ^{57}Co point source.^{11}C-erlotinib was injected via the tail vein catheter within 1 min and dynamic emission scan was started afterwards for 90-120 min
Flush with 20 IE/ml Heparin in NaCl physiologic over 30 sec
After the first emission scan inject ^{18}F-FDG via the tail vein catheter within 1 min and start a 30-60 min dynamic emission scan
20 IE/mL Heparin in NaCl Phys. was flushed in the vein for more than 30 seconds.
After the second emission scan, blood samples (retrobulbar) were taken and the animals could recover from the anesthesia. Radioactivity was measured in whole blood and plasma samples in the gamma counter (Figure 16).

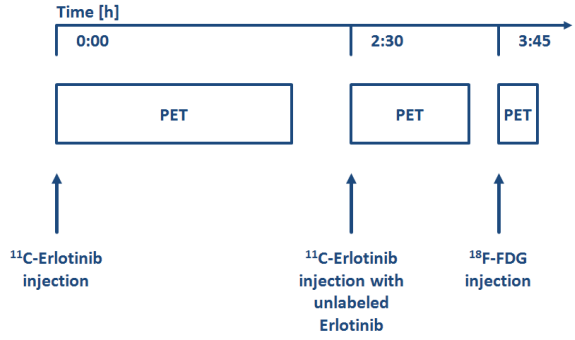

Figure 16: study design

3.9.2 Animals

Female BALB/c nude CAnN.Cg-Foxn1^{nu}/Crl mice (Charles River, Sulzfeld, Germany) aged 10–13 weeks, weighing 17.5–21.5 g, were housed in Markolon type 2 filter-top cages (6 mice per cage) under controlled environmental conditions (24±2°C, 40–70% humidity, 12-h light/dark cycle). An acclimatization period of >1 week was allowed before the animals were used in the experiments. A-431, HCC827, HCC827$_{EPR}$, and HCC827$_{ERLO}$ cells were harvested and re-suspended in serum-free RPMI-1640 medium, and 5–6×10^6 cells were subcutaneously injected into the right upper flank. When tumors had grown to a size of approximately 100 mm^3, the animals underwent PET imaging. All animal experiments were approved by the national authorities (Amt der Niederösterreichischen Landesregierung) and all study procedures were performed in accordance with the European Communities Council Directive of September 22, 2010 (2010/63/EU).

3.9.3 Positron Emission Tomography (PET) Imaging:

PET is a nuclear imaging technique which is performed using radioactive molecules as a radiotracer. The Fluorodeoxyglucose (F-18 FDG) is an analog of glucose, which is used in most of the cases for performing PET scanning as a radiotracer. F-18 FDG is consumed (as a sugar molecule) by metabolically active cells in the body for providing energy. Accumulation of FDG seen on PET images indicates high metabolic activity in that area (as in tumors). This can help to recognize whether a tumor has metastasized to other areas of the body. Thus, the PET scan can help pinpoint the extent of cancer's spread and help identify areas for further treatment or monitoring. Low or no metabolic activity can indicate areas of reduced blood flow or blockages due to stroke or heart attacks.

Erlotinib is labeled with 11C (^{11}C-erlotinib). To investigate the accumulation of erlotinib in tumors and different organs in mouse, Pet imaging was performed using ^{11}C-erlotinib as a radiotracer (Figure 17). PET was also performed using FDG as a control for scanning.

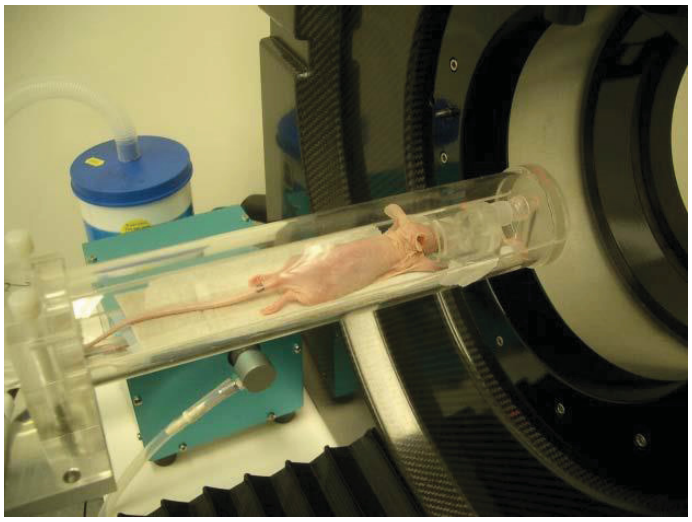

Figure 17: (PET) imaging set up used in this study

Prior to each experiment, the animals were placed in an induction box and anesthetized with 2.5% isoflurane. During the imaging period anesthesia was maintained with 1–2% isoflurane administered via a cone mask and the isoflurane level was adjusted depending on the depth of anesthesia. The respiratory rate and body temperature of the animals were constantly monitored during the data acquisition period. The animals were kept warm throughout the experiment at approximately 37°C. The animals were positioned in an imaging chamber and a lateral tail vein was cannulated for radiotracer administration.

For PET imaging a micro-PET Focus 220 scanner (Siemens Medical Solutions, Knoxville, TN) was used. Animals with A-431 tumors (n=3), HCC827 tumors

(n=4), HCC827/EPR tumors (n=5), and HCC827/Erlo tumors (n=4) underwent two consecutive dynamic PET scans with ^{11}C-erlotinib (injected activity 39±8 MBq for scan 1 and 27±9 MBq for scan 2). Scan 1 (120 min) was followed by scan 2 (60 min) in which unlabeled erlotinib (10 mg/kg) was co-administered with the radiotracer. At the end of scan 2, a static ^{18}F-FDG scan (20 min) was performed to facilitate the definition of tumor regions of interest (ROI).
For all groups, list-mode data were acquired for the defined time with an energy window of 250–750 keV and a 6 ns timing window. Before each PET scan, a transmission scan using a ^{57}Co point source was recorded for 10 min.
After completion of the imaging procedure, animals were killed by cervical dislocation while still under deep anesthesia. Tumors were excised and snap-frozen in liquid nitrogen Samples were stored at −80°C until further processing.

3.9.4 PET Data Analysis

The dynamic PET data were sorted into three-dimensional sinograms. Images were reconstructed using Fourier rebinning of the 3-D sinograms followed by two-dimensional filtered back-projection. The standard data correction protocol (normalization, decay correction, and injection decay correction) was applied to the data. Tumor ROIs were manually outlined over multiple planes in the static ^{18}F-FDG scans, muscle ROIs were outlined in the PET summation images (scan 1 and 2), and heart ROIS were outlined during the first 90 sec in the PET summation images (scan 1 and 2). ROIs were used to generate volumes of interest, which were then transferred to the PET images of the individual time frames. Time-activity curves (TAC), expressed as standardized uptake value (SUV= (radioactivity per cubic centimeter/injected radioactivity) x body weight), were calculated for each volume of interest. Furthermore, tumor-to-blood and muscle-to-blood ratios were calculated at 60 min after radiotracer injection.

4 Results:

First in vitro investigations were performed using four different cell models including parental HCC827 cells and its three EGFR TKI resistant sublines. HCC827 parental cells are were purchased from American Type Culture Collection (ATCC). HCC827/Erlo and HCC827/Gefi sublines were selected by treating the HCC827 parental cells with 20µM erlotinib and 20µM gefitinib, respectively. Selection of these cell lines was performed by Kushtrim Kryeziu. Besides that, HCC827/EPR subline was received from an international cooperation partner in Japan (Dr. Kenichi Suda, Kinki University, compare chapter 3.2.1).

4.1.1 The activity of EGFR inhibitors in HCC827 parental and EGFR TKI resistant sublines:

HCC827 and EGFR TKI selected sublines were treated with erlotinib (Figure 18). Erlotinib is categorized as a first-generation EGFR TKI. Generally, cell models harboring EGFR sensitizing mutation, e.g. L858R, in the tyrosine kinase domain are considered sensitive towards this compound (HCC827) [53]. Consequently, as expected the parental cell line was sensitive towards erlotinib. In contrast HCC827/Erlo, HCC827/Gefi and HCC827/EPR cells were resistant. HCC827/Erlo and HCC827/EPR, both selected with erlotinib, showed the highest levels of resistance (Figure 18).

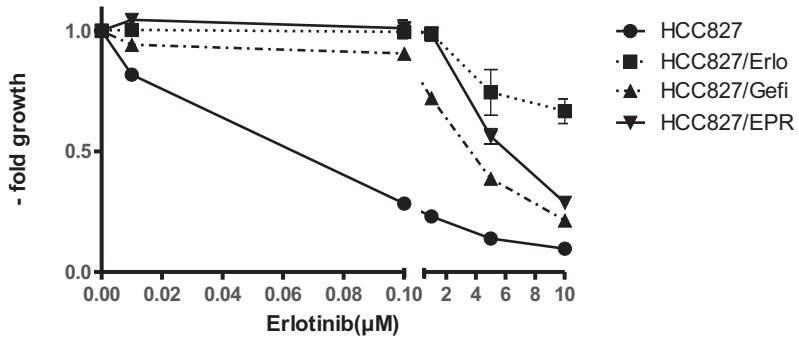

Figure 18: Sensitivity of HCC827 cell models towards erlotinib. Cells were seeded and after 24 h incubation, treated with the indicated concentrations of erlotinib for 72h.

To further investigate the mechanism underlying acquired erlotinib resistance, cells were treated with other EGFR TKIs, osimertinib and afatinib (Figure 19A and Figure 19B, respectively) and analyzed by viability assays (MTT).

Osimertinib (AZD9291) is a new third-generation EGFR TKI capable to inhibit EGFR harboring the resistance-causing T790M mutation, while cells with EGFR

sensitizing mutations only exhibit reduced but not completely lost sensitivity [51]. As Figure 19A indicates, HCC827, as well as HCC827/EPR cell models were sensitive against osimertinib. Highest sensitivity towards osimertinib was observed in the HCC827/EPR subline, proving the presence of T790M secondary mutation in this case. In contrast, HCC827/Erlo and HCC827/Gefi models were highly resistant against osimertinib, suggesting the involvement of other resistance mechanisms than the T790M mutation affecting also sensitivity against this third-generation EGFR inhibitor. This is in line with the results of earlier EGFR sequencing studies of the HCC827 cell models, where no secondary mutation could be detected in these two sublines.

Afatinib is an irreversible second-generation EGFR TKI that binds covalently to the ATP binding cassette of the EGFR tyrosine kinase domain. It inhibits EGFR in cells harboring sensitizing mutations regardless of secondary mutations [60]. Figure 19B shows that again HCC827, as well as HCC827/EPR cells, were sensitive, while HCC827/Erlo and HCC827/Gefi were highly resistant. This proved that EGFR TKI resistance is not caused by the presence of a secondary mutation in these cell models.

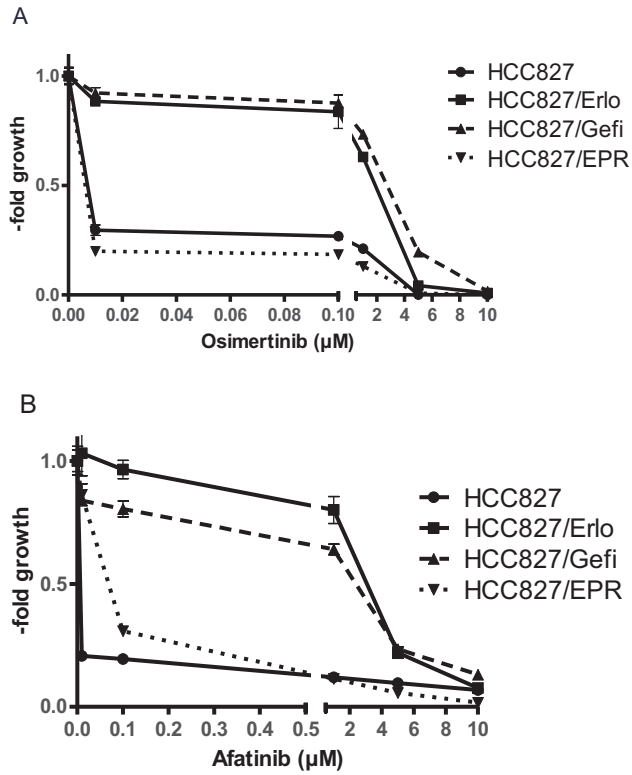

Figure 19: Sensitivity of HCC827 cell models towards osimertinib and afatinib. Cells were seeded and after 24 h incubation, treated with the indicated concentrations of (A) osimertinib and (B) afatinib for 72 h.

4.1.2 The activity of MET inhibitors in HCC827 parental and EGFR TKI resistant sublines:

It has been reported before, that activation of the MET pathway might play an important role in acquired EGFR TKI resistance [62]. To further analyze the role of MET activation and to investigate whether EGFR TKI resistance depends on it in our cell models, we next treated the cells with two MET-inhibitors PHA-665752 and crizotinib.

PHA-665752 is a selective small molecule c-MET inhibitor that strongly inhibits the tyrosine kinase domain of c-Met in comparison to other tyrosine or serine-threonine kinases [71].

Crizotinib is a c-MET/ALK inhibitor. Its function as a protein kinase inhibitor is due to competitive binding within the ATP-binding pocket of target kinases [72].

As shown in Figure 20, HCC827 and HCC827/EPR, as well as HCC827/Gefi and HCC827/Erlo cells, were all equally resistant towards both MET inhibitors, especially at lower concentrations. This suggested that HCC827/Erlo and HCC827/Gefi do not depend on MET pathway for their survival. However, both EGFR TKI resistant sublines generated in our group showed slightly reduced resistance at higher crizotinib concentrations as compared to the parental and HCC827/EPR cell model.

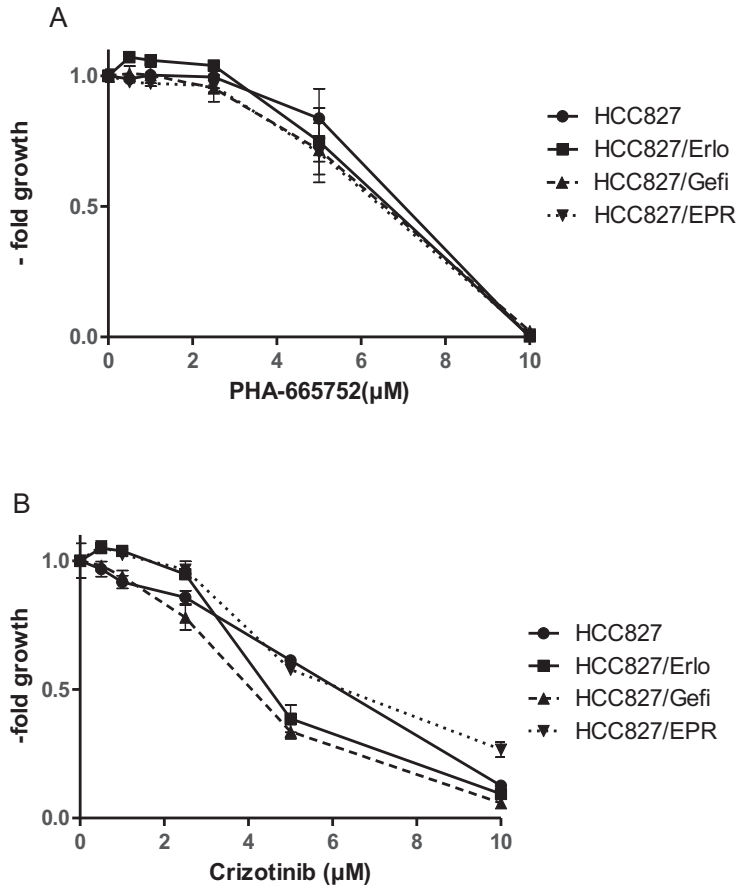

Figure 20 Sensitivity of HCC827 cell models towards PHA-665752 and crizotinib. Cells were seeded and after 24 h incubation, treated with the indicated concentrations of (A) PHA-665752 and (B) crizotinib for 72 h.

4.1.3 Combination treatment of EGFR and MET inhibitors in HCC827 parental and EGFR TKI-resistant sublines:

To test for the resensitizing effect of EGFR/MET inhibitors, we next treated the HCC827 cell models with erlotinib or osimertinib in combination with crizotinib (Figure 21 and Figure 22, respectively).

HCC827 cells were already highly sensitive towards erlotinib, and combination treatment with crizotinib did not result in a significant increase of cell sensitivity (Figure 21 A). In contrast, HCC827/Erlo cells were distinctly re-sensitized towards erlotinib upon inhibition of the MET pathway with crizotinib (Figure 21B). As shown in Figure 21 C, HCC827/Gefi cells were resistant towards erlotinib. When MET pathway was inhibited by crizotinib, cells became significantly re-sensitized towards erlotinib. Thus, in both HCC827/Erlo and HCC827/Gefi sublines a synergistic effect upon cotreatment of erlotinib and crizotinib was observed (Figure 21B and Figure 21C).

HCC827/EPR cells were resistant towards erlotinib as well as PHA and they also showed no significant increase in sensitivity upon combination treatment with

erlotinib and crizotinib (Figure 21D). In this experiment, they exhibited some sensitivity towards crizotinib, which contrasts to the experiment in Figure 20.

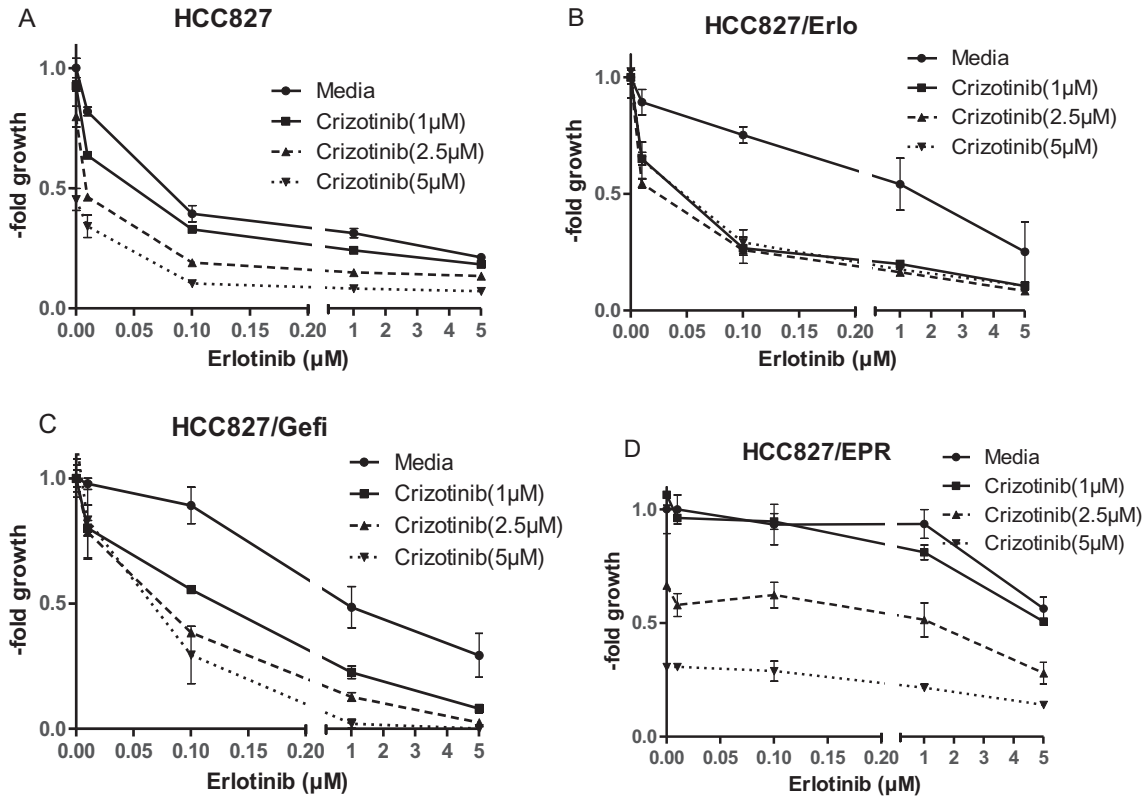

Figure 21: Viability assays of the indicated cell models treated with erlotinib in combination with crizotinib. Cells were seeded and after 24 h incubation, treated with the indicated drug concentrations for 72 h.

The same effects were observed upon combination treatment with osimertinib and crizotinib, except for HCC827/EPR cells, which showed high sensitivity towards osimertinib due to a secondary mutation.

Upon combination of osimertinib and crizotinib, high sensitivity for osimertinib and thus no significant re-sensitization in combination with crizotinib was seen for the parental and the HCC827/EPR cell model (Figure 22 A and D). In contrast, in HCC827/Erlo and HCC827/Gefi cells that were resistant to osimertinib, a strong resensitizing effect in the combination treatment was observed (Figure 22 B and C).

This suggests that MET pathway inhibition by crizotinib can re-sensitize HCC827/Erlo and HCC827/Gefi cells towards EGFR TKIs (Figure 21 B and C & Figure 22 B and C), indicating an important role of the MET pathway in acquired EGFR TKI resistance in the erlotinib and gefitinib-resistant sublines. However, simultaneous inhibition of both pathways is necessary to overcome acquired EGFR inhibitor resistance.

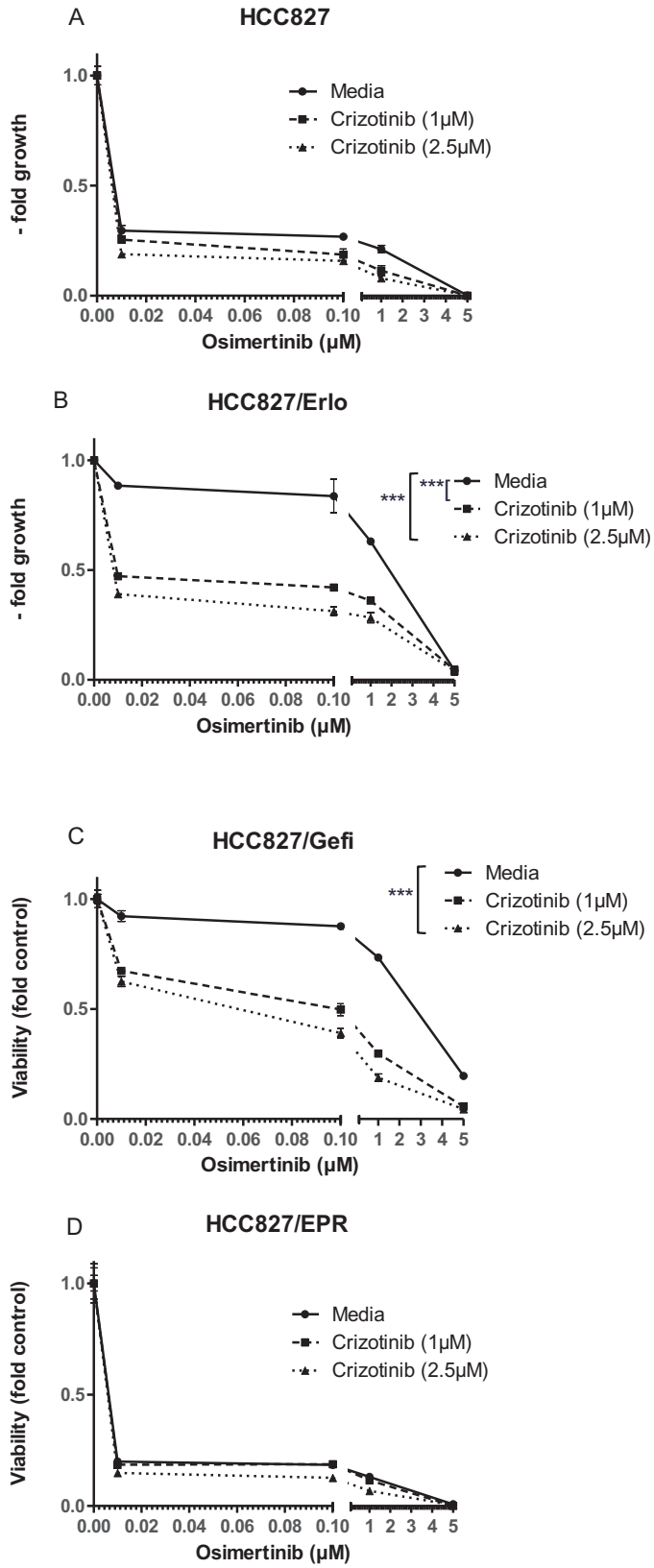

*Figure 22: Sensitivity of HCC827 cell models towards combination treatment with osimertinib and crizotinib. Cells were seeded and after 24 h incubations treated with the indicated concentrations of osimertinib and crizotinib for 72 h. *** indicates significance at p<0.05 by two-sided ANOVA*

Table 8 shows the IC_{50} values of different TKIs against HCC827 parental cell line as well as resistant cell models. HCC827/EPR cells were the most sensitive subline in comparison with HCC827, HCC827/Erlo, and HCC827/Gefi cell models.

Table 8: IC_{50} values of erlotinib, gefitinib, osimertinib, and crizotinib is calculated in different cell lines. n. a. stands for not analyzed.

	Erlotinib	Gefitinib	Osimertinib	Crizotinib
HCC827	0.165 ± 0.015	0.182 ± 0.004	0.145 ± 0.014	4.458 ± 0.250
HCC827/Erlo	> 10mM	n. a.	1.885 ± 0.029	>> 5µM
HCC827/Gefi	3.777 ± 0.644	> 10µM	2.736 ± 0.147	3.103 ± 0.768
HCC827/EPR	> 10µM	n. a.	0.129 ± 0.005	3.604 ± 0.268

4.1.4 Impact of combination treatment on signaling pathway activity:

In parallel, Western blots using total protein lysates of HCC827 and EGFR TKI resistant sublines were performed. Cells were exposed for 24 hours to the drugs (0.5 µM erlotinib, 0.5 µM crizotinib, as well as the combination) (Figure 23). Expression levels of EGFR, MET, AKT, and ERK, as well as the presence of their phosphorylated and, hence, activated forms were investigated.

Highest phosphorylation of EGFR (P-EGFR) was detected in HCC827, followed by HCC827/EPR, whereas it was undetectable in HCC827/Erlo and HCC827/Gefi cells. In contrast, P-MET was only detected in the HCC827/Erlo and HCC827/Gefi cell models. This data corresponds well with the viability assay data (Figure 21 A-D).

In HCC827 parental cells treated with erlotinib, P-EGFR, as well as p-Akt, was abolished. This was reflected by a high cell death rate (observed under the microscope). Upon inhibition of the MET pathway by treating the cells with crizotinib, cells were obviously able to survive via the EGFR pathway (signals for P-EGFR, P-ERK, and P-AKT were readily detectable). In case of combination treatment with erlotinib and crizotinib, cells again underwent cell death, and phosphorylation of EGFR and MET together with activation of the respective downstream cascades (measured as P-ERK and P-Akt) were completely abolished (Figure 23).

Both, the strong EGFR phosphorylation in the parental cell line, as well as the very weak one in the HCC827/Erlo and HCC827/Gefi cell models, had completely disappeared upon treatment with erlotinib. However, these two sublines showed phosphorylation of MET together with ERK and AKT, suggesting cell survival via activation of MET pathway.

As a result of MET pathway inhibition by crizotinib single treatment, P-MET vanished in HCC827/Erlo and HCC827/Gefi sublines, whereas P-ERK, as well as

P-AKT, was still detectable. Although some cells still survived, cell viability was decreased as compared to the parental cells (compare Figure 20).
Only concomitant inhibition of EGFR and MET pathway resulted in complete EGFR, MET, ERK, AKT phosphorylation inhibition, again accompanied by cell death induction as confirmed by the viability analyses (compare Figure 21).
Whereas MET expression was nearly absent or rather low in the HCC827 parental cells, both the HCC827/Erlo and HCC827/Gefi models expressed moderate to high levels of MET. In addition, in these two sublines also the activated P-MET could be detected which was totally absent in the HCC827 parent and HCC827/EPR subline. In the HCC827/EPR cells, as expected, neither inhibition of EGFR nor MET pathway resulted in cell death. This was observed also for the combination treatment, again in accordance with the MTT data (Figure 21 D).

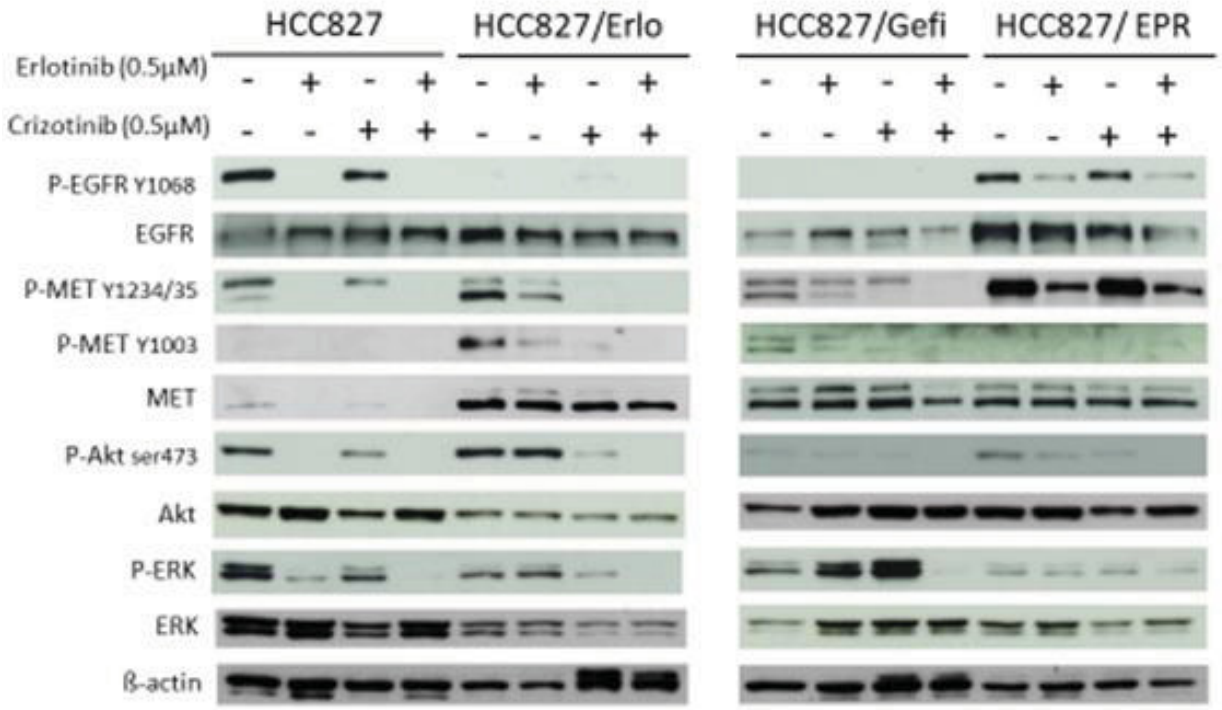

Figure 23: Western blot analysis of total protein lysates of HCC827 and EGFR –TKI resistant sublines. EGFR, MET, AKT, ERK as well as their phosphorylated (activated) forms and ß-actin were investigated in different cell models. ß-actin was served as a loading control. Cells were treated with 0.5mM erlotinib, as well as 0.5µM crizotinib as a single treatment and in combination for 72 hrs. The ß-actin level was analyzed as a housekeeping gene, to control whether comparable amounts of proteins were loaded in each slot.

4.1.5 EGFR and MET gene dose alterations in HCC827 and EGFR TKI resistant sublines:

Array CGH was performed in order to investigate genome-wide gene dose alterations in HCC827 and EGFR TKI-resistant sublines. Figure 24 shows an overview of genome-wide changes in all cell models.

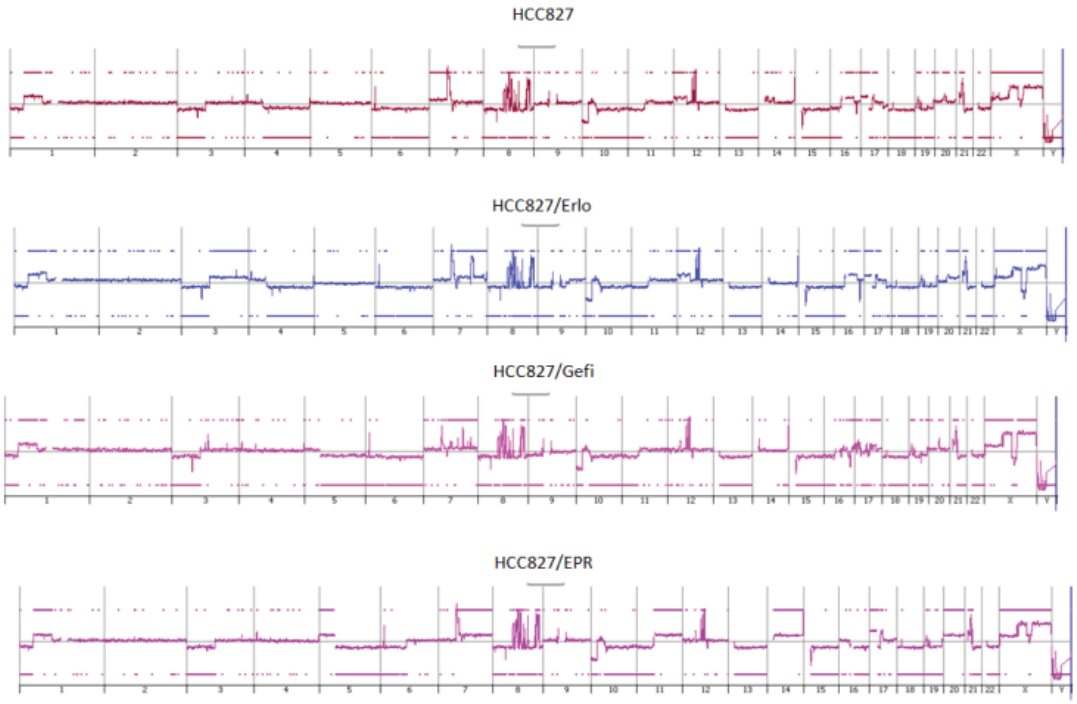

Figure 24: genome-wide gains and losses of HCC827 and EGFR TKI-resistant sublines.

In HCC827 parental and HCC827/EPR cells, a high-level amplification at chromosome 7p12 including the EGFR locus was detected. This EGFR amplification was also present in the HCC827/Erlo and HCC827/Gefi resistant sublines, however, at reduced levels with lowest values detected for the HCC827/Gefi subline (Figure 25 and Table 9).

During selection with EGFR TKI, both HCC827/Erlo and HCC827/Gefi developed a new amplification at chromosome 7q31 including the MET locus. This amplification was detected neither in HCC827 nor in HCC827/EPR cells (Figure 24, Figure 25 and Table 9). With regard to the structure, the amplicon spanned a wider region in HCC827/Erlo as compared to HCC827/Gefi, which harbored a focal high-level amplification of MET (Figure 25). Mean $\log_2$ ratios of EGFR and MET gene dose values investigated by array CGH are shown in Table 9.

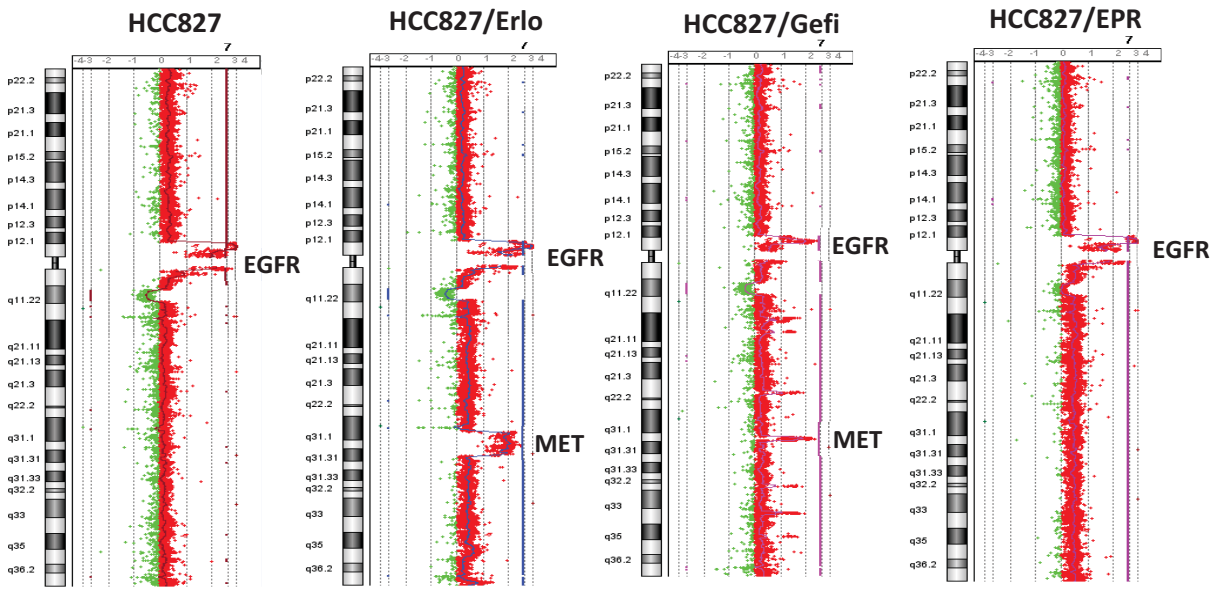

Figure 25: array CGH analyses depicting the profiles of chromosome 7 of HCC827 and EGFR TKI resistant sublines. All cell models show amplification of EGFR on 7p12. HCC827/Erlo and HCC827/Gefi sublines also harbor an additional amplification of MET on 7q31.

Table 9: Mean log_2 ratios of oligonucleotides for EGFR (n=201) and MET (n=140) in HCC827 and EGFR-TKI resistant cell lines investigated by array CGH.

	HCC827	HCC827/Erlo	HCC827/Gefi	HCC827/EPR
EGFR	4.76999223	3.851336308	2.071280567	4.680570848
MET	0.239267007	2.003693648	2.009496615	0.551784607

4.1.6 FISH analysis of EGFR and MET gene loci

In addition to array CGH, FISH experiments using locus-specific probes for EGFR and MET together with centromere 7 probes were performed. EGFR and MET loci were labeled with fluorescent dye in red (Texas Red for EGFR and Spectrum Red for MET), and centromere 7 in green (FITC or Spectrum Green) (see materials and methods).

EGFR amplification was readily detected in all 4 cell models in metaphase chromosomes as well as interphase nuclei. The amplicon was located on a marker chromosome, with a "caterpillar look", showing numerous consecutive copies of EGFR and centromere 7. In addition, also chromosomes with single copies of EGFR and centromere 7 were detected (Figure 26). Upon counting of interphase nuclei with or without EGFR amplification, a slightly reduced percentage of nuclei with EGFR amplicon in the HCC827/Erlo and HCC827/Gefi sublines were detected, corresponding to the array CGH results.

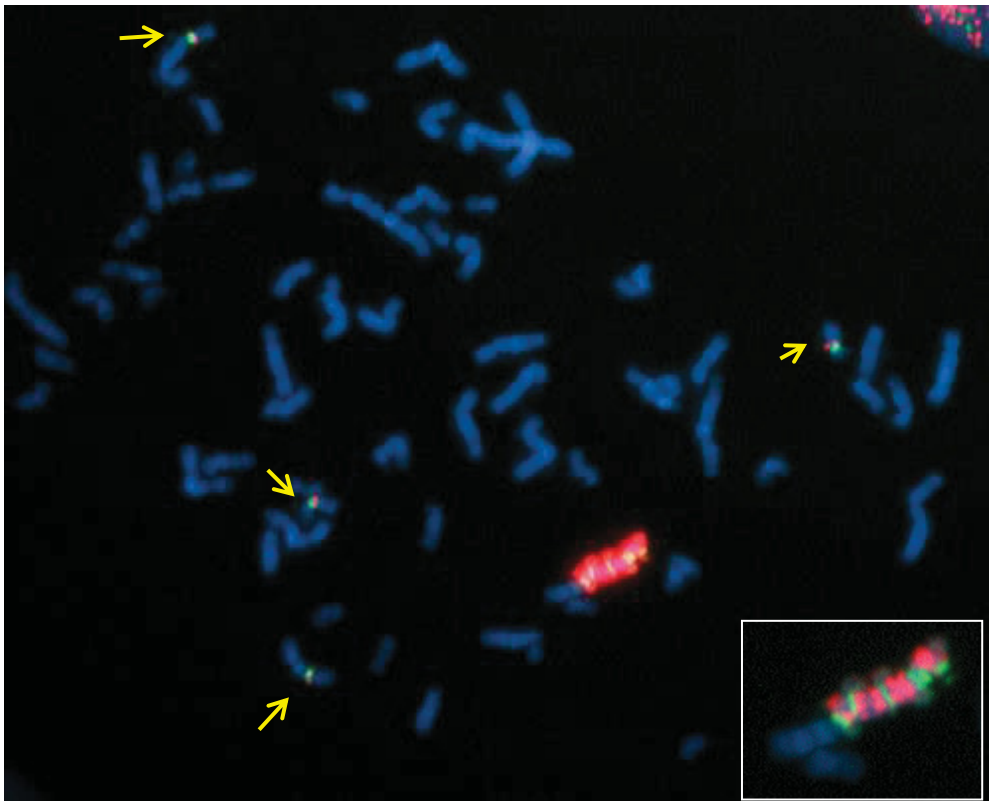

Figure 26: FISH of HCC827 parental cell line for EGFR (red) and centromere 7 (green) detects a huge amplicon as well as several single copies.

Another FISH experiment was performed to label the MET gene locus. MET amplification was observed in the HCC827/Erlo and HCC827/Gefi sublines (Figure 27 & Figure 28), but not in the parental and HCC827/EPR cell lines. In case of HCC827/Erlo, a complex re-arrangement including several times numerous consecutive MET copies together with centromere 7 was observed (Figure 27). In the HCC827/Gefi cells MET amplification was present in form of a homogeneously staining region (HSR) located either on a chromosome or separately, (probably as acentric chromosome fragment) (Figure 28). These data correspond again to the amplified regions of 7q detected by array CGH (Figure 25).

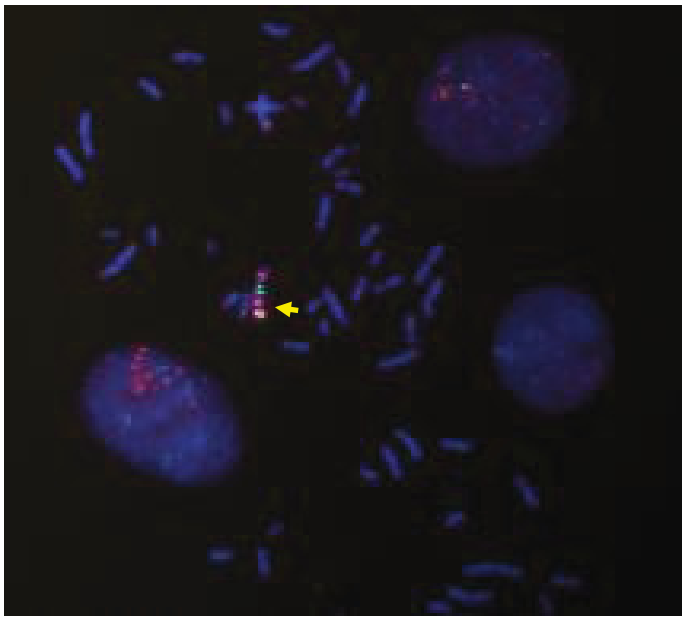

Figure 27: FISH shows the amplification of MET in HCC827/Erlo resistant subline. MET is labeled in red and centromere 7 in green. Amplification is marked by a yellow arrow.

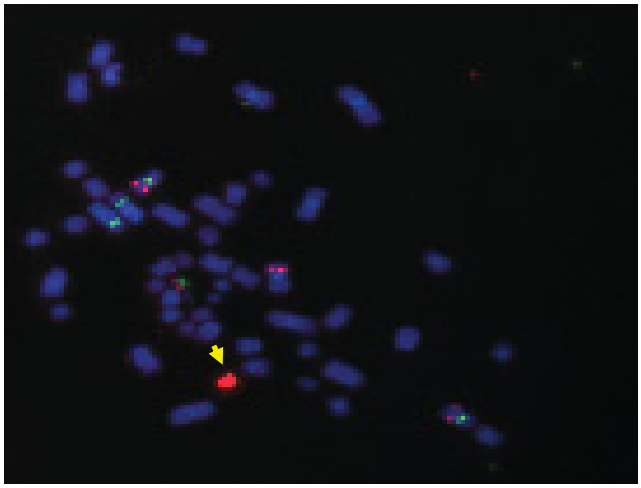

Figure 28: FISH shows MET amplification in the HCC827/Gefi cell line. MET is labeled in red and centromere 7 in green. Amplification is marked by a yellow arrow.

4.1.7 Whole genome gene expression arrays (mRNA microarrays) of the HCC827 and EGFR- TKI- resistant sublines:

In addition to aCGH, whole genome gene expression arrays were performed to investigate genome-wide alterations at the mRNA expression level in HCC827 and the EGFR inhibitor-resistant sublines.

Figure 29 shows normalized values of EGFR as well as MET mRNA levels in different cell models. The mRNA expression levels of EGFR and MET corresponded to gene dose alterations detected by array CGH and FISH.

The highest level of EGFR expression was again observed in the HCC827 parental cell line, while it was decreased in the resistant sublines. Again, EGFR displayed the lowest expression level in the HCC827/Gefi subline.

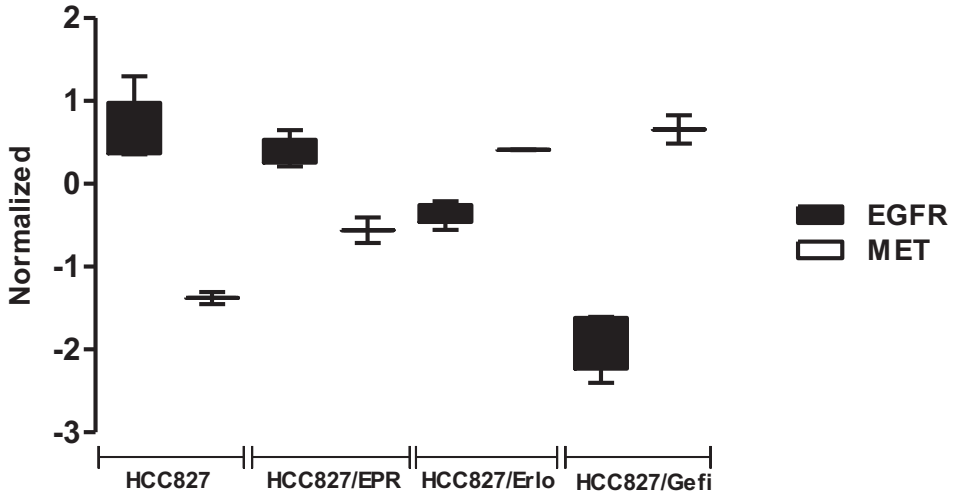

Figure 29: mRNA expression array data for EGFR and MET in HCC827, HCC827/Erlo, HCC827/Gefi, and HCC827/EPR resistant sublines.

4.1.8 Altered mRNA and protein expression of other RTKs:

Next, we looked for mRNA changes of other RTKs in the EGFR TKI- resistant sublines as compared to the parental line. Various receptors with distinct alterations were found. Genes/oligos that showed a more than 2×fold change in expression between either of the sublines in comparison to the HCC827 parental cell line are shown in Table 10, Table 11 and Table 12.

In addition to MET, AXL, and FGFR1 were upregulated in HCC827/Erlo subline in comparison to HCC827 parental cell line. HCC827/Gefi cells showed in addition to lower EGFR mRNA expression, upregulation of MET and FGFRL1 expressions at mRNA level in comparison to HCC827 cells (Table 11). EPHA4, INSR, and KIT were upregulated in HCC827/EPR cells in comparison to HCC827 cells (Table 12).

For confirmation of mRNA data, AXL and FGFR1 expression levels in HCC827 and EGFR TKI- resistant sublines were investigated by Western blot. However, neither change in AXL nor FGFR1 expression was detected at the protein level. FGFR1 was below the detection limit in all of the cell lines. For AXL, a weak band could be detected in all cell models, however, showed no difference between the cell lines (data not shown). A potential role of AXL, as well as

FGFR1 in acquired resistance of HCC827, derived cell models was investigated in detail in another study performed by Dina Baier.

*Table 10: mRNAs/oligos of RTK-coding genes changed more than 2- fold in the HCC827/Erlo cells as compared to the HCC827 parental cell line. * indicates significance at p-value<0.05.*

Gene Symbol	Regulation ([HCC/Erlo] vs. [HCC]) *	FC ([HCC/Erlo] vs. [HCC]) *
AXL	Up	6.475299
FGFR1	Up	3.5553048
FGFR1	Up	5.5289683
MET	Up	3.4598832
DDR1	Down	-2.0351572
EGFR	Down	-2.8249536

*Table 11: mRNAs/oligos of RTK-coding genes changed more than 2- fold in the HCC827/Gefi cells as compared to the HCC827 parental cell line. *indicates significance at p-value<0.05.*

Gene Symbol	Regulation ([HCC/Gefi] vs. [HCC]) *	FC ([HCC/Gefi] vs. [HCC]) *
MET	Up	4.099865
FGFRL1	Up	2.2482095
EGFR	Down	-6.286855
EGFR	Down	-7.7401643
EGFR	Down	-5.2221737

*Table 12: mRNAs/oligos of RTK-coding genes changed more than 2- fold in the HCC827/EPR cells as compared to the HCC827 parental cell line. * indicates significance at p-value<0.05.*

Gene Symbol	Regulation ([HCC EPR] vs. [HCC]) *	FC ([HCC EPR] vs. [HCC]) *
EPHA4	Up	3.5271685
INSR	Up	2.20097
KIT	Up	54.976753
AXL	Down	-2.865051

*Up/down-regulated in the HCC827/TKI resistant subline as compared to the parental cell line. FC stands for fold change. Significant data was represented at p-value<0.05.

4.1.8.1 VENN diagram:

Gene expression data was further investigated using Venn diagram. Figure 30 shows the overlap of genes/oligonucleotides which differ between

HCC827/Erlo and HCC827/Gefi cells as compared to the parental cell models. The red circle represents 193 entities which differ between HCC827/Erlo and HCC827 parental cells.
All entities (432) altered in HCC827/Erlo subline in comparison to HCC827 subline was shown in blue.
There are only 58 overlapping genes that are altered in terms of mRNA expression in both HCC827/Erlo and HCC827/Gefi cells in comparison to the HCC827 cell model. This suggests that these two sublines acquired EGFR-TKI resistance by involving at least to some extent different molecular mechanisms reflected by the small portion of genes altered in common. This might be based on interaction of the two different EGFR inhibitors with other cellular targets or differing susceptibility against off-target resistance like drug efflux pumps (compare chapter 4.3 for ABC transporters) or metabolization processes.

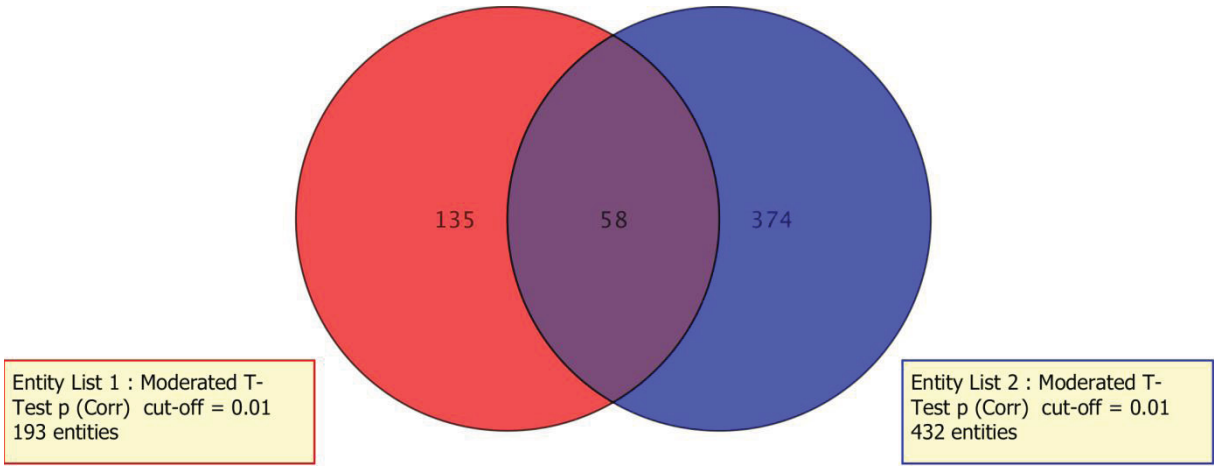

Figure 30: Venn diagram of HCC827 vs. HCC827/Erlo and HCC827 vs. HCC827/Gefi

HCC827/Erlo and HCC827/Gefi vs. HCC27 parental cell line IPA diagram including fold changes in the expression at RNA level.
Figure 31 and Figure 32 show schematic diagrams generated with the Ingenuity Pathway Analysis (IPA) software [73]. It shows expression level alterations of several genes as well as their interactions in HCC827/Erlo and HCC827/Gefi in comparison to HCC827 parental cell line respectively. Red and blue color indicate up and downregulations respectively.
MET is upregulated in HCC827/Erlo and HCC827/Gefi sublines (Shown in red) in comparison to HCC827 parental cells, whereas, FGFR2 is downregulated (Figure 31).

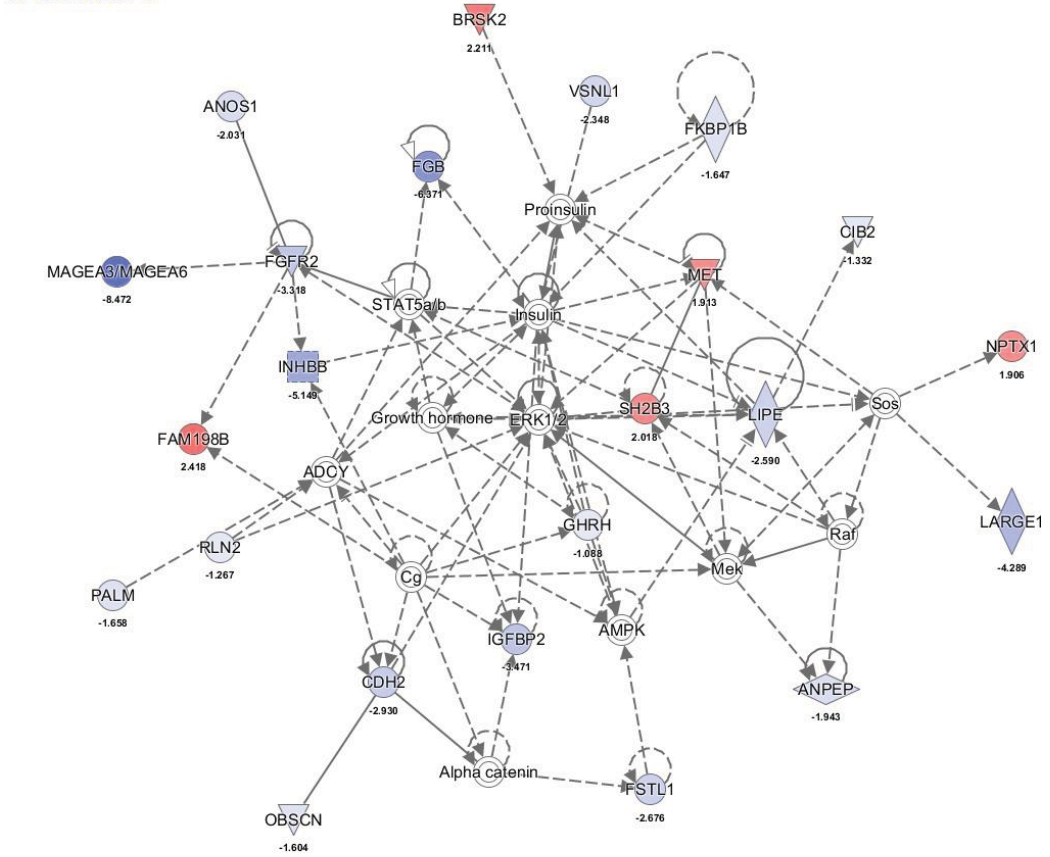

Figure 31: IPA diagram of HCC827/Erlo and HCC827/Gefi vs. HCC27 parental cell line

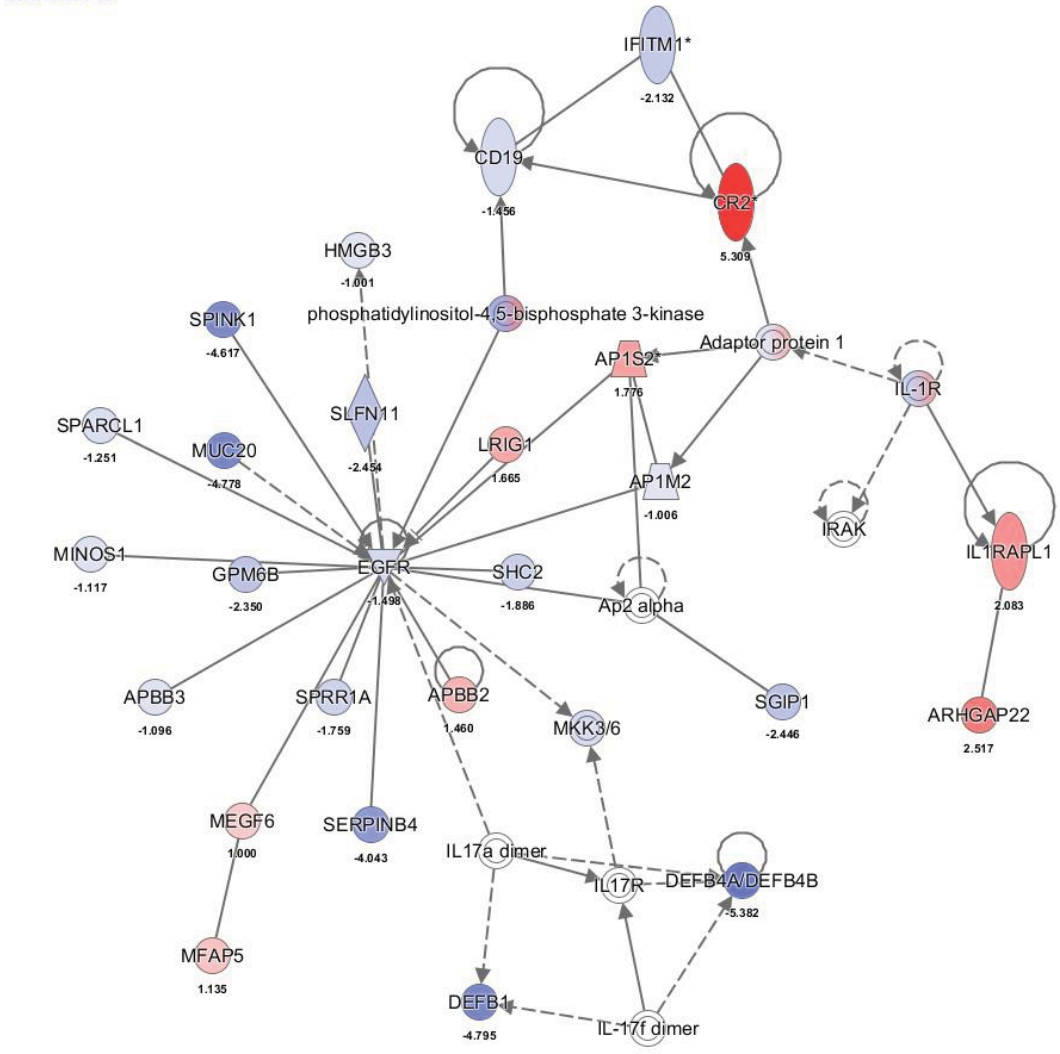

Figure 32: IPA diagram of HCC827/Erlo vs. HCC27 parental cell line

4.2 Generation of crizotinib-resistant sublines:

MET amplification was already suggested as the mechanism underlying resistance towards erlotinib and gefitinib [58, 62]. We were interested in the cross-talk between EGFR and MET. Therefore, selection for HCC827/Erlo and HCC827/Gefi cells was continued with crizotinib, either alone or in combination with the respective EGFR TKI (Table 3, Figure 8 and Figure 9).

4.2.1 The sensitivity of HCC827/Erlo-derived, double-selected sublines towards erlotinib and crizotinib:

HCC827, HCC827/Erlo, HCC827/ErloCrizo, and HCC827/Erlo+Crizo were treated with erlotinib and analyzed by cell viability assays (Figure 33 A). The resistant HCC827/Erlo and the sensitive parental HCC827 lines were included as controls. HCC827/ErloCrizo and HCC827/Erlo+Crizo both showed even higher resistance against erlotinib as compared to the HCC827/Erlo cell model.

HCC827, HCC827/Erlo as well as the crizotinib selected sublines were treated with different concentrations of crizotinib. All cell lines represented resistance against crizotinib (Figure 33 B). This led us to the conclusion that none of these cells had developed a dependency on c-MET-mediated signals for survival.

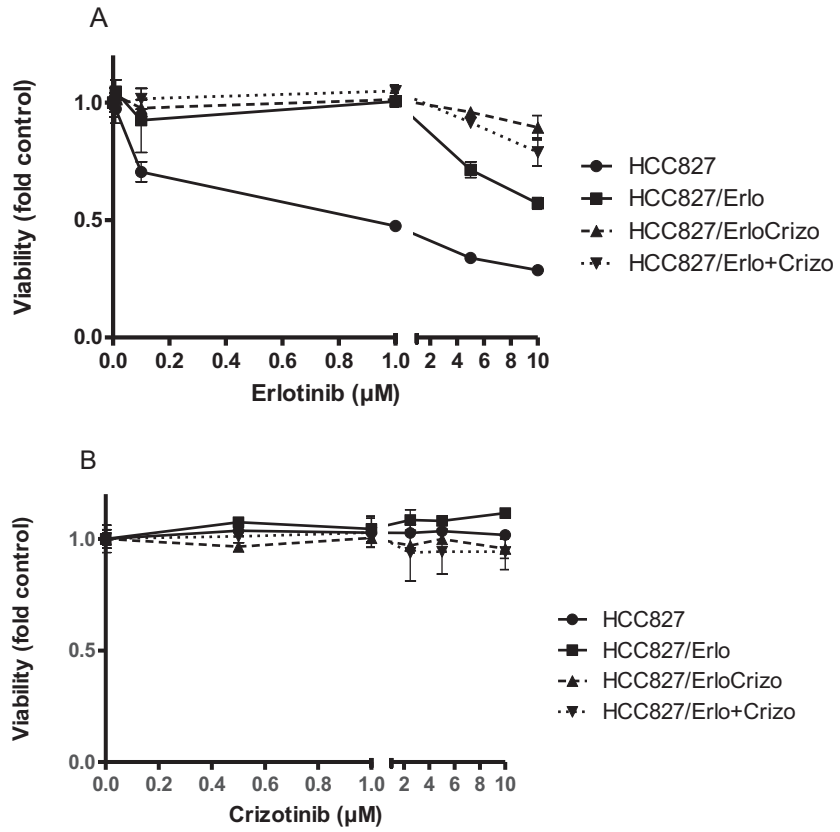

Figure 33: Viability assay of HCC827, HCC827/Erlo, HCC827/ErloCrizo, HCC827/Erlo+Crizo. (A) cells were treated with erlotinib or (B) crizotinib at the indicated concentrations.

Next, HCC827/Erlo and the crizotinib -selected derivatives were co-treated with erlotinib and crizotinib (Figure 34). As shown before, all cells were resistant towards erlotinib (Figure 33 A). However, in the experiment shown in Figure 34, HCC827/Erlo cells were slightly sensitive against erlotinib. In our treatment scheme, HCC827/Erlo cells got erlotinib only 1x per month and became a bit sensitive again after 2 weeks hence, slightly re-gained sensitivity. Therefore, this graph reflects the time point after the last drug selection (Figure 34 A).
Upon combination treatment with crizotinib, HCC827/Erlo, as well as HCC827/ErloCrizo cells, became re-sensitized towards erlotinib and/or vice versa (Figure 34A and Figure 34B). However, HCC827/Erlo+Crizo cells stayed highly resistant even to the combination of both drugs. This indicates a newly acquired resistance mechanism in HCC827/Erlo+Crizo cells (Figure 34 C, no IC_{50} value could be reached, see also Table 8).

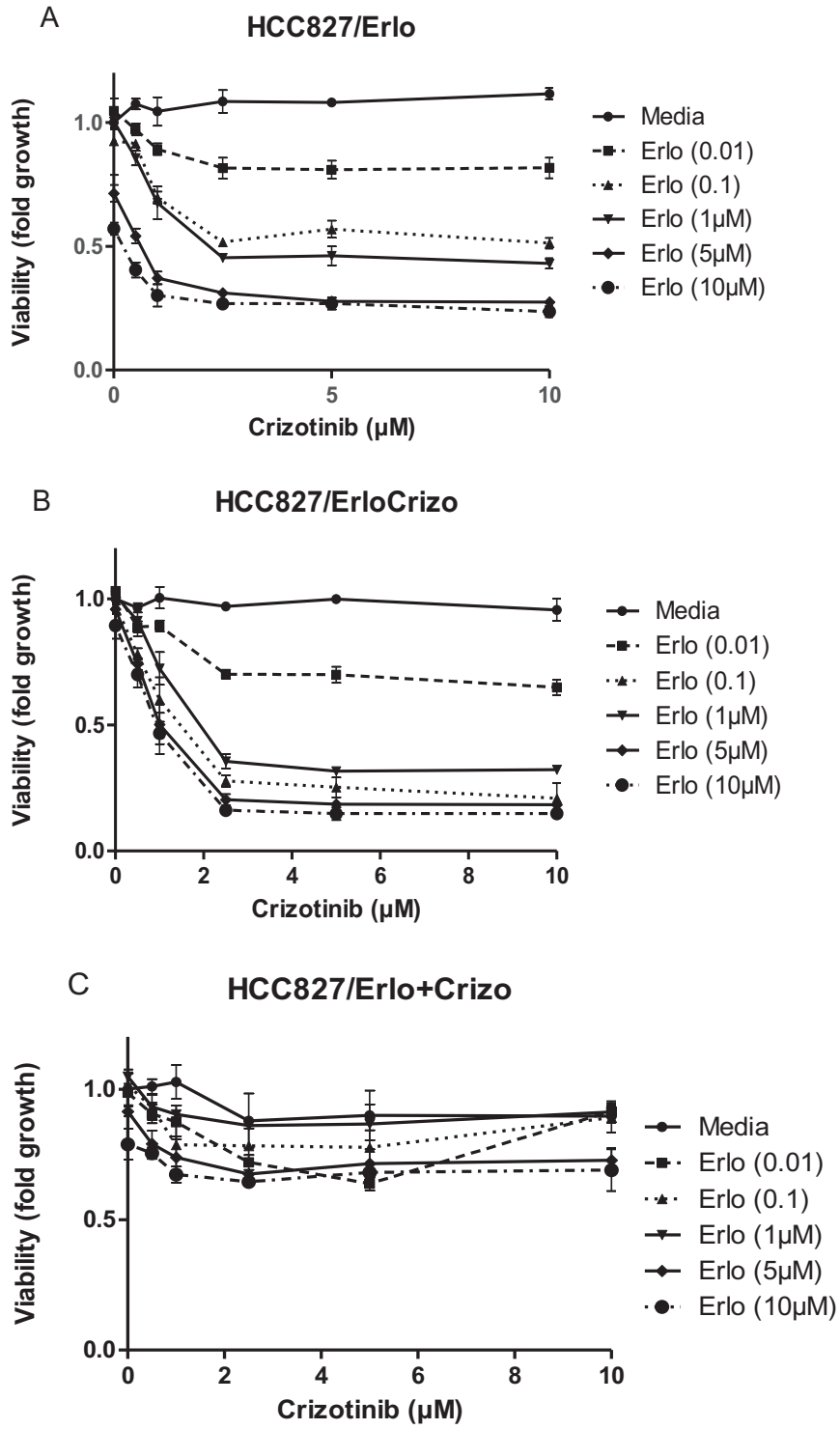

Figure 34: HCC827/Erlo and the crizotinib selected sublines were treated with erlotinib in combination with crizotinib. A, B and C show viability assays of HCC827/Erlo, HCC827/ErloCrizo and HCC827/Erlo+Crizo respectively. Cells were treated with erlotinib and crizotinib, at the indicated concentration levels.

4.2.2 Osimertinib sensitivity in HCC827/Erlo and HCC827/Gefi-subfamilies:

In parallel, osimertinib sensitivity was investigated to indirectly check for the presence of the secondary T790M mutation as a mechanism responsible for the acquired resistance after combination treatment in the HCC827/Erlo+Crizo and HCC827/Gefi+Crizo cell lines (Figure 35 A and B). HCC827/EPR cells were used as a control for sensitivity.

For both EGFR-TKI-resistant families, the crizotinib selected sublines, as well as the respective parental cells, were resistant to osimertinib. Only HCC827/GefiCrizo cells showed slight sensitivity. However, this effect was not comparable to the high sensitivity observed for the HCC827/EPR model (Figure 35 and B).

Therefore, we concluded that in those sublines selected with both EGFR-TKI and crizotinib (HCC827/Erlo+Crizo and HCC827/Gefi+Crizo), the T790M mutation does not cause the resistance against combination treatment.

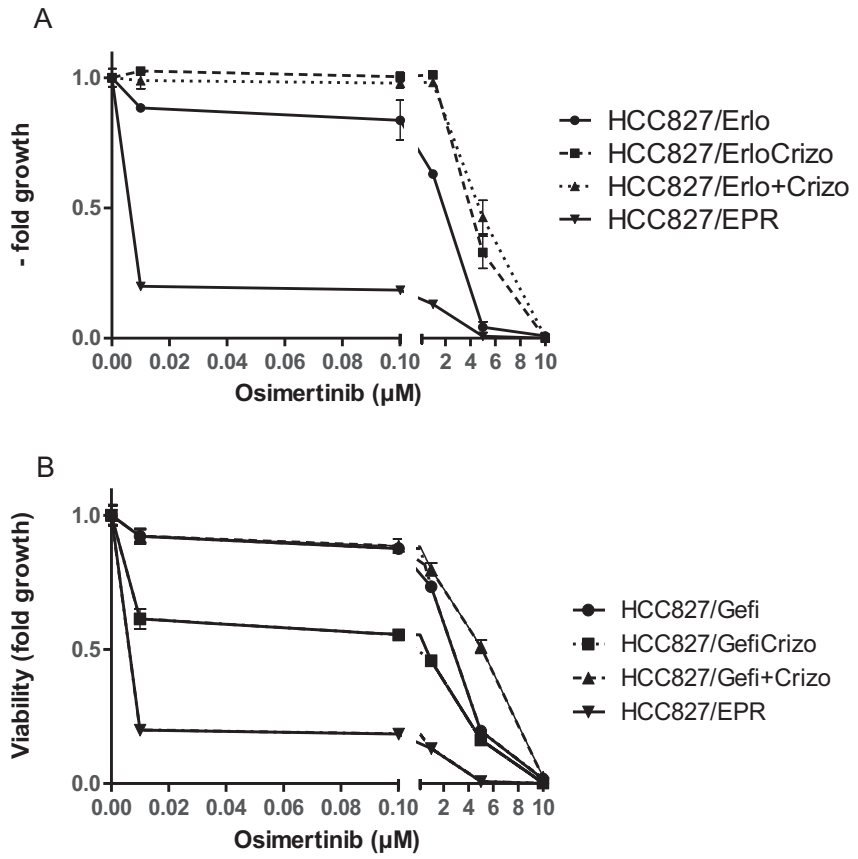

Figure 35: Osimertinib sensitivity of the (A) HCC827/Erlo- and (B) HCC827/Gefi-subfamily HCC827/EPR cells were included as positive control.

4.2.3 Analysis of protein lysates of HCC827/Erlo plus crizotinib selected sublines:

HCC827/Erlo and the two crizotinib selected sublines derived from HCC827/Erlo were treated with erlotinib and crizotinib (as single agents and in combination). After 72 h, cells were harvested, and total protein lysates were prepared and analyzed by Western blotting. Each cell line was treated in 4 different ways:

1. Control cells (only medium was added).
2. Cells treated with 0.5 µM erlotinib (single treatment)
3. Cells treated with 0.5 µM crizotinib (single treatment)
4. Cells co-treated with 0.5 µM erlotinib and 0.5 µM crizotinib (combination treatment)

As shown in Figure 36, HCC827/Erlo and HCC827/ErloCrizo cells had a higher level of total MET in comparison to and HCC827/Erlo+Crizo cells. MET phosphorylation of y1234/35 was detected only in the HCC827/Erlo cells, whereas it was downregulated in HCC827/ErloCrizo and completely undetectable in the in HCC827/Erlo+Crizo subline.

These results correspond well to data observed at DNA and mRNA level by array CGH and expression array, respectively (see next chapters).

In the HCC827/Erlo subline, EGFR phosphorylation was downregulated upon application of erlotinib. However, cells obviously survived via activation of the MET pathway (P-MET level was upregulated by erlotinib single treatment). Upon inhibition of the MET pathway by crizotinib, MET activation vanished and P-EGFR has upregulated again. Correspondingly, after a single treatment, AKT, as well as ERK phosphorylation levels could still be detected. In contrast, upon application of the combination (erlotinib and crizotinib) both P-AKT and P-ERK disappeared in HCC827/Erlo as well as HCC827/ErloCrizo cells, corresponding the cell death observed by MTT upon application of both drugs (Figure 34A and Figure 34B).

In HCC827/Erlo+Crizo cells downregulation of EGFR was observed. The level of total AKT, but not P-AKT, was distinctly upregulated in the HCC827/Erlo+Crizo cells in comparison to HCC827/Erlo and HCC827/ErloCrizo sublines. Both ERK expression and also phosphorylation were increased in the HCC827/Erlo+Crizo model. Interestingly, weak P-AKT and P-ERK levels were still seen upon combination treatment in the double-selected cell model, obviously enabling cell survival. This corresponds to the highly proliferative phenotype and again supports activation of a new TKI resistance activated in the in vitro cell culture model.

The ß-actin level was analyzed as a housekeeping gene, to control whether the same amount of proteins was loaded in each slot.

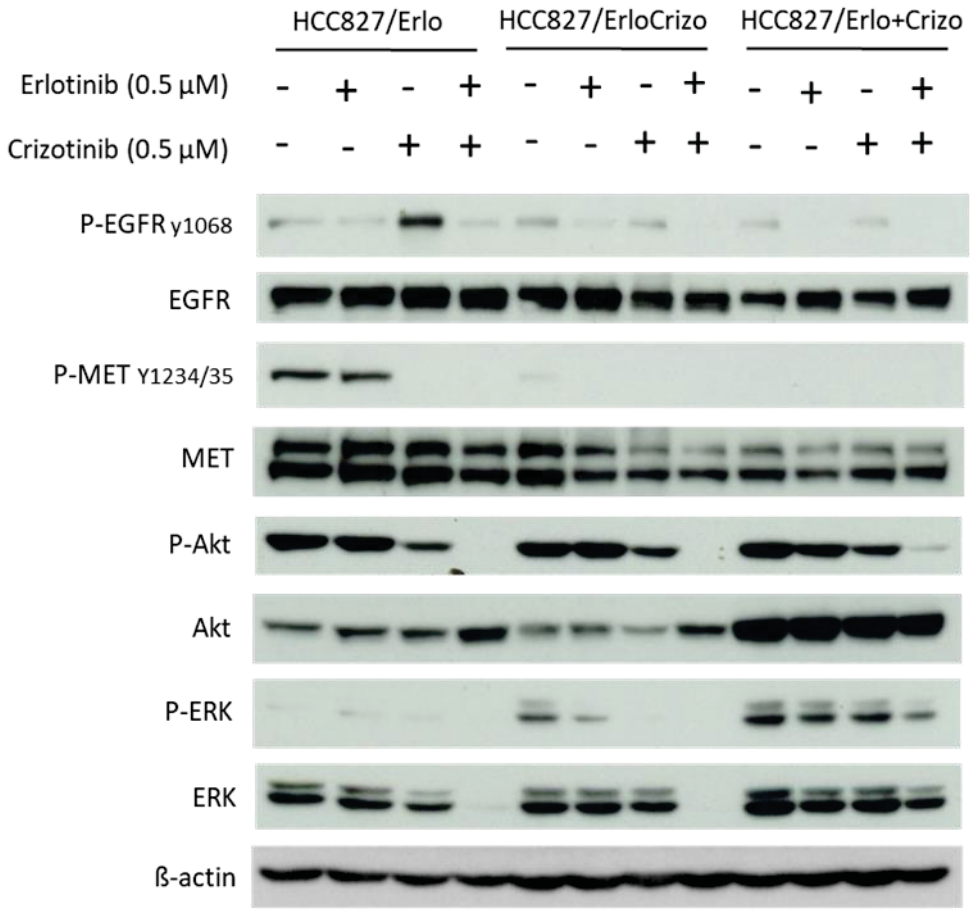

Figure 36: Analysis of total protein cell lysates of HCC827/Erlo, HCC827/ErloCrizo, and HCC827/Erlo+Crizo cell models. EGFR, MET, AKT, ERK, and the respective phosphorylated forms were investigated. ß-actin served as a loading control.

In contrast to the HCC827/Erlo sub-family, during the selection of sublines in vitro, the HCC827/Gefi sub-family showed greater variations in cell behavior and growth patterns, making interpretations of analyses and data difficult. The project of this thesis aimed to focus more on the HCC827/Erlo sub-family. Hence, the HCC827/Gefi sub-family was investigated in detail in another study performed by Dina Baier.

4.2.4 Array CGH analysis of the crizotinib-selected cell models:

Gene dose alterations were investigated in crizotinib-selected sublines by indirect array CGH, comparing crizotinib-selected sublines to their corresponding parental cell line.

For the parental HCC827/Erlo and HCC827/Gefi cell lines direct aCGH analysis had already been performed as described in 4.1.5 and 4.1.6. In this case, the tumor DNA was compared to a normal human male DNA sample.

4.2.5 EGFR and MET alterations in HCC827/Erlo-derived sublines:

Figure 37 shows genome-wide genomic changes (gains and losses) in HCC827/Erlo (direct CGH, upper panel) and changes between the respective crizotinib-selected sublines as compared to progenitor HCC827/Erlo cells (indirect CGH, middle and lower panel). Figure 38 represents log2 ratios of EGFR and MET gene dose alterations in HCC827/ErloCrizo and HCC827/Erlo+Crizo sublines as compared to the HCC827/Erlo subline.

Interestingly, HCC827/ErloCrizo cells selected with crizotinib gained back EGFR and lost MET gene copies. In contrast, HCC827/Erlo+Crizo cells, co-selected against EGFR-TKI and MET inhibitor, lost gene copies of both targets.

Moreover, we detected a new amplicon on the long arm of chromosome 17 (17q12) in the HCC827/Erlo+Crizo subline. This region harbored various interesting gene loci, among them SOCS7, which is involved in JAK/Stat signaling (Figure 39). This was also further investigated by mRNA gene expression array (chapter 4.2.6 Whole genome expression array).

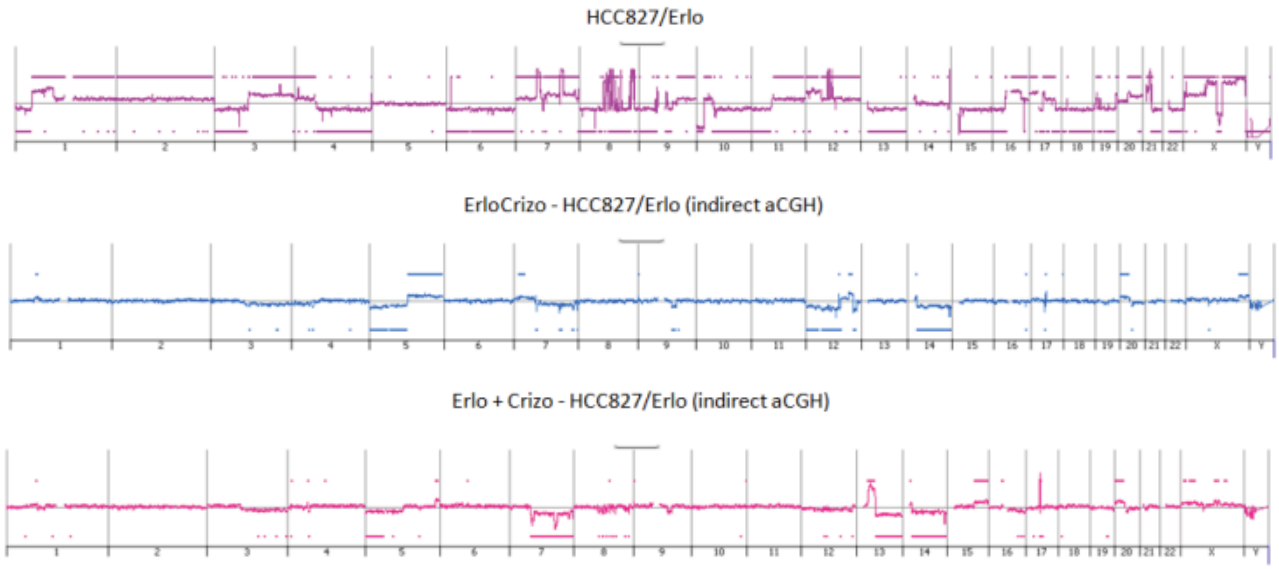

Figure 37: genome-wide gains and losses of HCC827/Erlo and Crizotinib-selected sublines. Genomic DNA of HCC827/Erlo cells was investigated by direct aCGH (compared to male Agilent DNA template) whereas, genomic DNA of HCC827/ErloCrizo and HCC827/Erlo+Crizo cells was investigated by indirect aCGH (compared to genomic DNA of HCC827/Erlo cells).

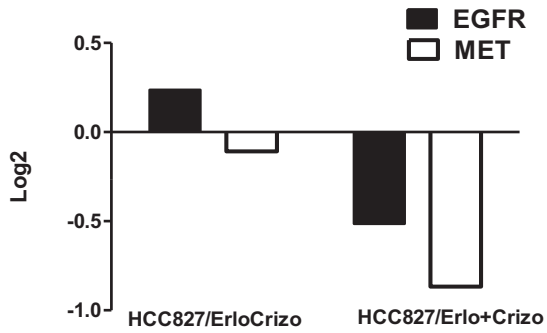

Figure 38: gene dose alterations of EGFR and MET in comparison to the corresponding parental cell line (HCC827/Erlo).

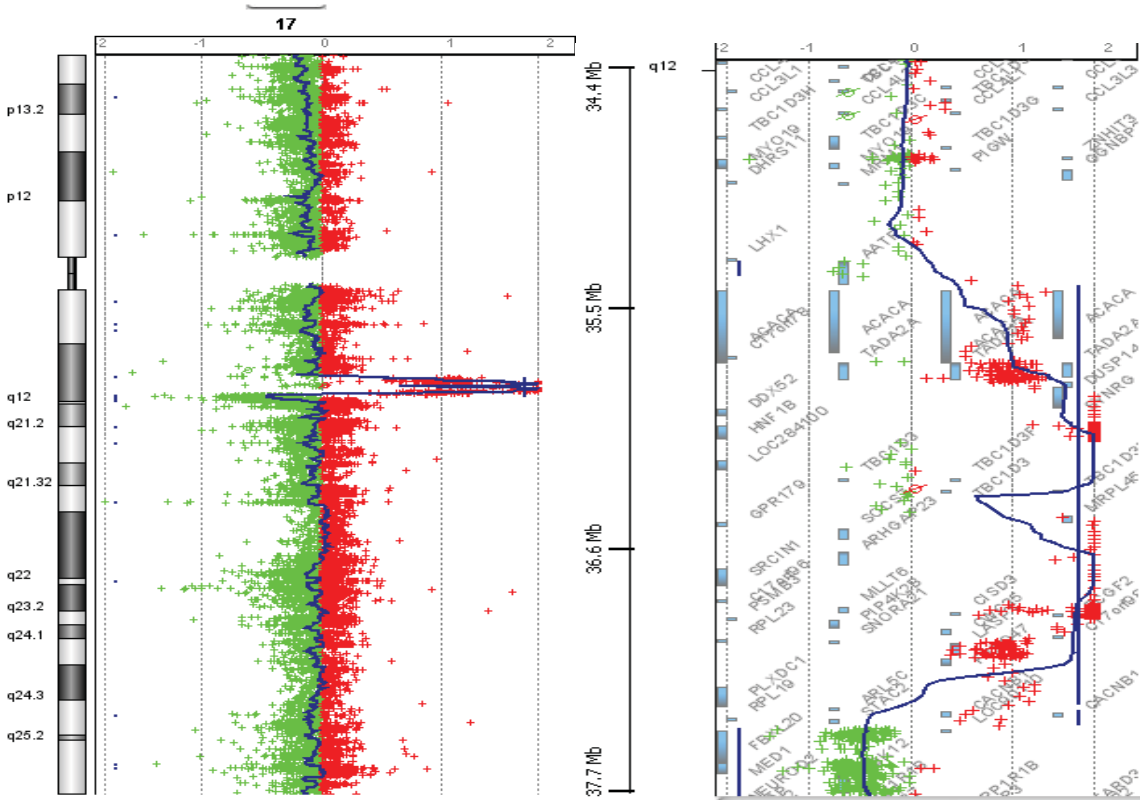

Figure 39: A new amplicon was observed at chromosome 17 of HCC827/Erlo+Crizo subline.

4.2.6 Whole genome expression changes of the crizotinib selected cell models:

Whole genome gene expression analysis of the investigated cell models was performed based on gene expression arrays. Especially, we were interested to investigate genes selectively amplified in the HCC827/Erlo+Crizo subline. Thus, expression of the genes located within the 17q12 amplicon were extracted from whole genome expression array data. HCC827/Erlo, HCC827/ErloCrizo, and HCC827/Erlo+Crizo transcriptomes were analyzed by Gene spring software. Table 13 presents genes located within the chromosome 17q12 amplicon that were highly upregulated at mRNA level (with fold change >2) in HCC827/Erlo+Crizo in comparison to HCC827/Erlo as their corresponding progenitor cell model.

Table 13 expression array was performed including HCC827/Erlo HCC827/ErloCrizo and HCC827/Erlo+Crizo. Fold change in the mRNA level of HCC827/Erlo+Crizo in comparison to HCC827/Erlo.

Gene Symbol	FC ([HCC827/ Erlo+Crizo] vs. [HCC827/ Erlo])
SYNRG	20.196947
SYNRG	7.2854395
SYNRG	4.2194314
DDX52	5.378543
DUSP14	4.561416
MRPL45	3.6923983
MRPL45	3.1328945
TADA2A	3.6549764
MLLT6	3.3295622
MLLT6	2.9264312
SOCS7	3.1208982
PCGF2	2.3717134
HNF1B	2.2995524
CWC25	2.2072377

4.2.7 Altered expression of additional RTK in HCC827/Erlo derived subfamily:

According to expression array data, FGFR1, FGFR2, FGFR3, ERBB2, ERBB3 as well as EPHA4 are RTK genes highly overexpressed at mRNA level in HCC827/ErloCrizo cells in comparison to HCC827/Erlo subline.

*Table 14: mRNAs/oligos of RTKs changed more than 2-fold in the HCC827/ErloCrizo as compared to the HCC827/Erlo cells. * indicates significance at p-value<0.05.*

Gene Symbol	Regulation*	Fold Change
EPHB3	Up	6.904964
FGFR2	Up	6.133229
FGFR3	Up	2.6003125
ERBB2	Down	-2.7843127

In HCC827/Erlo+Crizo cells, AXL, EPHA4, ERBB3, FGFR1, FGFR2, and FGFR3 were significantly upregulated at mRNA level in comparison to their expression level in HCC827/Erlo. Among them, especially FGFR2 is highly upregulated (Table 15 and Figure 40).

*Table 15: mRNAs/oligos of RTKs changed more than 2-fold in the HCC827/Erlo+Crizo as compared to the HCC827/Erlo cells. * indicates significance at p-value<0.05.*

Gene Symbol	Regulation*	Fold Change
AXL	Up	2.154899
EPHA4	Up	7.264242
ERBB3	Up	2.950841
ERBB3	Up	2.309517
FGFR1	Up	7.020714
FGFR1	Up	5.773517
FGFR2	Up	25.47384
FGFR2	Up	219.2002
FGFR3	Up	4.323212
EPHA1	Down	-2.0705
IGF2R	Down	-3.01599
INSR	Down	-2.67775
MET	Down	-2.7549

In addition to the RTK-specific approach, changes in signal interaction networks were analyzed based on genome-wide gene expression data using Ingenuity software (IPA). The most significantly enriched gene networks are presented [73]. As shown in Figure 40, not only FGFR2 but also several

interaction partners like Alp/ALPP and FLRT3 were significantly upregulated in HCC827/Erlo+Crizo cells in comparison to their progenitor cell model (HCC827/Erlo).

In contrast, the transcription factor TOX2 was selectively down-regulated in double-selected subline (HCC827/Erlo+Crizo) in comparison to HCC827/Erlo cell model.

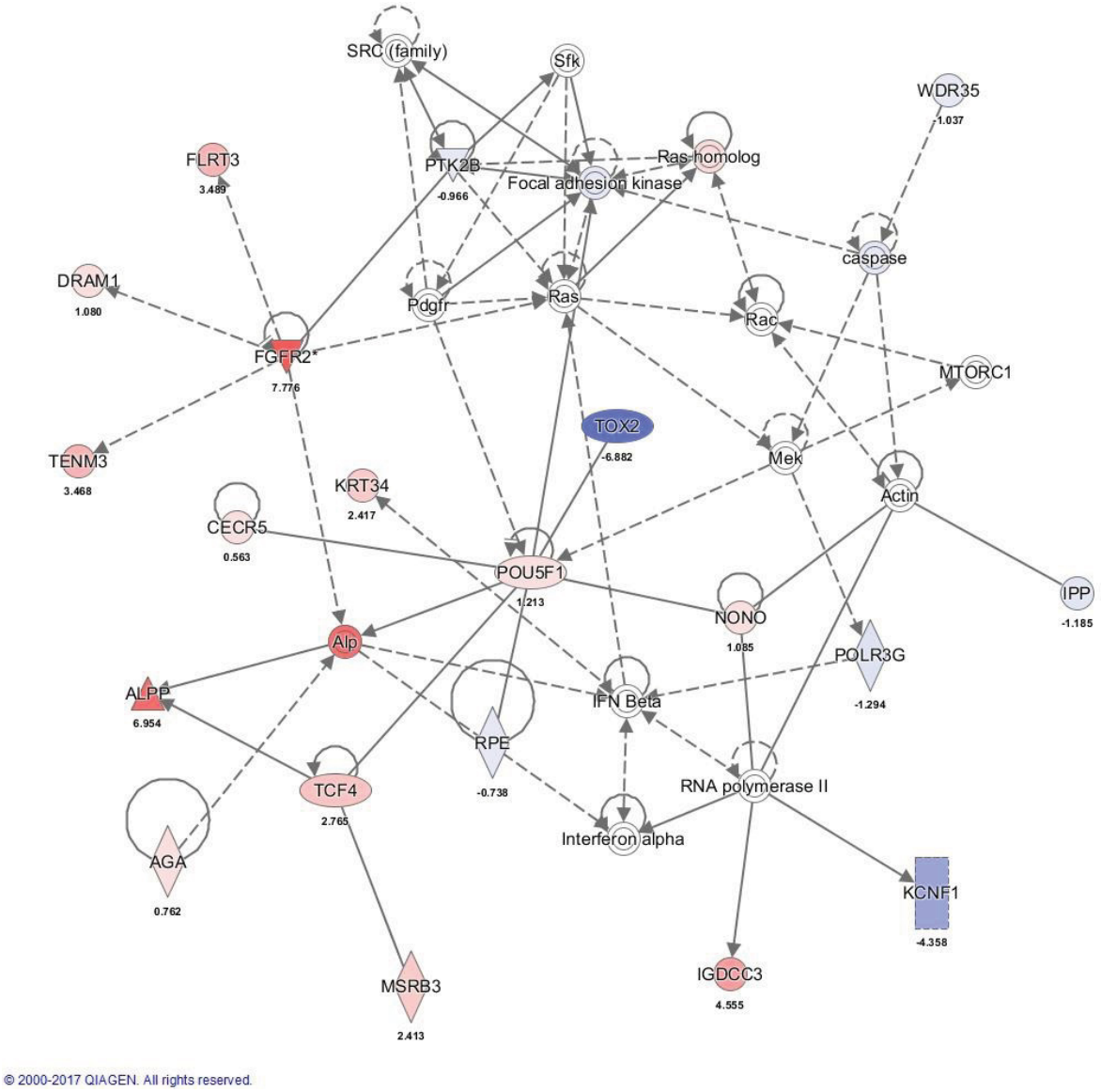

Figure 40: IPA diagram of HCC827/Erlo+Crizo vs. HCC827/Erlo

When comparing the single crizotinib-selected to the double selected cell model, in HCC827/ErloCrizo cells EPHA1, EPHB3, IGF2R, and INSR were upregulated at the mRNA level in comparison to the HCC827/Erlo+Crizo subline (Table 16). Conversely, EPHA4, FGFR1, FGFR2, ERBB2, and ERBB3 were upregulated in the double selected as compared to the single selected subline.

*Table 16: mRNAs/oligos of RTKs changed more than 2-fold in the HCC827/ErloCrizo cells as compared to the HCC827/Erlo+Crizo. * indicates significance at p-value<0.05.*

Gene Symbol	Regulation*	Fold Change*
EPHA1	Up	2.04068
EPHB3	Up	3.843482
IGF2R	Up	2.723755
INSR	Up	2.32361
AXL	Down	-3.14675
EPHA4	Down	-11.1758
ERBB2	Down	-3.23226
ERBB3	Down	-3.00706
ERBB3	Down	-2.39755
FGFR1	Down	-7.45787
FGFR1	Down	-7.64535
FGFR2	Down	-10.7646
FGFR2	Down	-35.7398
ROR1	Down	-2.07262

4.2.7.1 Gene expression alterations by Pathview:

The gene expression data was further analyzed using Pathview [74, 75]. As EGFR and RTK inhibitors were the focus of this study, “EGFR tyrosine kinase inhibitors” pathway from KEGG was chosen. Figure 41 and Figure 42 represent the genes involved in EGFR TK inhibitor resistance with altered expression in recently generated in comparison to their progenitor cell line. The upregulated genes in Progenitor and newly generated resistant cell models were shown in blue and red respectively. In the crizotinib single-selected HCC827/ErloCrizo cell line the RTK-ligand PDGFα, several members of the MAK cascade and especially FGFR3 were found upregulated. In accordance with Western blot analyses, the crizotinib target MET was downregulated also at the mRNA level. Unexpectedly, also the RTK AXL and H-RAS were strongly downregulated upon drug selection. In contrast, the crizotinib/erlotinib double-selection led to distinct upregulation of AXL while its ligand GAS6 was downregulated. However, ERBB3 and again FGFR3 were massively upregulated. This would suggest that crizotinib selection generally induces FGFR3 gene expression in HCC827 cells. Additionally, bcl2 mRNA was strongly induced in the double-resistant cell model pointing towards acquisition of general apoptosis resistance.

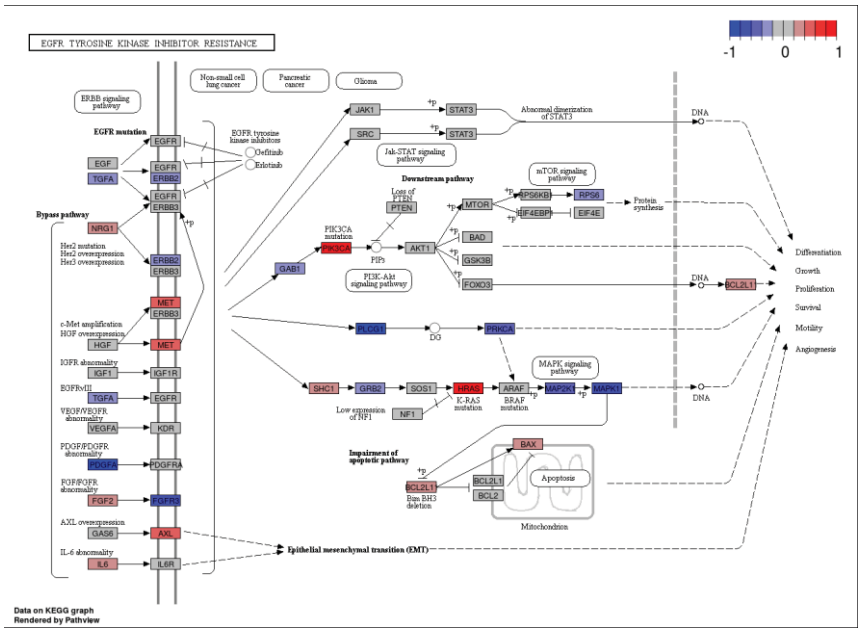

Figure 41: Colored "EGFR Tyrosine Kinase Inhibitor Resistance" KEGG pathway of HCC827/Erlo vs. HCC827/ErloCrizo cell models. Upregulated genes in HCC827/Erlo vs. HCC827/ErloCrizo were shown in red and downregulated genes in blue color.

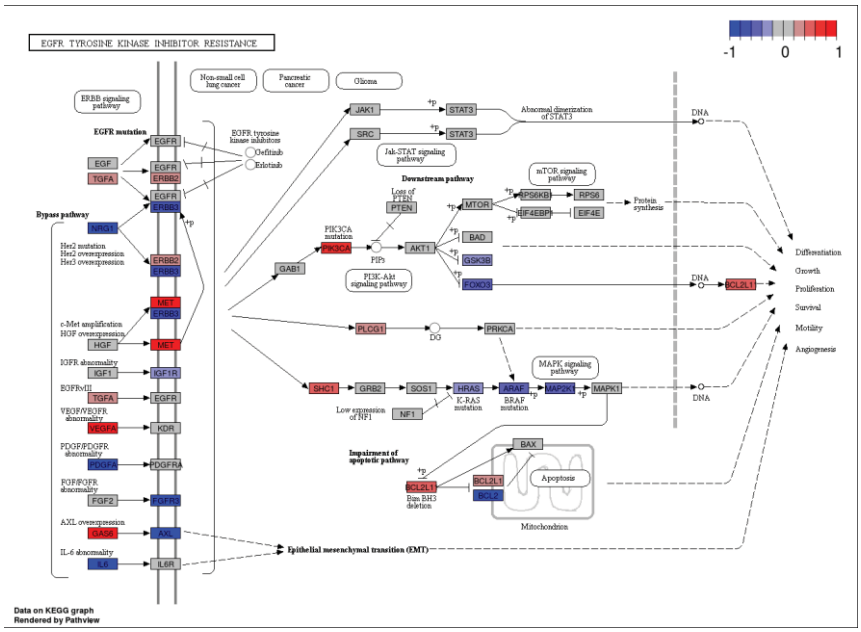

Figure 42: Colored "EGFR Tyrosine Kinase Inhibitor Resistance" KEGG pathway of HCC827/Erlo vs. HCC827/Erlo+Crizo cell models. Upregulated genes in HCC827/Erlo vs. HCC827/Erlo+Crizo were shown in red and downregulated genes in blue color.

4.2.8 Gene Set Enrichment Analysis (GSEA):

The gene expression data was also analyzed using GSEA allowing estimation of altered pathways and biochemical signals in the investigated cell models [76]. As this was done in collaboration with Dina Baier, the HCC827/GefiCrizo and HCC827/Gefi+Crizo the respective data are described in detail in her thesis.

Figure 43 depicts the enrichment plots with significant KEGG gene set alterations of HCC827/ErloCrizo cells as compared to the erlotinib-resistant subline (as progenitor cell model). The “calcium ion regulated exocytosis of neurotransmitter”, “Rho protein signal transduction”, “renal system process involved in regulation of blood volume”, “negative regulation of neural precursor cell proliferation” and “regulation of peptidyl threonine phosphorylation” represented altered gene sets with false discovery rate (FDR) < 0.001.

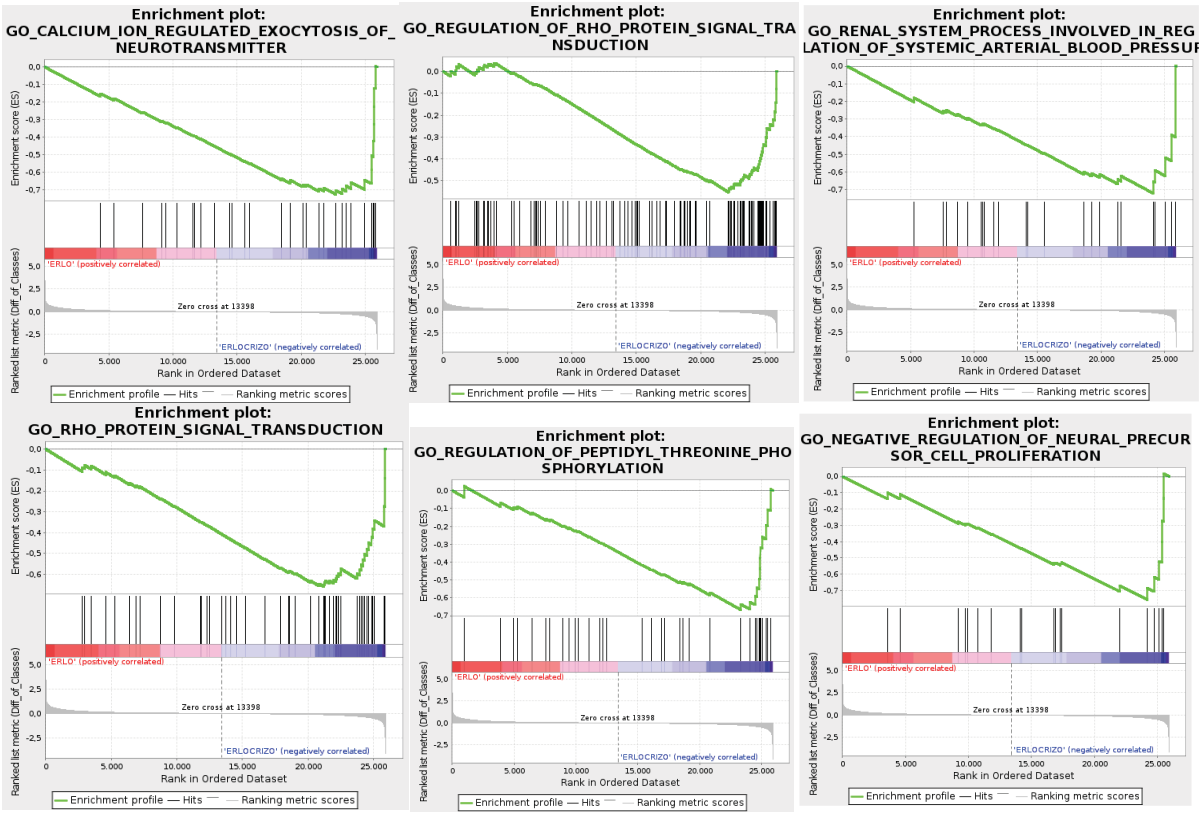

Figure 43: GSEA analysis of HCC827/ErloCrizo in comparison to HCC827/Erlo cell model. The green line represents the running Enrichment Score (ES), each black line in the lower part shows a member of related investigated gene set in that plot. The genes were arranged by their log fold change at the x-axis. The y-axis represents the log fold change (FC) in each gene, shown by the waterfall.

Figure 44 presents the GSEA waterfall plats interpreted by comparing HCC827/Erlo+Crizo with HCC827/Erlo as its progenitor cell model. “regulation of epithelial cell apoptotic process”, “regulation of apoptotic signaling pathway”, “regulation of protein maturation”, “flavonoid metabolic process”, “protein activation cascade”, and “negative regulation of protein maturation” represented altered gene sets with false discovery rate (FDR) < 0.001.

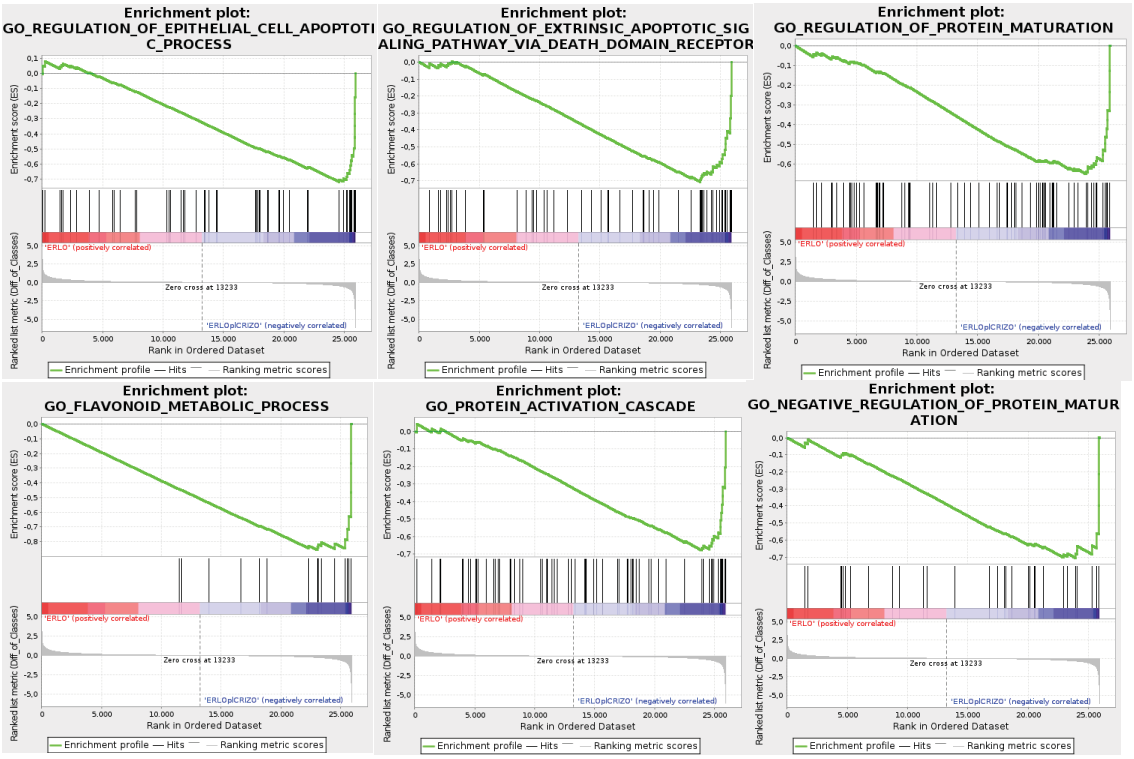

Figure 44: GSEA analysis of HCC827/Erlo+Crizo in comparison to HCC827/Erlo cell model. The green line represents the running Enrichment Score (ES), each black line in the lower part shows a member of related investigated gene set in that plot. The genes were arranged by their log fold change at the x-axis. The y-axis represents the log fold change (FC) in each gene, shown by the waterfall.

4.3 Role of ABC transporters:

Not only the activity of classical chemotherapy but also of several TKI is markedly influenced by ABC transporter efflux pumps [37]. Hence, the expression level of ABC transporters most strongly associated with cancer therapy resistance was investigated.

4.3.1 ABCB1 & ABCG2:

ABC transporters have an important role in multi-drug resistance. Among them, ABCB1 and ABCG2 are already known to be responsible for acquired resistance against erlotinib [38]. As doxorubicin is a substrate of ABCB1, HCC827, as well as HCC827/Erlo cells, were selected against doxorubicin. The expression of ABCB1, a major efflux pump for doxorubicin and erlotinib, was investigated at the protein level (Figure 45). However, ABCB1 was neither expressed in HCC827/Dox nor in HCC827/ErloDox sublines. KBC-1, an ABCB1 overexpressing cell model derived from KB3-1 cell line, was included as positive control.

ABCG2, another member of the ABC transporter family, was also investigated in this study. HCC827/Erlo and HCC827/Gefi resistant sublines were selected with 1µM mitoxantrone as a substrate of ABCG2. However, Western blot analysis again did not indicate any expression of ABCG2 in the HCC827/ErloMx and HCC827/GefiMx.

In summary, these data indicate that HCC827 cells are not very susceptible to ABC efflux pump activation by drug selection neither using classical therapeutics nor substrate TKI.

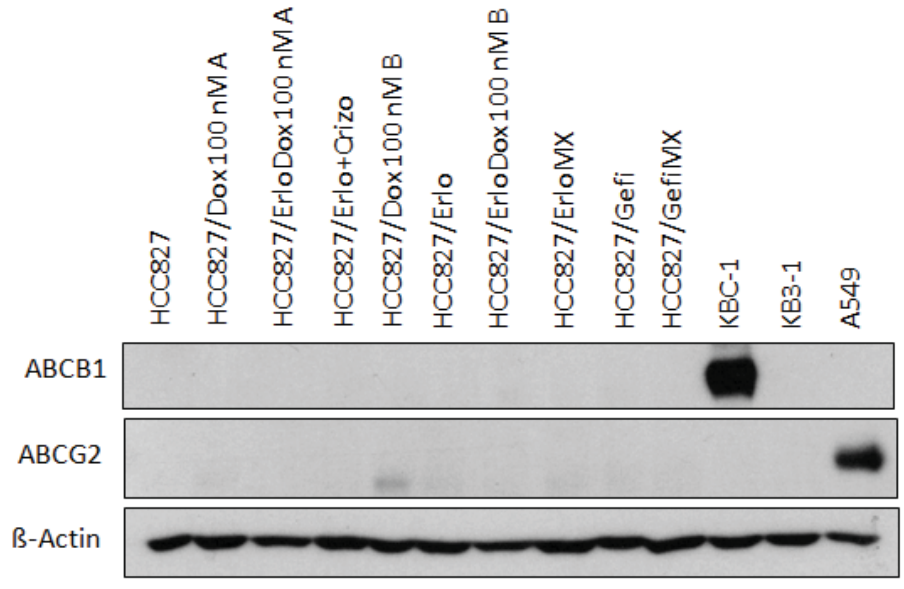

Figure 45: Western blot analysis of ABCB1 and ABCG2 expression in the indicated cell models. KBC-1 and A549 cell models were included as ABCB1 and ABCG2-positive controls, respectively.

However, in order to be able to test whether ABC transporters generally modify erlotinib activity and organ distribution, HCC827 were transfected with an ABCB1-coding plasmid. Transfection efficiency was proven by Western blot (Figure 46A). ABCB1 overexpression was observed in HCC827/ABCB1 cells in comparison to the parental cell line which displayed no detectable expression of ABCB1. ABCB1 expression level was investigated further including KBC-1 cell line as an ABCB1 overexpressing model (Figure 46B).

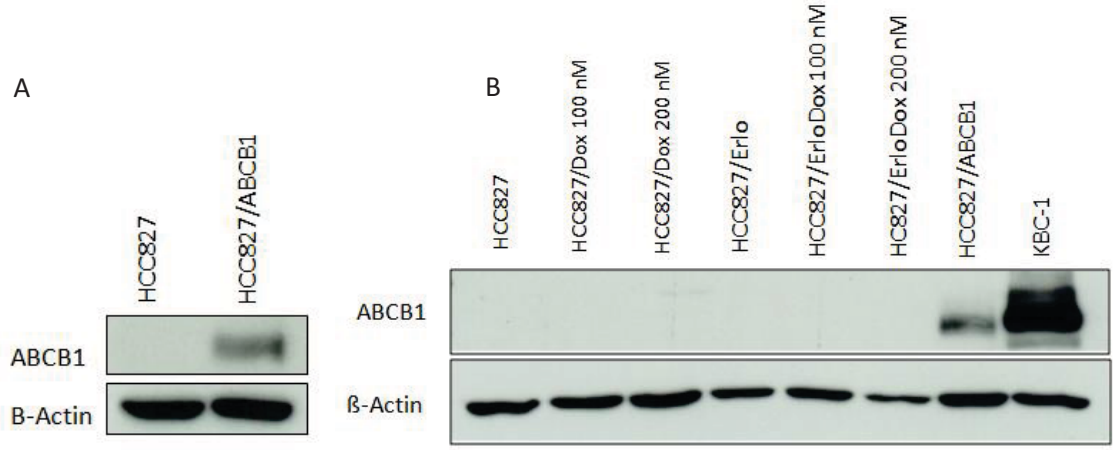

Figure 46: Western bot analysis of ABCB1 in the indicated cell models. A- HCC827 and HCC827/ABCB1 control model. B- HCC827-derived cell models as indicated.

4.3.2 Anti-proliferative effect of doxorubicin in ABCB1 overexpressing cell models:

The functional activity of ABCB1 was proven in the ABCB1 transfected cell line in comparison to the parental cell line (Figure 47 A). Cells were treated with different concentrations of doxorubicin for 72 h. HCC827/ABCB1 cells were significantly less sensitive towards doxorubicin as a cytotoxic agent.

The contribution of ABCB1 to doxorubicin resistance was further investigated by inhibiting the pump with elacridar. Cells were treated with different concentration of doxorubicin as cytotoxic agent and elacridar as ABCB1 modulator for 72 h (Figure 47 B, C & D). DMS/NIN; another ABCB1 overexpressing cell model (compare Figure 47 A), was included as positive and HCC827 as negative controls. DMS/NIN cells were resistant towards doxorubicin, and a significant re-sensitizing effect was observed by modulating ABCB1. In HCC827 cells, which were sensitive towards doxorubicin, and harbored no detectable ABCB1 expression, no significant resensitizing effect with elacridar was observed. In contrast, in the HCC827/ABCB1 cell model modulating ABCB1 by elacridar lead to re-sensitization of the cells towards doxorubicin.

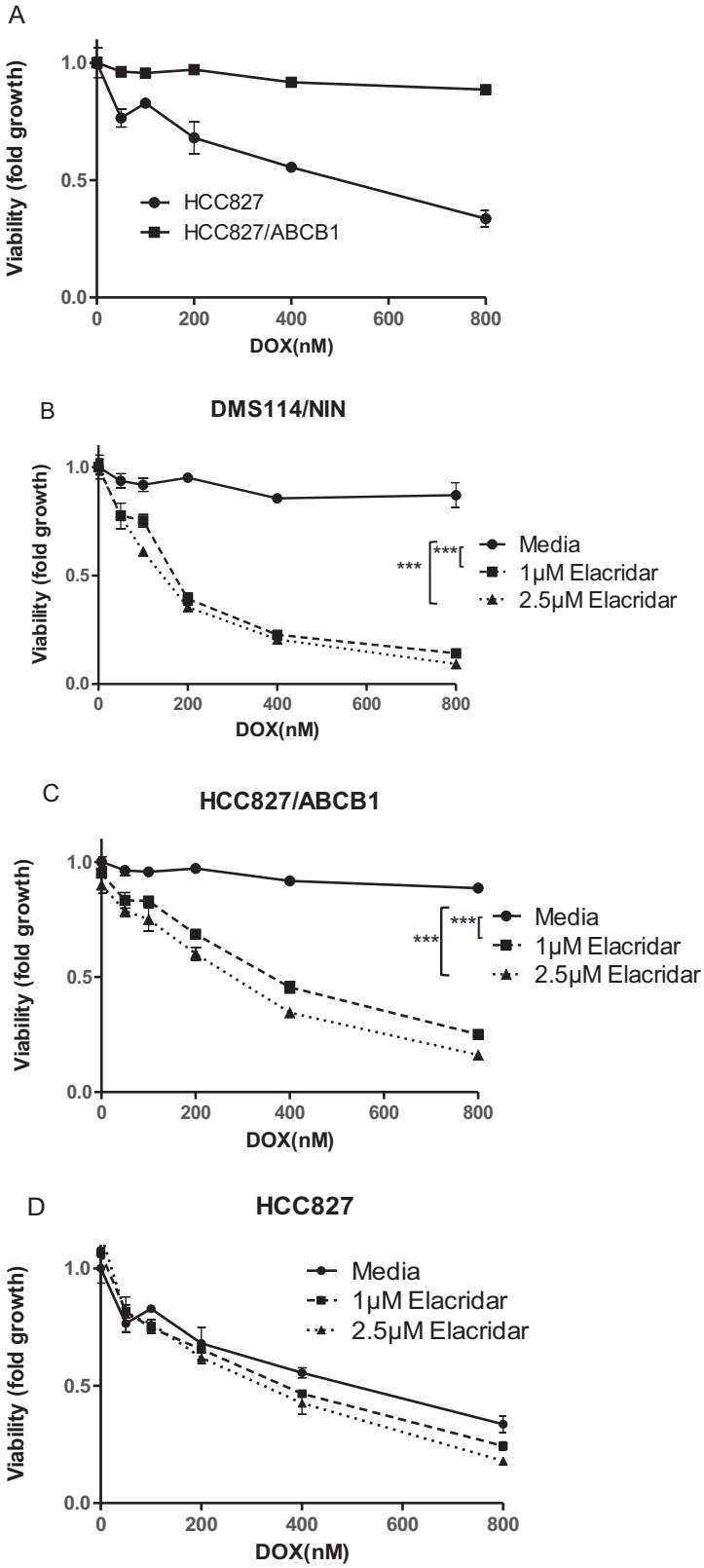

*Figure 47: Role of ABCB1 in resistance towards doxorubicin. A: Sensitivity of ABCB1 transfected cells towards doxorubicin was investigated in comparison to the parental cell line. Cells were treated with the indicated doxorubicin concentrations without and with Elacridar for 72 h.DMS114/NIN cells were included as positive and parental cell line as a negative control. *** indicates significance at p<0.05 by two-sided ANOVA.*

4.3.3 Impact of ABCB1 on erlotinib cytotoxicity:

The sensitivity of the ABCB1 overexpressing cell model against erlotinib was investigated performing viability assays. HCC827 and HCC827/ABCB1 cells were treated with different concentrations of erlotinib for 72 hours (Figure 48). The cell viability assay indicated no significant difference between HCC827/ABCB1 and HCC827 cell models. Hence, ABCB1 is not able to protect HCC827 cells against erlotinib.

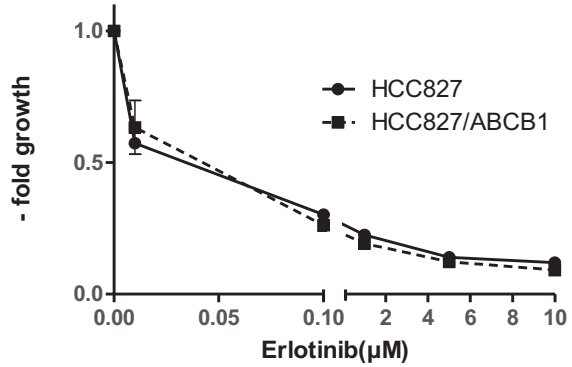

Figure 48: sensitivity of HCC827 and HCC827/ABCB1 against erlotinib. Cells were treated with the indicated erlotinib concentrations for 72 hours.

To analyze the role of ABCB1 in cell sensitivity of our cell models towards erlotinib, HCC827, as well as HCC827/ABCB1 cells, were treated with Erlotinib in combination with elacridar (as ABCB1 modulator) different concentrations. As shown in Figure 48, HCC827/ABCB1 cells are only very slightly less sensitive towards erlotinib in comparison to HCC827. Accordingly, HCC827/ABCB1 cells became slightly more sensitive towards erlotinib by ABCB1 inhibition using elacridar. Additionally, the difference did not reach significance.

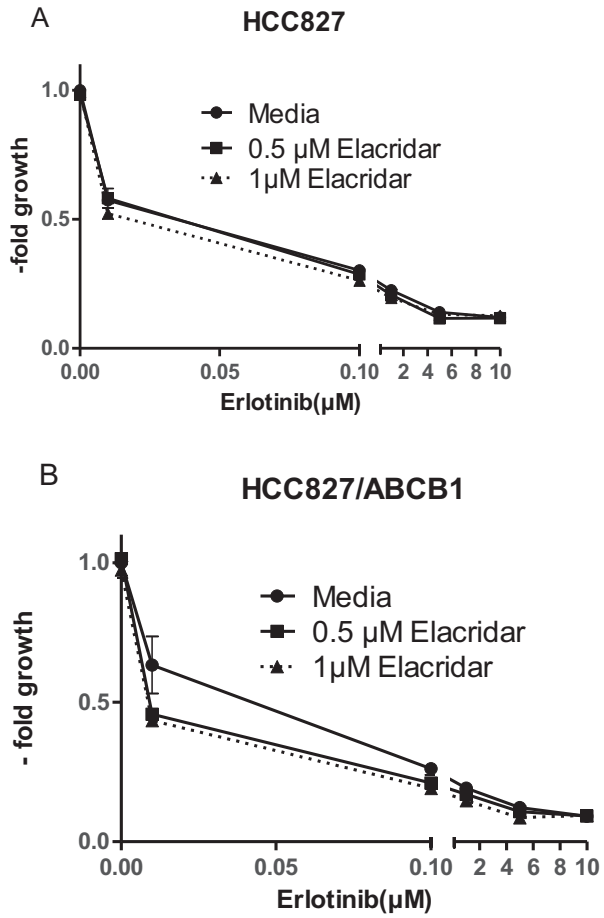

Figure 49: Activity of Erlotinib co-treatment with elacridar after 72 hours exposure of HCC827 and HCC827/ABCB1 cells. The included cells were treated with 0, 0.01, 0.1, 1, 5, 10 µM erlotinib in combination with 0, 0.5, 1 µM elacridar as ABCB1 modulator.

4.3.4 Role of ABCB1 in osimertinib sensitivity:

The sensitivity of HCC827/ABCB1 and HCC827 cell lines against osimertinib was investigated. Cells were treated with osimertinib in different concentrations. As shown in Figure 50, ABCB1 overexpressing cells (HCC827/ABCB1) are slightly less sensitive towards osimertinib in comparison to HCC827 cells. This leads us to conclude that osimertinib is not a very efficient substrate of ABCB1-mediated drug efflux.

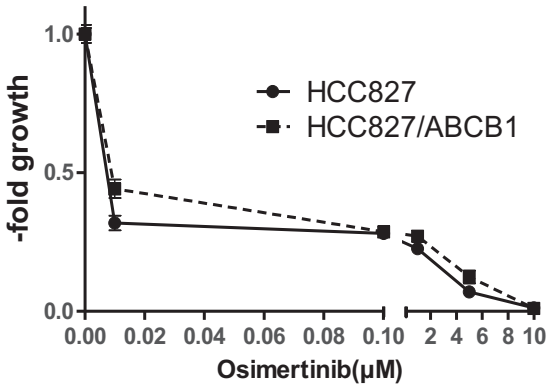

Figure 50: viability of HCC827 and HCC827/ABCB1 towards osimertinib. Cells were treated with 0, 0.1, 0.01, 1, 5, 10 µM osimertinib for 72 hours.

4.4 In vivo investigations:

Accumulation of ^{11}C erlotinib in different tumor xenografts developed in mice was detected by PET scanning. PET scan was not able to distinguish tumors derived from the parental HCC827 cell line harboring mutated EGFR and the indicated erlotinib-resistant sublines derived from in vitro drug selection. No significant difference in ^{11}C erlotinib accumulation was observed in tumors derived from different cell models (Figure 51). This was performed in collaboration with Prof Oliver Langer group at the Austrian Institute of Technology (AIT). The respective data have been published recently with me as a co-author [77].

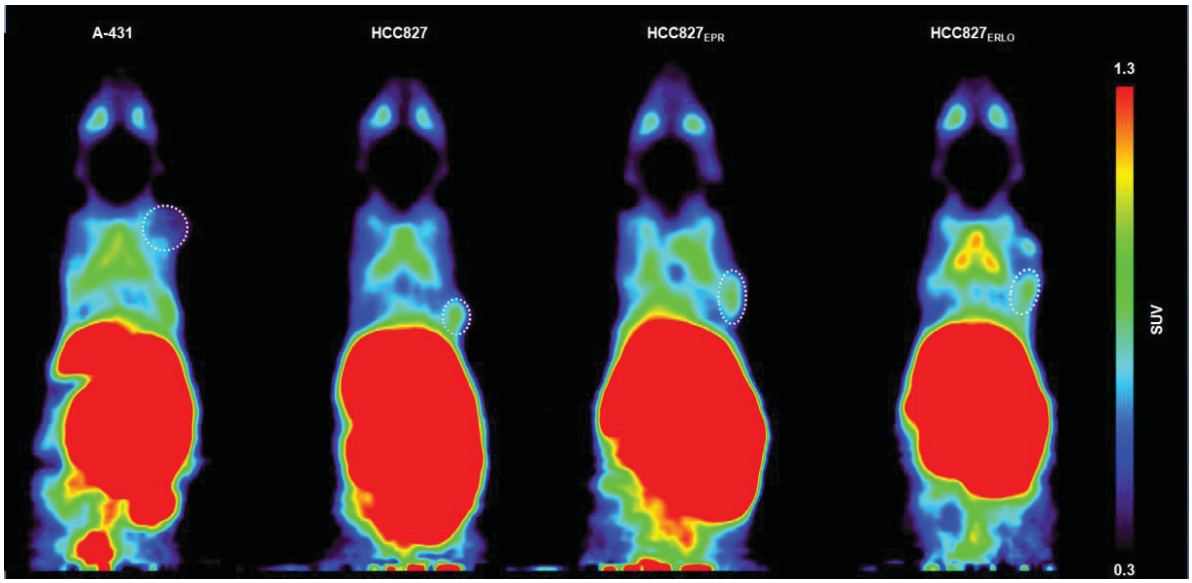

Figure 51: PET scan images of the xenograft mouse injected with different EGFR expressing cell models. Tumor area is marked by a pointed line.

5 Discussion

5.1 EGFR inhibitor resistance models of EGFR-mutated lung cancer

EGFR is an important oncogenic driver in a subgroup of NSCLC harboring activating mutations of this receptor tyrosine kinase. This makes it an important target for precision therapy, however, resistance against EGFR inhibitors also in lung cancer is still an unsolved problem [45]. Hence, the aim of this thesis project was to investigate the mechanisms responsible for TKI resistance in EGFR-driven NSCLC cell models and to develop novel strategies to prevent or circumvent resistance development. HCC827 is an NSCLC cell model harboring an EGFR gain-of-function mutation that makes these cells sensitive towards diverse EGFR-targeting TKIs [78].

In this thesis work, we especially aimed to dissect acquired resistance mechanisms against various EGFR inhibitors of different generations and the specific contributions of ABCB1, an important multidrug resistance efflux pump, known to transport several small-molecule TKI [79]. The role of EGFR was investigated in HCC827 cells as well as EGFR TKI resistant sublines selected against the first-generation EGFR inhibitors erlotinib and gefitinib. As already shown repeatedly by other research groups, HCC827 cells are most sensitive towards erlotinib, afatinib, and osimertinib (all different kinds and generations of EGFR-TKIs) (4.1.1), proofing so-called oncogene addiction (cells depend on EGFR). According to published data, cell models harboring the secondary resistance mutation T790M (HCC827/EPR), obtained from a cooperation partner in Japan, were resistant against first-line EGFR TKI but responded well to the third-generation inhibitor osimertinib[22].

Several mechanisms of acquired resistance to EGFR TKI have been described before based on in vitro models or therapy failure in the clinics, including besides resistance mutations like T790M, also a switch to alternative receptor tyrosine kinase signals [80-82]. Hence, the upregulation of MET has been reported as a frequent mechanism underlying acquired EGFR TKI (erlotinib and gefitinib) resistance [57, 62]. As mentioned, HCC827/Erlo and HCC827/Gefi sublines were resistant towards first-generation EGFR-TKIs but did not harbor a secondary resistance mutation. In contrast, investigations of DNA and RNA (4.1.5, 4.1.6) showed high levels of MET amplification and over-expression in both HCC827/Gefi and HCC827/Erlo cells. It was proven in this study that MET overexpression, based on gene amplification, plays a major role in acquired EGFR-TKI resistance of the HCC827/Erlo as well as HCC827/Gefi models. Interestingly, a dramatic response to crizotinib monotherapy has been reported in NSCLC patient with acquired EGFR inhibitor resistance after 12

month therapy with erlotinib [83]. Accordingly, we investigated whether EGFR TKI driven sublines depend on MET signaling. Surprisingly, despite high levels of MET expression, no MET addiction was observed based on unchanged sensitivity against MET inhibitors 4.1.2). This indicates that, in contrast to the in vivo situation mentioned above, HCC827/Erlo cells do not develop a full dependency on MET-mediated growth signals. Interestingly, in our hands only combined exposure to the EGFR and the MET TKIs (like erlotinib and crizotinib) completely resensitized the resistant cell models (4.1.3). This suggests, that EGFR and c-MET are cooperating in the resistance phenotype and that, depending on the TKI present, the downstream signals are rescued by the respective alternative pathway. Accordingly, phosphorylation of ERK as a readout for MAPK pathway activity was completely inhibited only in the EGFR/MET inhibitor combination setting. Respective, cooperative RTK networks involving EGFR and MET have been suggested in other cell types driven by mutated or activated EGFR [84]. Whether direct interaction of EGFR with the MET RTK in the plasma membranes of the resistant cell clones is underlying this phenomenon is addressed in ongoing investigations. Interestingly, Wang et al. have suggested cooperation between MET or IGFR1 with ERBB3 in EGFR inhibitor resistance [85]. Moreover, MET-EGFR dimerization has been recently suggested to depend on the status of EGFR mutation in lung adenocarcinoma and was sensitive to the inhibition of MET kinase [86]. A comparable mechanism might also be active clinically even against third-generation EGFR inhibitors. Hence, in an EGFR T790M-positive brain metastasis of an osimertinib-resistant NSCLC patient, a MET amplicon was detected. Interestingly, only a combined treatment with ERBB (afatinib) and MET (capmatinib) inhibitor completely inhibited the growth of this tumor as xenograft suggesting again cooperative action of these two RTK molecules [87, 88].

5.2 Acquired MET TKI resistance mechanism:

Consequently, we were aiming to model the treatment failure of EGFR inhibitor-resistant HCC827 cell clones towards single MET (crizotinib) and double MET/EGFR inhibitor exposure. New resistant sublines derived from HCC827/Gefi cells (HCC827/GefiCrizo and HCC827/Gefi+Crizo) will be investigated in depth in another study performed by Dina Baier. In contrast, in my thesis, I have focused on sublines derived from the erlotinib-resistant cell clones that I had selected against crizotinib (HCC827/ErloCrizo) or crizotinib + erlotinib (HCC827/Erlo+Crizo).

First, we focused on whether again an RTK switch was underlying the resistance phenotypes of these cell models. Different genetic alterations concerning alternative RTK molecules were already reported in the frame of acquired TKI resistance including other ERBB molecules like HER2, but also MET, FGFR1, FGFR2, and FGFR3 amplifications Consequently, these RTK molecules were investigated for alterations in this study. According to gene expression analysis, in single MET inhibitor-selected resistant cell model (HCC827/ErloCrizo) expression of various RTKs were upregulated including FGFR2, FGFR3, ERBB2 and EPHB3 at least at the mRNA level. This proves the idea that a possible cross talk between different RTKs could be the responsible mechanism to bypass the oncogenic driver inhibition. Accordingly, FGFR2 and FGFR3 gene transcription were upregulated due to EGFR inhibition by either gefitinib or Erbitux in NSCLC cells [89]. While no association was published regarding EPHB3 and EGFR/MET inhibition, EPHB3 is upregulated via FGFR inhibition by AZD4547 treatment, and contribute to FGFR inhibitor resistance via mTOR signaling [90].

A dramatic alteration was observed concerning EGFR and MET genes during resistance selection against both RTK inhibitors and their combinations. In the only crizotinib selected subline (HCC827/ErloCrizo), a massive loss of the c-MET amplicon was detected, characterizing the erlotinib-selected derivative. Conversely, array CGH revealed a re-gain of EGFR gene locus copies downregulated during erlotinib selection before. Accordingly, a gain of MET amplification was accompanied even by loss of the T790M mutation-positive EGFR amplicon during third-generation EGFR TKI rociletinib selection [91]. However, the HCC827/ErloCrizo cells stayed resistant against erlotinib single treatment, which enhances the possibility of resistance due to other RTK or ERBB family crosstalks as outlined above.

To the best of our knowledge, we are the first research group aiming to model MET/EGFR inhibitor resistance in an acquired EGFR inhibitor resistance background based on MET gene amplification. Concomitant selection of EGFR inhibitor (erlotinib) and MET inhibitor (crizotinib), lead to loss of both EGFR and MET amplifications in HCC827/Erlo+Crizo cells. These cells were highly proliferative and completely resistant towards combination treatment of erlotinib and crizotinib. This points towards activation of highly potent alternative oncogenic driver and resistance mediator during the double selection process. No Osimertinib (T790M mutation selective EGFR inhibitor) sensitivity was observed. Hence, neither MET amplification nor T790M secondary mutation may be considered as responsible for the newly acquired resistance phenotype. Selection against crizotinib has been shown to induce

EMT connected to overexpression of the RTK AXL in H2228 lung cancer cells [92]. Additionally, there are reports suggesting upregulation of other RTKs such as AXL for the acquisition of erlotinib resistance [93, 94]. Interestingly, a significant upregulation of other RTKs including, AXL but also FGFR1, FGFR2 as well as ERBB family members such as ERBB2 and ERBB3 was observed in double selected subline (HCC827/Erlo+Crizo). It was already shown, that ERBB3 could be upregulated in EGFR TKI (gefitinib and osimertinib) acquired resistance, and has an important role in the receptor internalization [95]. This led us to investigate possible cross talks between upregulated RTKs underlying acquired resistance. Afatinib as dual ERBB2 and EGFR kinase inhibitor might be used to indicate the contribution of the possible dimerization, and further activation of both receptors as an important mechanism of cell growth and survival. This is discussed in detail in the study performed by Dina Baier. Interestingly, ERBB3 is significantly upregulated only in the double selected subline (HCC827/Erlo+Crizo). ERBB3 and its ligand neuregulin have been implicated in acquired alectinib (another ALK inhibitor) resistance [92]. Additionally, ERBB3 activation via ERBB1 and SRC signaling pathway mediated afatinib resistance in lung cancer cells [96]. Additionally, it needs to be considered that FGFR1 and AXL, both upregulated in crizotinib-resistant sublines, have been shown to have a role in EMT [97]. EMT was suggested to be central to acquired EGFR TKI resistance in NSCLC tumors [58, 97, 98] Hence, AXL and FGFR1 could also be an important reason for newly acquired TKI resistance via activating EMT in selected sublines. This leads us to suggest the upregulated receptors as possible underlying resistance elements to bypass the double selection. This will be further investigated in our research lab.

A second strategy to identify molecular mechanisms underlying erlotinib/crizotinib double resistance was based on genome-wide DNA dose analysis by aCGH. A new amplicon was found on chromosome 17q12 of double selected subline (HCC827/Erlo+Crizo), which contains different gene loci. Among them, the SOCS7 gene was also amplified. Suppressor of cytokine signaling7 (SOCS7) overexpression was proven at mRNA level by whole-genome expression array in double selected subline (HCC827/Erlo+Crizo). Members of SOCS family are important molecules in cellular signal transduction. Activation of RTKs leads to SOCS protein binding. It was shown that SOCS7 interacts with tyrosine domain of EGFR by the SH2 domain [99, 100]. Additionally, it has also a negative regulatory function in JAK/STAT pathway. Besides that, it was shown that inhibition of EGFR/STAT3 activation leads to apoptosis in human NSCLC cells (despite EGFR activating mutations) [101]. In contrast to our observations,

Jak2 inhibition was suggested to re-sensitize EGFR inhibitor-resistant lung cancer cells towards erlotinib by uncoupling EGFR from its negative regulator SOCS5 [102]. Whether SOCS7 might interfere with this signal loop needs to be established in further investigations.

Besides that, IPA analysis of whole genome gene expression revealed massive downregulation of TOX2 at mRNA level. Box protein family member 2 (TOX2) is a transcription factor and has an important role during maturation of Natural Killer (NK) cells during development [103]. It was shown in another study that TOX2 is unmethylated in normal lung cells. However, there is a hyper-methylated CPG island within TOX2 promoter in lung (28% of the tumors) and breast (23% of the cases) cancer cells [104]. This leads to expression alteration of many downstream genes during cancer development. The reduced expression of TOX2 and the related downstream target genes in the double selected subline suggests that TOX2 might play a role in the sensitivity of investigated sublines towards combined EGFR/MET inhibition.

It was already shown that Synergin has a role in the internalization of plasma membrane receptors [105, 106]. According to the whole genome expression data (performed in this study), Synergin is highly upregulated in the HCC827/Erlo+Crizo cells. Additionally, big vesicles were observed in these cells as indicated by phase contrast microscopy. Thus, synergin could have a major role in the internalization of receptors.

5.3 Genome instability:

Many studies have proven a massive heterogeneity of cancer cells in solid tumors on the basis of genomic alterations and epigenetic deregulation [107-109]. Consequently, there is an open discussion ongoing about the major mechanism driving therapy resistance development. Either there was a pre-existing resistant sub-clone that was surviving drug exposure (selection), or the cells have developed new resistance features e.g. based on secondary mutations (adaptation). Concerning the T790M resistance mutation in EGFR, several studies have suggested that this mutation might preexist in a minor cancer cell subclone of tumors harboring activating EGFR mutations [110, 111]. This would argue for a selection process of resistance development. Indeed, preexisting T790M subclones in 25% of NSCLC cases harboring activating EGFR mutations correlated with a worse clinical outcome of EGFR inhibitor therapy [112]. Preexisting EGFR mutations were also observed in EGFR TKI (afatinib) resistant NSCLC cells according to next-generation sequencing (NGS), which leads to low progression-free survival (PFS) [113]. However, recent studies

suggested that the fixation process of paraffin-embedded specimen leads to artifacts in the sequencing process and that preexisting T790M mutation is frequently artifact [114]. Accordingly, a very recent study suggested that the T790M mutation might be acquired during gefitinib selection by NFκB-mediated activation of activation-induced cytidine deaminase (AICDA) finally causing the additional resistance mutation [115].

Regarding the here established and investigated resistance models, various subpopulations concerning EGFR and MET copy numbers were observed by the FISH investigation. However, in both gefitinib and erlotinib single drug selection resistance via MET amplification was observed. This strongly argues against preexisting T790M-positive subclones in this cell model. Also, another study investigated different subpopulations of HCC827 during Erlotinib selection, their gene dose alterations as well as sensitivity towards different TKIs. In agreement with our data, they observed EMT transition parallel to MET amplification in different sub-clones [58]. NGS investigations have already shown the possibility of double and triple mutations in single tumors and their effects on anticancer drug sensitivity and therapy success [116]. The shift back to predominant EGFR gene amplification and loss of MET gene copy numbers during the crizotinib single selection of HCC827/Erlo to establish HCC827/ErloCrizo strongly suggest selection of the respective tumor cell subclones. Interestingly, double selection of HCC827/Erlo cells (harboring the massive MET amplicon) against erlotinib plus crizotinib did not induce a T790M mutation in HCC827/Erlo+Crizo cells. In contrast, selection of treatment-naive HCC827 cells against erlotinib plus PHA-665752 led to the establishment of the HCC827/EPR model characterized by a uniform T790M mutated background. Together with our observation concerning MET gene amplification, this suggests that the T790M mutation is acquired during the selection process against combined EGFR/MET TKI in HCC827/EPR cells. Together our data suggests that selection and adaptation processes of genomic alterations might cooperate in acquired TKI resistance development. Also, another study showed that both mechanisms could be involved [117]

From a clinical point of view, these data suggest that the sequence of EGFR inhibition and combination with other TKI might be relevant concerning the activated resistance mechanisms. It has to be kept in mind that MET-amplified cell models are also resistant against the third-generation EGFR inhibitor osimertinib developed to inhibit T790M-positive tumors. Interestingly, besides additional resistance mutations in the EGFR gene, MET amplifications were

found a second most frequent genetic alteration in patients developing osimertinib resistance [118]
Hence, MET inhibition is suggested to be essential for avoiding EGFR inhibitor resistance. Accordingly, we modeled EGFR/MET double selection after erlotinib failure in the HCC827/Erlo+Crizo cells. Cross-sensitivity profiles suggested acquisition of no additional resistance mutation and also no clear RTK amplicon was detected by aCGH. Nevertheless, alternative RTK molecules like AXL, FGFRs, EPHA4 and also ERBB3 were overexpressed at the mRNA level. Additionally, alternative amplicons like the one including the SOCS7 gene were detected. The genetic basis and actual contribution of these alterations to the resistance phenotype need to be established in the ongoing studies.

5.4 ABC transporters:

ABC transporters are a family of transmembrane proteins able to transport various substrates including in many cases anticancer compounds. These do not only include classical chemotherapeutics but also TKIs. Hence, erlotinib and gefitinib are well- known substrates of the most prominent MDR efflux pump ABCB1 and ABCG2 [38, 119, 120]. This would suggest that selection against these drugs should readily induce overexpression of these drug transporters. Surprisingly, we could not detect any meaningful expression of either ABCB1 or ABCG2 in the EGFR inhibitor selected HCC827 sublines. Only in HCC827/Erlo+Crizo cells expression of ABCB1 was highly upregulated at the mRNA level, but not corresponding to substantial protein detection by Western blot. Additionally, no ABCB1 overexpression was observed in crizotinib selected cell models. In a nutshell, activation of ABC transporters does not play a major role in acquired EGFR and MET resistance at least in the HCC827 lung cancer model. As doxorubicin is also a substrate of ABCB1, doxorubicin selection was chosen as a second strategy to induce ABCB1 overexpression induction. Therefore, HCC827 parental and HCC827/Erlo cells were selected by doxorubicin treatment. However, no overexpression of ABCB1 was observed via doxorubicin selection. This suggests that HCC827 cells are generally not prone to activate ABCB1 drug transporter overexpression. To allow monitoring of 11C- erlotinib in vivo, we decided to transfect the cells with an ABCB1 coding plasmid. The resulting ABC overexpressing cells (HCC827/ABCB1) could be used to investigate the accumulation of different drugs in vitro and in vivo. Surprisingly, despite the high resistance of these cells to doxorubicin completely reversible by ABCB1 blockade, only a very weak cross-resistance to erlotinib and osimertinib was found 4.3.4). This suggests that either the TKIs

are only weak ABCB1 substrates or that the particular nature of the EGFR mutated HCC827 cell background impacts on this TKI resistance mechanism. It might be hypothesized that ABCB1 is able to avoid doxorubicin interaction with DNA in the cell nucleus but not TKI interaction with RTK molecule kinase domain at the inner side of the plasma membrane.
Summarizing, our data suggest that ABC transporters are not major drivers of acquired EGFR/MET inhibitor resistance.

5.5 In Vivo investigations:

^{11}C- erlotinib PET scan has already been shown as an approach capable to distinguish the NSCLC tumor harboring EGFR activating mutation (del746-A750) from tumors with wild type EGFR [121]. To assess in vivo specificity of ^{11}C-erlotinib accumulation, PET scan was performed in BALB/c nude mice with subcutaneous tumor xenografts. Four cell models were used including, epidermoid carcinoma A431 as erlotinib-sensitive cell line harboring wild type EGFR, and three EGFR mutated NSCLC cell model HCC827, HCC827/Erlo, HCC827/Gefi, HCC827/EPR investigated in this thesis work. However, no significant differences in erlotinib accumulation were found by PET scan between tumors grown in mice model in this study [77]. It needs to be investigated in further studies why ^{11}C- erlotinib binding does not differ in HCC827 and its derivative EGFR TKI resistant sublines in our in vivo experiments. This shows the necessity to develop other radiolabeled drugs specifically designed to selectively bind to activating EGFR mutations, as a more promising strategy for screening for EGFR mutations and resistance mechanisms based on PET scanning.

6 Conclusion:

In this study, various molecular mechanisms underlying acquired EGFR TKI resistance mechanisms were investigated using EGFR mutated cell models. To this end, EGFR mutations, MET pathway and overexpression of ABCB1 and ABCG2 were the main focus of investigations. Among them, only HCC827/EPR subline depicted sensitivity against the third-generation EGFR TKI osimertinib, corresponding to the presence of the secondary T790M resistance mutation. Interestingly, no overexpression of ABC transporters was found in HCC827 and its sublines selected against EGFR- and MET-targeting TKI. Hyperactivation of the MET pathway was shown to play the major role in acquired first-generation EGFR TKI resistance (HCC827/Erlo and HCC827/Gefi). Neither single inhibition of EGFR nor MET pathway alone was able to overcome this resistance and induce lung cancer cell death. However, double inhibition of the two of them led to massive cell death induction and resistance reversal. This proved the major role of the interplay between EGFR and MET pathway in erlotinib and gefitinib resistance.

To dissect the Interplay of EGFR and MET receptor, crizotinib selected sublines were generated using the erlotinib-resistant HCC827/Erlo model as progenitor subline. Crizotinib single treatment was not capable to resensitized the single crizotinib and double-selected subline (crizotinib and erlotinib). ERBB family members as well as AXL was found as a possible mechanism responsible for newly acquired resistance in the single and double EGFR/MET inhibitor resistance cell models. Hence, a combination Of ERBB and/or AXL TKI together with EGFR inhibitors could be a promising strategy to overcome acquired TKI resistance based on MET gene amplification. However, more investigations are needed to achieve a more precise understanding of these complex molecular resistance mechanisms against clinically used anticancer TKI and their complex interactions.

7 Abbreviations:

ABC	ATP-binding cassette transporter
ALL	Acute Lymphoblastic Leukemia
APS	Ammonium per sulfate
Array CGH	Comparative Genomic Hybridization
ATP	Adenosine triphosphate
BBB	Blood-brain barrier
BCRP	Breast cancer resistant protein
Crizo	Crizotinib
DAPI	4; 6-diamino-2-phenylindole
DMSO	Dimethyl sulfoxide
DNA	Deoxyribonucleic acid
EGF	Epidermal Growth factor
EGFR	Epidermal growth factor receptor
Erlo	Erlotinib
FACS	Fluorescence-activated cell sorting
FBS	Fetal bovine serum
FDA	Food and drug administration
FISH	Fluorescence In Situ Hybridization
Gefi	Gefitinib
GFP	Green fluorescent protein
GSEA	Gene set enrichment analysis
HGF	Hepatocyte growth factor
HGFR	Hepatocyte growth factor receptor
IGF	Insulin-like growth factor
IPA	Ingenuity pathway analysis
MAPK	Mitogen-activated protein kinase
MDR	Multi-drug resistance
MRP	Multi-drug resistance-associated protein
MTT	Dimethyl thiazolyl diphenyl tetrazolium salt
MW	Molecular weight
MTX	Methotrexate
MX	Mitoxantrone
NSCLC	Non-small cell lung carcinoma
PBS	Phosphate buffered saline
PET	Positron emission tomography
PFS	Progression-free survival
P-gp	p-glycoprotein

PMSF	Phenylmethanesulfonylfluoride
PDVF	Polyvinylidene fluoride
RPMI	Roswell Park Memorial Institute
RTK	Receptor tyrosine kinase
SCLC	Small cell lung cancer
SDS-PAGE	Sodium dodecyl sulfate-polyacrylamide gel electrophoresis
STAT	Signal Transducer and Activator of Transcription
TBST	Tris-buffered saline with tween

8 Bibliography

1. Bray, F., et al., *Global cancer statistics 2018: GLOBOCAN estimates of incidence and mortality worldwide for 36 cancers in 185 countries.* CA Cancer J Clin, 2018.
2. Thomas, A., et al., *Refining the treatment of NSCLC according to histological and molecular subtypes.* Nat Rev Clin Oncol, 2015. **12**(9): p. 511-26.
3. Detterbeck, F.C., et al., *The Eighth Edition Lung Cancer Stage Classification.* CHEST, 2017. **151**(1): p. 193-203.
4. Osmani, L., et al., *Current WHO guidelines and the critical role of immunohistochemical markers in the subclassification of non-small cell lung carcinoma (NSCLC): Moving from targeted therapy to immunotherapy.* Semin Cancer Biol, 2018. **52**(Pt 1): p. 103-109.
5. Utada, M., S. Yonehara, and K. Ozasa, *Historical Changes in Histological Diagnosis of Lung Cancer.* J Epidemiol, 2018.
6. Gridelli, C., et al., *Non-small-cell lung cancer.* Nature Reviews Disease Primers, 2015. **1**: p. 15009.
7. Saladi, L., et al., *Adenocarcinoma of Lung and Bronchial Carcinoid Presenting as Double Synchronous Primary Lung Cancer: A Case Report and Review of Literature.* World J Oncol, 2018. **9**(4): p. 110-114.
8. Ebell, M.H., T.N. Thai, and K.J. Royalty, *Cancer screening recommendations: an international comparison of high income countries.* Public Health Rev, 2018. **39**: p. 7.
9. Shi, L., et al., *Radiomics for Response and Outcome Assessment for Non-Small Cell Lung Cancer.* Technol Cancer Res Treat, 2018. **17**: p. 1533033818782788.
10. Mlika, M., et al., *Liquid Biopsy as Surrogate to Tissue in Lung Cancer for Molecular Profiling: A Meta-Analysis.* Curr Respir Med Rev, 2018. **14**(1): p. 48-60.
11. Politi, K. and R.S. Herbst, *Lung cancer in the era of precision medicine.* Clin Cancer Res, 2015. **21**(10): p. 2213-20.
12. O'Neill, A.C., et al., *Hallmarks of Cancer in the Reading Room: A Guide for Radiologists.* (1546-3141 (Electronic)).
13. Rotow, J. and T.G. Bivona, *Understanding and targeting resistance mechanisms in NSCLC.* Nature Reviews Cancer, 2017. **17**: p. 637.
14. Zugazagoitia, J., et al., *Biological therapies in nonsmall cell lung cancer.* Eur Respir J, 2017. **49**(3).
15. Herbst, R.S., D. Morgensztern, and C. Boshoff, *The biology and management of non-small cell lung cancer.* Nature, 2018. **553**: p. 446.
16. Su, Y., H.B. Fang, and F. Jiang, *An epigenetic classifier for early stage lung cancer.* Clin Epigenetics, 2018. **10**: p. 68.
17. Govindan, R., *Chemotherapy for metastatic NSCLC: current status and future direction.* Nature Clinical Practice Oncology, 2005. **2**: p. 238.
18. Chabner, B.A. and T.G. Roberts Jr, *Chemotherapy and the war on cancer.* Nature Reviews Cancer, 2005. **5**: p. 65.
19. Rosell, R. and N. Karachaliou, *Optimizing lung cancer treatment approaches.* Nature Reviews Clinical Oncology, 2014. **12**: p. 75.
20. Daly, M.E., A.M. Monjazeb, and K. Kelly, *Clinical Trials Integrating Immunotherapy and Radiation for Non-Small-Cell Lung Cancer.* J Thorac Oncol, 2015. **10**(12): p. 1685-93.
21. Wraith, D.C., *The Future of Immunotherapy: A 20-Year Perspective.* Front Immunol, 2017. **8**: p. 1668.
22. Anagnostou, V.K. and J.R. Brahmer, *Cancer immunotherapy: a future paradigm shift in the treatment of non-small cell lung cancer.* Clin Cancer Res, 2015. **21**(5): p. 976-84.
23. Meyers, D.E., et al., *Targeting the PD-1/PD-L1 axis for the treatment of non-small-cell lung cancer.* Curr Oncol, 2018. **25**(4): p. e324-e334.

24. Barnet, M.B., et al., *Immunotherapy in Non-Small Cell Lung Cancer: Shifting Prognostic Paradigms.* J Clin Med, 2018. **7**(6).
25. Moya-Horno, I., et al., *Combination of immunotherapy with targeted therapies in advanced non-small cell lung cancer (NSCLC).* Ther Adv Med Oncol, 2018. **10**: p. 1758834017745012.
26. Viteri, S., et al., *Results of clinical trials with anti-programmed death 1/programmed death ligand 1 inhibitors in lung cancer.* Transl Lung Cancer Res, 2015. **4**(6): p. 756-62.
27. Liang, H., X. Liu, and M. Wang, *Immunotherapy combined with epidermal growth factor receptor-tyrosine kinase inhibitors in non-small-cell lung cancer treatment.* Onco Targets Ther, 2018. **11**: p. 6189-6196.
28. Yin, W., et al., *Remodeling Tumor-Associated Macrophages and Neovascularization Overcomes EGFR(T790M) -Associated Drug Resistance by PD-L1 Nanobody-Mediated Codelivery.* Small, 2018: p. e1802372.
29. Chen, S., B. Hu, and H. Li, *A meta-analysis of nivolumab for the treatment of advanced non-small-cell lung cancer.* Onco Targets Ther, 2018. **11**: p. 7691-7697.
30. Kong, L.L., et al., *Current progress and outcomes of clinical trials on using epidermal growth factor receptor-tyrosine kinase inhibitor therapy in non-small cell lung cancer patients with brain metastases.* Chronic Dis Transl Med, 2017. **3**(4): p. 221-229.
31. Drilon, A., et al., *Targeting MET in Lung Cancer: Will Expectations Finally Be MET?* J Thorac Oncol, 2017. **12**(1): p. 15-26.
32. Pakkala, S. and S.S. Ramalingam, *Personalized therapy for lung cancer: Striking a moving target.* JCI Insight, 2018. **3**(15).
33. Recondo, G., et al., *Making the first move in EGFR-driven or ALK-driven NSCLC: first-generation or next-generation TKI?* Nature Reviews Clinical Oncology, 2018. **15**(11): p. 694-708.
34. Hanahan, D. and R.A. Weinberg, *Hallmarks of cancer: the next generation.* Cell, 2011. **144**(5): p. 646-74.
35. Pao, W. and J. Chmielecki, *Rational, biologically based treatment of EGFR-mutant non-small-cell lung cancer.* Nat Rev Cancer, 2010. **10**(11): p. 760-74.
36. Dean, M., A. Rzhetsky, and R. Allikmets, *The human ATP-binding cassette (ABC) transporter superfamily.* Genome Res, 2001. **11**(7): p. 1156-66.
37. Gottesman, M.M., T. Fojo, and S.E. Bates, *Multidrug resistance in cancer: role of ATP–dependent transporters.* Nature Reviews Cancer, 2002. **2**: p. 48.
38. Marchetti, S., et al., *Effect of the ATP-binding cassette drug transporters ABCB1, ABCG2, and ABCC2 on erlotinib hydrochloride (Tarceva) disposition in in vitro and in vivo pharmacokinetic studies employing Bcrp1-/-/Mdr1a/1b-/- (triple-knockout) and wild-type mice.* Mol Cancer Ther, 2008. **7**(8): p. 2280-7.
39. Eid, S.Y., et al., *Natural Products Modulate the Multifactorial Multidrug Resistance of Cancer.* Pharmacology & Pharmacy, 2015. **06**: p. 146-176.
40. Asao, T., F. Takahashi, and K. Takahashi, *Resistance to molecularly targeted therapy in non-small-cell lung cancer.* Respir Investig, 2018.
41. Imai, K. and A. Takaoka, *Comparing antibody and small-molecule therapies for cancer.* Nat Rev Cancer, 2006. **6**(9): p. 714-27.
42. Gschwind, A., O.M. Fischer, and A. Ullrich, *The discovery of receptor tyrosine kinases: targets for cancer therapy.* Nature Reviews Cancer, 2004. **4**: p. 361.
43. Morrison, J., et al., *Epidermal growth factor receptor blockers for the treatment of ovarian cancer.* Cochrane Database of Systematic Reviews, 2018(10).
44. Turk, H.F. and R.S. Chapkin, *Analysis of epidermal growth factor receptor dimerization by BS(3) cross-linking.* Methods Mol Biol, 2015. **1233**: p. 25-34.
45. Linardou, H., et al., *Somatic EGFR mutations and efficacy of tyrosine kinase inhibitors in NSCLC.* Nature Reviews Clinical Oncology, 2009. **6**: p. 352-366.
46. Walther, A., et al., *Genetic prognostic and predictive markers in colorectal cancer.* Nature Reviews Cancer, 2009. **9**: p. 489.

47. Passiglia, F., et al., *EGFR inhibition in NSCLC: New findings.... and opened questions?* Crit Rev Oncol Hematol, 2017. **112**: p. 126-135.
48. Sullivan, I. and D. Planchard, *Next-Generation EGFR Tyrosine Kinase Inhibitors for Treating EGFR-Mutant Lung Cancer beyond First Line.* Front Med (Lausanne), 2016. **3**: p. 76.
49. Ricciuti, B., et al., *Afatinib in the first-line treatment of patients with non-small cell lung cancer: clinical evidence and experience.* Ther Adv Respir Dis, 2018. **12**: p. 1753466618808659.
50. Ulivi, P., et al., *Gene mutation analysis in EGFR wild type NSCLC responsive to erlotinib: are there features to guide patient selection?* Int J Mol Sci, 2014. **16**(1): p. 747-57.
51. Costa, D.B. and S.S. Kobayashi, *Whacking a mole-cule: clinical activity and mechanisms of resistance to third generation EGFR inhibitors in EGFR mutated lung cancers with EGFR-T790M.* Translational lung cancer research, 2015. **4**: p. 809-15.
52. Chen, L., et al., *Recent Progress of Small-Molecule Epidermal Growth Factor Receptor (EGFR) Inhibitors against C797S Resistance in Non-Small-Cell Lung Cancer.* J Med Chem, 2018. **61**(10): p. 4290-4300.
53. Sharma, S.V., et al., *Epidermal growth factor receptor mutations in lung cancer.* Nature Reviews Cancer, 2007. **7**: p. 169.
54. Salgia, R., *MET in Lung Cancer: Biomarker Selection Based on Scientific Rationale.* Mol Cancer Ther, 2017. **16**(4): p. 555-565.
55. Supriya Rajanna, A.S., *c-Met: A Potential Target for Current Non-Small-Cell Lung Cancer Therapeutics.* Chemotherapy: Open Access, 2014. **03**(03).
56. Saito, A., M. Horie, and T. Nagase, *TGF-beta Signaling in Lung Health and Disease.* Int J Mol Sci, 2018. **19**(8).
57. Peters, S. and A.A. Adjei, *MET: a promising anticancer therapeutic target.* Nature Reviews Clinical Oncology, 2012. **9**: p. 314-326.
58. Jakobsen, K.R., et al., *MET amplification and epithelial-to-mesenchymal transition exist as parallel resistance mechanisms in erlotinib-resistant, EGFR-mutated, NSCLC HCC827 cells.* Oncogenesis, 2017. **6**: p. e307.
59. Ghafoor, Q., et al., *Epidermal Growth Factor Receptor (EGFR) Kinase Inhibitors and Non-Small Cell Lung Cancer (NSCLC) - Advances in Molecular Diagnostic Techniques to Facilitate Targeted Therapy.* Pathol Oncol Res, 2017.
60. Abdallah, S.M. and V. Hirsh, *Irreversible tyrosine kinase inhibition of epidermal growth factor receptor with afatinib in EGFR activating mutation-positive advanced non-small-cell lung cancer.* Curr Oncol, 2018. **25**(Suppl 1): p. S9-S17.
61. Miranda, O., M. Farooqui, and J.M. Siegfried, *Status of Agents Targeting the HGF/c-Met Axis in Lung Cancer.* Cancers (Basel), 2018. **10**(9).
62. Engelman, J.A., et al., *MET Amplification Leads to Gefitinib Resistance in Lung Cancer by Activating ERBB3 Signaling.* Science, 2007. **316**.
63. Xu, Y. and Y. Fan, *Responses to crizotinib can occur in c-MET overexpressing nonsmall cell lung cancer after developing EGFR-TKI resistance.* Cancer Biology & Therapy, 2018: p. 1-5.
64. Kim, S., et al., *Acquired Resistance of MET-Amplified Non-small Cell Lung Cancer Cells to the MET Inhibitor Capmatinib.* J Korean Cancer Assoc, 2018. **0**(0): p. 0-0.
65. Fruman, D.A. and C. Rommel, *PI3K and cancer: lessons, challenges and opportunities.* Nature Publishing Group, 2014. **13**.
66. Engelman, J.A., *Targeting PI3K signalling in cancer: opportunities, challenges and limitations.* Nat Rev Cancer, 2009. **9**(8): p. 550-62.
67. Liu, P., et al., *Targeting the phosphoinositide 3-kinase pathway in cancer.* Nat Rev Drug Discov, 2009. **8**(8): p. 627-44.
68. Franke, T.F., *PI3K/Akt: getting it right matters.* Oncogene, 2008. **27**: p. 6473-6488.
69. Kim, H.J. and D. Bar-Sagi, *Modulation of signalling by Sprouty: a developing story.* Nature Reviews Molecular Cell Biology, 2004. **5**: p. 441.

70. Bejjani, B.A. and L.G. Shaffer, *Application of array-based comparative genomic hybridization to clinical diagnostics.* J Mol Diagn, 2006. **8**(5): p. 528-33.
71. Christensen, J.G., et al., *A selective small molecule inhibitor of c-Met kinase inhibits c-Met-dependent phenotypes in vitro and exhibits cytoreductive antitumor activity in vivo.* Cancer Res, 2003. **63**(21): p. 7345-55.
72. Ou, S.H., *Crizotinib: a novel and first-in-class multitargeted tyrosine kinase inhibitor for the treatment of anaplastic lymphoma kinase rearranged non-small cell lung cancer and beyond.* Drug Des Devel Ther, 2011. **5**: p. 471-85.
73. Kramer, A., et al., *Causal analysis approaches in Ingenuity Pathway Analysis.* Bioinformatics, 2014. **30**(4): p. 523-30.
74. Luo, W. and C. Brouwer, *Pathview: an R/Bioconductor package for pathway-based data integration and visualization.* Bioinformatics, 2013. **29**(14): p. 1830-1.
75. Luo, W., et al., *Pathview Web: user friendly pathway visualization and data integration.* Nucleic Acids Res, 2017. **45**(W1): p. W501-W508.
76. Bateman, A.R., et al., *Importance of collection in gene set enrichment analysis of drug response in cancer cell lines.* Sci Rep, 2014. **4**: p. 4092.
77. Traxl, A., et al., *[(11)C]Erlotinib PET cannot detect acquired erlotinib resistance in NSCLC tumor xenografts in mice.* Nucl Med Biol, 2017. **52**: p. 7-15.
78. Girard, L., et al., *Genome-wide allelotyping of lung cancer identifies new regions of allelic loss, differences between small cell lung cancer and non-small cell lung cancer, and loci clustering.* (0008-5472 (Print)).
79. Eadie, L.N., et al., *The clinical significance of ABCB1 overexpression in predicting outcome of CML patients undergoing first-line imatinib treatment.* (1476-5551 (Electronic)).
80. Oxnard, G.R., et al., *Acquired resistance to EGFR tyrosine kinase inhibitors in EGFR-mutant lung cancer: distinct natural history of patients with tumors harboring the T790M mutation.* (1078-0432 (Print)).
81. Bell, D.W., et al., *Inherited susceptibility to lung cancer may be associated with the T790M drug resistance mutation in EGFR.* (1061-4036 (Print)).
82. Zhang, K. and Q. Yuan, *Current mechanism of acquired resistance to epidermal growth factor receptor-tyrosine kinase inhibitors and updated therapy strategies in human nonsmall cell lung cancer.* (1998-4138 (Electronic)).
83. Yoshimura, K., et al., *Successful crizotinib monotherapy in EGFR-mutant lung adenocarcinoma with acquired MET amplification after erlotinib therapy.* Respir Med Case Rep, 2017. **20**: p. 160-163.
84. Guo, A., et al., *Signaling networks assembled by oncogenic EGFR and c-Met.* (1091-6490 (Electronic)).
85. Wang, D.D., et al., *Contribution of EGFR and ErbB-3 Heterodimerization to the EGFR Mutation-Induced Gefitinib- and Erlotinib-Resistance in Non-Small-Cell Lung Carcinoma Treatments.* (1932-6203 (Electronic)).
86. Ortiz-Zapater, E., et al., *MET-EGFR dimerization in lung adenocarcinoma is dependent on EGFR mtations and altered by MET kinase inhibition.* (1932-6203 (Electronic)).
87. Martinez-Marti, A., et al., *Dual MET and ERBB inhibition overcomes intratumor plasticity in osimertinib-resistant-advanced non-small-cell lung cancer (NSCLC).* (1569-8041 (Electronic)).
88. Guo, A., et al., *Signaling networks assembled by oncogenic EGFR and c-Met.* Proc Natl Acad Sci U S A, 2008. **105**(2): p. 692-7.
89. Ware, K.E., et al., *Rapidly acquired resistance to EGFR tyrosine kinase inhibitors in NSCLC cell lines through de-repression of FGFR2 and FGFR3 expression.* (1932-6203 (Electronic)).
90. Lee, S.Y., et al., *Upregulation of EphB3 in gastric cancer with acquired resistance to a FGFR inhibitor.* (1878-5875 (Electronic)).
91. Mizuuchi, H., et al., *Oncogene swap as a novel mechanism of acquired resistance to epidermal growth factor receptor-tyrosine kinase inhibitor in lung cancer.* (1349-7006 (Electronic)).

92. Kim, H.R., et al., *Epithelial-mesenchymal transition leads to crizotinib resistance in H2228 lung cancer cells with EML4-ALK translocation.* (1878-0261 (Electronic)).
93. Romaniello, D., et al., *A Combination Of Approved Antibodies Overcomes Resistance Of Lung Cancer To Osimertinib By Blocking Bypass Pathways.* Clin Cancer Res, 2018.
94. Rho, J.K., et al., *MET and AXL Inhibitor NPS-1034 Exerts Efficacy against Lung Cancer Cells Resistant to EGFR Kinase Inhibitors Because of MET or AXL Activation.* Cancer Research, 2014. **74**(1): p. 253-262.
95. Yonesaka, K., et al., *An HER3-targeting antibody-drug conjugate incorporating a DNA topoisomerase I inhibitor U3-1402 conquers EGFR tyrosine kinase inhibitor-resistant NSCLC.* Oncogene, 2018.
96. Booth, L., et al., *The afatinib resistance of in vivo generated H1975 lung cancer cell clones is mediated by SRC/ERBB3/c-KIT/c-MET compensatory survival signaling.* (1949-2553 (Electronic)).
97. Thomson, S., et al., *Epithelial to mesenchymal transition is a determinant of sensitivity of non-small-cell lung carcinoma cell lines and xenografts to epidermal growth factor receptor inhibition.* Cancer Res, 2005. **65**(20): p. 9455-62.
98. Yauch, R.L., et al., *Epithelial versus mesenchymal phenotype determines in vitro sensitivity and predicts clinical activity of erlotinib in lung cancer patients.* Clin Cancer Res, 2005. **11**(24 Pt 1): p. 8686-98.
99. Sasi, W., et al., *Observations on the effects of Suppressor of Cytokine Signaling 7 (SOCS7) knockdown in breast cancer cells: their in vitro response to Insulin Like Growth Factor I (IGF-I).* Clin Transl Oncol, 2014. **16**(5): p. 476-87.
100. Kazi, J.U., et al., *SOCS proteins in regulation of receptor tyrosine kinase signaling.* Cell Mol Life Sci, 2014. **71**(17): p. 3297-310.
101. Park, H.J., et al., *Induction of apoptosis by morusin in human non-small cell lung cancer cells by suppression of EGFR/STAT3 activation.* Biochem Biophys Res Commun, 2018. **505**(1): p. 194-200.
102. Gao, S.P., et al., *JAK2 inhibition sensitizes resistant EGFR-mutant lung adenocarcinoma to tyrosine kinase inhibitors.* (1937-9145 (Electronic)).
103. Vong, Q.P., et al., *TOX2 regulates human natural killer cell development by controlling T-BET expression.* Blood, 2014. **124**(26): p. 3905-13.
104. Tessema, M., et al., *Differential epigenetic regulation of TOX subfamily high mobility group box genes in lung and breast cancers.* PLoS One, 2012. **7**(4): p. e34850.
105. Hirst, J., et al., *The aftiphilin/p200/gamma-synergin complex.* Mol Biol Cell, 2005. **16**(5): p. 2554-65.
106. Mills, I.G., et al., *EpsinR: an AP1/clathrin interacting protein involved in vesicle trafficking.* J Cell Biol, 2003. **160**(2): p. 213-22.
107. Testa, U., G. Castelli, and E. Pelosi, *Lung Cancers: Molecular Characterization, Clonal Heterogeneity and Evolution, and Cancer Stem Cells.* Cancers (Basel), 2018. **10**(8).
108. O'Flaherty, L., H. Wikman, and K. Pantel, *Biology and clinical significance of circulating tumor cell subpopulations in lung cancer.* Transl Lung Cancer Res, 2017. **6**(4): p. 431-443.
109. Zhang, J., et al., *Intratumor heterogeneity in localized lung adenocarcinomas delineated by multiregion sequencing.* Science, 2014. **346**(6206): p. 256-9.
110. Ding, D., et al., *The predictive role of pretreatment epidermal growth factor receptor T790M mutation on the progression-free survival of tyrosine-kinase inhibitor-treated non-small cell lung cancer patients: a meta-analysis.* (1178-6930 (Print)).
111. Su, K.Y., et al., *Pretreatment epidermal growth factor receptor (EGFR) T790M mutation predicts shorter EGFR tyrosine kinase inhibitor response duration in patients with non-small-cell lung cancer.* (1527-7755 (Electronic)).
112. Lee, Y., et al., *Clinical outcome according to the level of preexisting epidermal growth factor receptor T790M mutation in patients with lung cancer harboring sensitive epidermal growth factor receptor mutations.* (1097-0142 (Electronic)).

113. Iwama, E., et al., *Exploration of resistance mechanisms for epidermal growth factor receptor-tyrosine kinase inhibitors based on plasma analysis by digital polymerase chain reaction and next-generation sequencing.* Cancer Sci, 2018.
114. Ye, X., et al., *High T790M detection rate in TKI-naive NSCLC with EGFR sensitive mutation: truth or artifact?* (1556-1380 (Electronic)).
115. El Kadi, N., et al., *The EGFR T790M Mutation Is Acquired through AICDA-Mediated Deamination of 5-Methylcytosine following TKI Treatment in Lung Cancer.* (1538-7445 (Electronic)).
116. Schildgen, V. and O. Schildgen, *The lonely driver or the orchestra of mutations? How next generation sequencing datasets contradict the concept of single driver checkpoint mutations in solid tumours - NSCLC as a scholarly example.* Semin Cancer Biol, 2018.
117. Hata, A.N., et al., *Tumor cells can follow distinct evolutionary paths to become resistant to epidermal growth factor receptor inhibition.* Nat Med, 2016. **22**(3): p. 262-9.
118. Le, X., et al., *Landscape of EGFR-Dependent and -Independent Resistance Mechanisms to Osimertinib and Continuation Therapy Beyond Progression in EGFR-Mutant NSCLC.* (1078-0432 (Print)).
119. Traxl, A., et al., *Breast Cancer Resistance Protein and P-Glycoprotein Influence In Vivo Disposition of 11C-Erlotinib.* J Nucl Med, 2015. **56**(12): p. 1930-6.
120. Sugano, T., et al., *Inhibition of ABCB1 Overcomes Cancer Stem Cell-like Properties and Acquired Resistance to MET Inhibitors in Non-Small Cell Lung Cancer.* (1538-8514 (Electronic)).
121. Abourbeh, G., et al., *Identifying erlotinib-sensitive non-small cell lung carcinoma tumors in mice using [(11)C]erlotinib PET.* EJNMMI Res, 2015. **5**: p. 4.

9 Table of figures